



The Effect of Colloidal Aggregates on Fat Crystal Networks

Raamanand Raj Chauhan

Christ Church
University of Oxford

Supervisors: Prof. Dirk G. A. L. Aarts and
Prof. Krassimir P. Velikov

A thesis submitted for the degree of
Doctor of Philosophy

Hilary Term 2017

Abstract

The effect of fumed silica aggregates on fat crystal networks is studied using a combination of rheology, differential scanning calorimetry and polarized light microscopy. We probe a model system for fat-structured foods with the aim of reducing the amount of fat whilst retaining the desirable mechanical and thermal properties. We begin with oscillatory rheology to investigate the effect of added silica and different fat concentrations on the resulting gel networks. The addition of silica is shown to increase the linear viscoelastic region, without significantly changing the storage modulus within this region. Differential scanning calorimetry measurements show that the presence of silica slightly increases the crystallization temperature but does not act as a seed for nucleation or significantly affect the melting profile of the system. We propose the formation of a composite gel network structure with a layer of silica on the surface of the fat crystal chains. We demonstrate that it is possible to create reduced-fat alternatives with similar rheological behaviour and thermal properties as the full-fat systems through the addition of colloidal silica. Next, we look at the effects of silica concentration, surface area and surface chemistry on the model system. In particular, we focus on the storage modulus, the length of the linear viscoelastic region and the rate of network breakdown after the linear region. We interpret these results in terms of hydrogen bonding between the silica aggregates and its role in reinforcing the fat crystal networks. Then, we study the time-dependent rheological behaviour of this system using the three interval thixotropy test. We measure the deformation under an applied stress and the recovery of structure once the applied stress is removed. We show that, under certain conditions, both fat and silica networks are thixotropic, leading to a full recovery after an applied deformation. We observe a synergistic effect leading to much stronger gel networks when fat and silica are present together. We use polarized light microscopy to gain a more direct insight into the effect of silica aggregates on the fat crystal microstructure. In particular, we study the effects of different fat concentrations, cooling rates, silica concentrations and silica surface chemistries. We use various image analysis techniques to quantify the fat crystal microstructure and find no significant difference in the presence of silica, at low concentrations.

Declaration

This thesis is submitted for the degree of Doctor of Philosophy in Physical and Theoretical Chemistry at the University of Oxford. No part of this thesis has been accepted or is currently being submitted for any degree, diploma, certificate or other qualification in this University or elsewhere. This thesis is wholly my own work, except where indicated.

Contents

Abstract	i
Declaration	iii
1 Introduction	1
1.1 Scope of the Thesis	3
2 Background and Experimental Methods	5
2.1 Experimental Model System	6
2.1.1 Fat Crystal Networks	6
2.1.2 Fumed Silica Aggregates	11
2.2 Experimental Methods	12
2.2.1 Rheology	12
2.2.2 Differential Scanning Calorimetry	15
2.2.3 Polarized Light Microscopy	16
2.2.4 Confocal Scanning Laser Microscopy	18
2.2.5 Infrared Spectroscopy	18
3 The Structure of Fat Crystal Networks with Colloidal Aggregates	21
3.1 Introduction	22
3.2 Experimental Methods	23

3.2.1	Chemicals	23
3.2.2	Sample Preparation	24
3.2.3	Rheology	24
3.2.4	Differential Scanning Calorimetry	26
3.3	Results	26
3.3.1	Rheology	26
3.3.2	Differential Scanning Calorimetry	31
3.4	Discussion	33
3.4.1	Suspensions	33
3.4.2	Single Component Gels	33
3.4.3	Composite Gels	34
3.5	Conclusions	36

4 Exploring Concentration, Surface Area and Surface Chemistry

	Effects of Colloidal Aggregates on Fat Crystal Networks	37
4.1	Introduction	38
4.2	Experimental Methods	40
4.2.1	Chemicals	40
4.2.2	Sample Preparation	40
4.2.3	Rheology	41
4.2.4	Differential Scanning Calorimetry	41
4.2.5	Infrared Spectroscopy	41
4.3	Results & Discussion	41
4.3.1	Silica Concentration	41
4.3.2	Silica Surface Area	44
4.3.3	Silica Surface Chemistry	45
4.3.4	Infrared Spectroscopy	49
4.4	Conclusions	50

5	The Deformation and Recovery of Fat Crystal Networks with Colloidal Aggregates	53
5.1	Introduction	54
5.2	Experimental Methods	56
5.2.1	Chemicals	56
5.2.2	Sample Preparation	57
5.2.3	Rheology	57
5.3	Results & Discussion	58
5.3.1	Different Stress Values	58
5.3.2	Different Fat Concentrations	60
5.3.3	Different Silica Concentrations	62
5.3.4	Fixed Stress Value	63
5.3.5	5 wt.% Fat with Different Silica Concentrations	65
5.3.6	5 wt.% Fat with Different Silica Surface Areas	67
5.3.7	5 wt.% Fat with Different Silica Surface Chemistries	68
5.4	Conclusions	70
6	Observing and Analysing Fat Crystal Networks	73
6.1	Introduction	74
6.2	Experimental Methods	75
6.2.1	Sample Preparation	75
6.2.2	Differential Scanning Calorimetry	75
6.2.3	Polarized Light Microscopy	75
6.2.4	Confocal Scanning Laser Microscopy	75
6.2.5	Image Analysis	76
6.3	Results & Discussion	79
6.3.1	Time Series Experiments	79
6.3.2	Measuring Crystallization with Polarized Light Microscopy	81

6.3.3 Polarized Light Microscopy Image Analysis	83
6.3.4 Confocal Scanning Laser Microscopy	89
6.4 Conclusions	92
Summary	95
Appendix	99
Bibliography	103
List of Publications	113
Acknowledgement of Funding	115
Acknowledgements	117

Chapter 1

Introduction

Our experience of the world tells us that matter cannot be neatly categorized into the three classical states of matter: solid, liquid and gas. We observe that commonplace materials can possess very different properties depending on how we manipulate them. For example, toothpaste flows out of the tube like a liquid, but will sit on the bristles of a toothbrush like a solid. The way these substances behave under mechanical stress plays a huge part in consumer experience and can be directly linked to the microstructure present [1]. In particular, foods offer many examples of complex behaviour due to their microstructure, such as the classic problem of getting ketchup out of the bottle [2].

Soft matter is a broad field of research interested in the physical properties of materials which lie between liquids and solids. These materials are easily deformed: the relevant energy scale is set by the thermal energy, $k_B T$, where k_B is Boltzmann's constant and T the absolute temperature [3,4]. Soft matter substances are made up of structural units, with typical colloidal lengthscales ranging from one nanometre to one micron in size [5], and it is these units that determine the macroscopic physical properties of the material.

Food science can be considered as a subset of soft matter [6–8]. There are a many different structural units in foods, including oil droplets in mayonnaise [9] and ice cream [10] and gas bubbles in bread [11] and beer [12]. Food science aims to understand these building blocks, the interactions between them and the way in which they self-assemble into larger structures [13]. The snap of chocolate and the way it melts in the mouth can be directly linked to the fat crystal units present [14]. These crystals form a network that spans the entire sample and this

microstructure is responsible for many of these desirable properties. Similarly, the spreadability of butter and the way it melts on hot toast is related to the fat crystal network properties.

The microstructure of foods can also determine the response to an applied stress and the recovery once the stress is removed. During the manufacturing of food products, it is crucial to understand how materials will behave during mixing or pumping in order to optimise flow through the production system and to avoid causing irreversible damage to the product. A clear illustration of the importance of this effect is a material which shows a decrease in viscosity with time under a constant applied stress, which will show different flow properties at different distances in a long section of pipe [15]. It is also important to understand how these materials recover after deformation; for example, mayonnaise will flow under an applied stress, but once the stress is removed, the viscosity will increase again [16]. This is a useful characteristic, since it allows flow during the manufacture and bottle-filling processes, but the recovery of structure means that the amount of separation and sedimentation during transportation and storage will be reduced, which can improve the shelf-life of the product.

Fats are a fundamental part of our diet: as an energy source, a supply of essential fatty acids and a carrier for fat-soluble vitamins [17,18]. Although the links between dietary fat and health risks are still debated [19], there is an ongoing effort by food manufacturers to remove or reduce the amount of saturated fat in their products. However, since the fat networks give rise to the desirable properties, lower-fat substitutes are often less appealing. This has directed research into a reduction in the amount of fat whilst trying to retain the desirable properties that consumers expect in their products [20–22]. One approach focuses on replacing the solid fat with other substances like waxes [23,24] to form organogels, whilst others look at forming novel structures like ‘aqueous-organic’ bigels [25], gel-in-oil-in-gel structured emulsions [26] or quiescent water-in-oil Pickering emulsions [27,28].

Our approach is to use colloidal fumed silica aggregates to reinforce the fat networks so that less fat is required to produce similar mechanical properties. Fumed silica is generally recognized as safe (GRAS) for the food industry [29] and is used as an anti-caking and anti-foaming agent in foods such as grated cheese, soups and flavoured salts [30]. There have been many different studies on the effects of adding extra components into fat networks [31]. A common reason for adding new components is to control the crystallization behaviour and the resulting crystal polymorphs, which is of paramount importance in the chocolate industry [32,33]. Added particles

can also act as seeds to create a more homogeneous microstructure. For example, solid sugar and cocoa particles have been used in chocolate model systems to reduce the risk of fat bloom [34,35]. More recently additives have been introduced into fat crystal networks to provide health benefits, like β -carotene which is an anti-oxidant and a precursor of vitamin A [36].

1.1 Scope of the Thesis

In this thesis, we use a model system of fat crystal networks in oil to investigate the effect of added colloidal aggregates. Our overall aim is to understand the link between the microstructure and the macroscopic properties in order to guide the design of reduced-fat foods that have thermal and mechanical properties which are not significantly different from their full-fat counterparts. In particular, we focus on the strength of the resulting networks, the crystallization and melting properties and the microstructure of the fat crystals.

In the following chapter we begin by introducing the model system and the various levels of structure that make up the fat crystal networks. We then describe the colloidal silica aggregates we use to manipulate the fat networks. This is followed by a brief explanation of each of the experimental techniques we use to study our model system.

In Chapter 3, we study the fat crystal network structure at different fat concentrations and in the presence of hydrophilic silica. We show that both the fat and the silica are capable of forming soft, gelled networks at the concentrations of interest. We use oscillatory stress sweep rheology to measure the strength of these networks and differential scanning calorimetry to obtain information on the different crystallization and melting behaviours. We examine the interplay between the fat and silica and propose a composite gel network structure. This chapter demonstrates that it is possible to use colloidal aggregates to create lower-fat samples with similar rheological and thermal properties to higher-fat systems.

In Chapter 4, we expand our study of the model system to look at different silica concentrations, silica surface areas and silica surface chemistries. These results show that the silica is not behaving as a seed for crystal nucleation. Furthermore, variations in the surface area and chemistry both result in a change in the number of surface silanol groups on the aggregates available for bonding. Therefore, this work highlights the importance of hydrogen bonding via these groups in this system. Finally, we use infrared spectroscopy in an attempt to measure this

hydrogen bonding.

In Chapter 5, we investigate the time-dependent rheological properties of the model system. We introduce the three interval thixotropy test for observing the deformation of samples under a constant applied stress and their recovery once the stress is removed. We show that, under certain conditions, both the fat and the silica are able to form networks with thixotropic behaviour. Moreover, when these components are present together we see the formation of much stronger composite networks via a synergistic effect.

In Chapter 6, we use polarized light microscopy to image the microstructure of the fat crystal networks. We focus on four aspects of fat crystallization in our model system: fat concentration, cooling rate, silica concentration and silica surface chemistry. We image the system during the crystallization process and track crystal growth as a function of time. Then, we analyse the final microstructures by measuring individual crystal sizes, extracting typical lengthscales via Fourier transforms and determining two-dimensional fractal dimensions. We also use confocal scanning laser microscopy to build a three-dimensional reconstruction of the fat crystal network microstructure.

Finally, we present a summary of this work to link the findings from the different chapters and to reiterate the key findings. We also suggest several ideas for future work.

Chapter 2

Background and Experimental Methods

ABSTRACT

In this chapter we introduce fat crystal networks and fumed silica aggregates as the key components of our model system. In particular, we focus on the different levels of structure present and the interactions at play. This is followed by a brief introduction into each of the experimental techniques used in this study.

2.1 Experimental Model System

2.1.1 Fat Crystal Networks

The model system used throughout this study consists of a continuous oil phase structured by a fat crystal network. This is a simplified model for fat-structured foods like chocolate and butter, which would normally contain additional components such as sugar crystals, cocoa particles and water droplets [13]. Fat crystal networks have many different levels of structure, which are illustrated in Figure 2.1a, and all of these are able to impact the macroscopic properties of the resulting sample in some way. Therefore, many studies have been conducted to understand this hierarchical structure, and they have been recently summarized by Acevedo et al. [37].

On the molecular scale, fat is made up of triglyceride molecules which are esters formed from the reaction of three fatty acids with glycerol (propane-1,2,3-triol). The number of double bonds and the length of the alkyl chains on the fatty acids has a very large effect on the macroscopic properties of triglycerides, and will determine whether a sample is solid or liquid at room temperature. In fact, both fat and oil are made up of triglycerides and the only distinction is their physical state at room temperature. The fatty acid components in the triglycerides can be denoted by their lipid numbers, which take the form $C:D$, where C is the number of carbon atoms in the fatty acid chain and D is the number of double bonds present. For our model system we use 85% pure tripalmitin fat, shown in Figure 2.1b, which is made up of 84.9% tripalmitin (PPP), 10.6% PPS and 3.2% MPP, where M denotes myristic acid (14:0), P is palmitic acid (16:0) and S is stearic acid (18:0) [38]. For the continuous phase we use soybean oil which is a complex mixture of saturated, mono-unsaturated and poly-unsaturated fatty acids. A detailed list of the components in soybean oil is given in Table 2.1.

There are several different crystal structures, known as polymorphs, which these molecules can arrange themselves into during crystallization from an isotropic melt. Tripalmitin has been shown by differential scanning calorimetry and X-ray diffraction to have three possible polymorphs, α , β' and β , where α is the least stable and β is the most stable [39, 40]. Different polymorphs have different melting temperatures due to the level of molecular order and density of the crystal structures. The polymorph obtained during crystallization can be controlled by the process conditions which is of paramount importance in the manufacture of chocolate. Co-

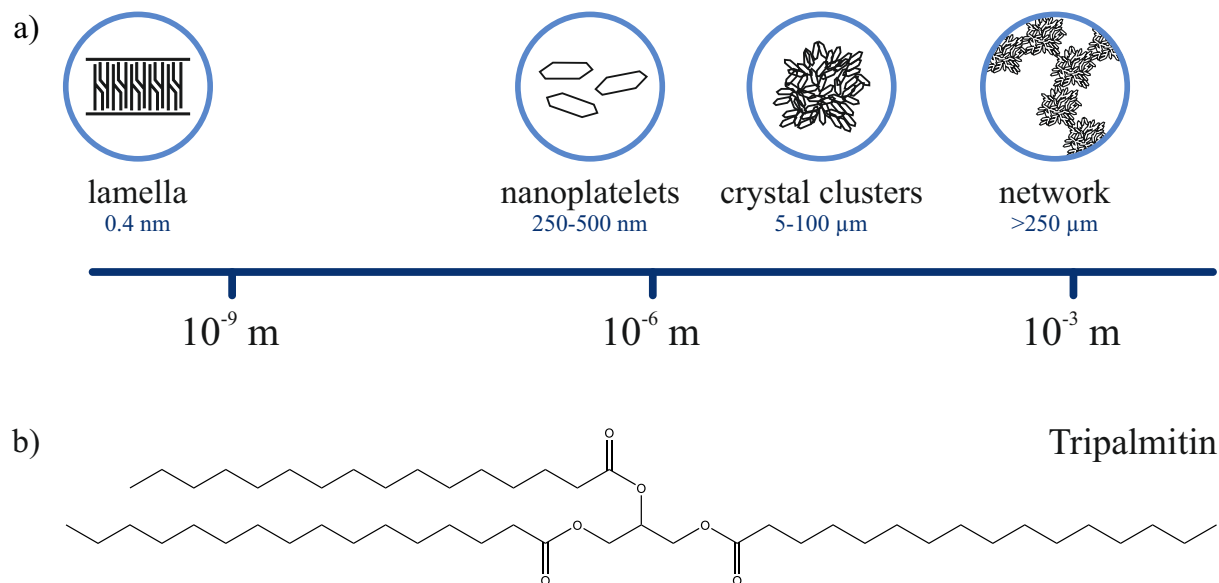


Figure 2.1: a) The different levels of structure present in fat crystal networks [37]. b) The molecular structure of tripalmitin fat.

Saturated Fat		Mono-unsaturated Fat		Poly-unsaturated Fat	
Lipid Number	%	Lipid Number	%	Lipid Number	%
16:0	10.455	18:1	22.55	18:2	50.952
17:0	0.034	20:1	0.233	18:3	6.789
18:0	4.435				
19:0	0.361				
20:0	0.366				
Total	15.651		22.783		57.741

Table 2.1: Fatty acid moieties present in soybean oil. Lipid numbers take the form $C:D$, where C is the number of carbon atoms and D is the number of double bonds present in the chain. Data taken from the USDA National Nutrient Database [42].

coa butter has six polymorphic forms, and as well as the melting temperature, the polymorphs can affect the texture, appearance and resistance to fat bloom [41].

X-ray crystallography has shown various possible conformations for the triglyceride molecules in different polymorphs including a chair and tuning fork configuration [43, 44]. In these conformations, the triglyceride molecules can self-assemble to form lamella structures, which then stack to form nanoplatelets. These lamellae and nanoplatelets can be observed and quantified by a novel technique of cold solvent extraction prior to cryogenic transmission electron microscopy (cryo-TEM) imaging [45]. Aggregation of these nanoplatelets is thought to be driven by Van der Waals interactions [46–48] and leads to the formation of crystal clusters. Depending on the crystallization conditions these clusters can range from approximately 1–100 μm , with smaller clusters being formed at faster cooling rates. This aggregation process has been

investigated in depth recently using computer simulation and ultra-small angle X-ray scattering (USAXS) [49–53].

The crystal clusters loosely pack to form chains and eventually a three-dimensional gel network that is able to span the entire volume of the sample. Narine et al. define microstructure to encompass all structures on a lengthscale of 1–140 μm , which includes the crystal clusters and the chains they form [14]. This microstructure is closest to the macroscopic structure and dictates the majority of the mechanical properties of the product, including spreadability, texture and yield stress [14, 54].

Fat Crystallization

The way in which fat crystal networks form has a large impact on the resulting macroscopic sample properties including the rheological and melting behaviour [55]. Therefore, in all of our experiments we take great care to control the fat crystallization process. At the beginning of all our experiments we heat the samples to form a homogeneous melt and destroy any crystal memory. This is then followed by a cooling process during which fat crystals nucleate and grow.

Classical nucleation theory describes the free energy (ΔG) required to form a nucleus [56], and the key relation is

$$\Delta G = V\rho\Delta\mu + S\gamma \quad (2.1)$$

where $\Delta\mu$ is the chemical potential difference between the bulk solid and bulk liquid, ρ is the density of the nucleus, γ is the surface free energy and V and S are the volume and surface area of the nucleus respectively. The volume term is favourable towards nucleation and describes the difference in free energy between the nucleating phase and the liquid. The second term describes the penalty for increasing the interfacial surface area between the liquid and the nucleating crystal. These terms compete and at small nucleus sizes, the interfacial cost is too high and small nuclei will breakdown. But at greater nucleus sizes the volume term dominates and so larger nuclei will continue to grow in size to form a crystal. This balance leads to an energy barrier for crystallization with a critical size being required before a crystal can grow.

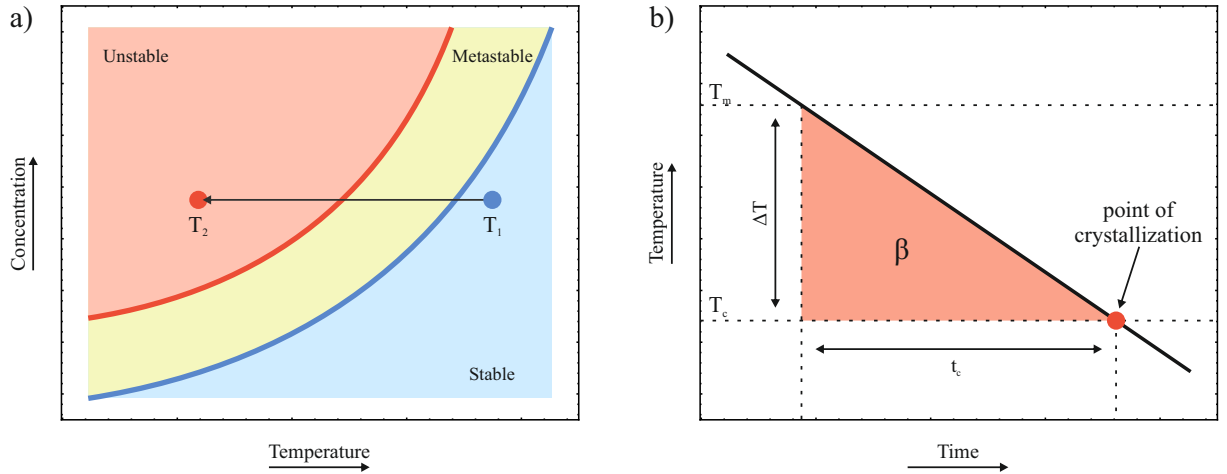


Figure 2.2: a) A schematic solubility curve diagram showing that a temperature decrease from T_1 to T_2 can lead to crystallization. b) The temperature profile for non-isothermal nucleation with a constant cooling rate.

The size of this activation energy barrier is concentration and temperature dependent. This means that it is possible to construct a solubility curve [57], as illustrated in Figure 2.2a. Below the solubility curve the system is stable and crystallization will not occur. However, a decrease in temperature will take the sample into the region where the system is unstable and crystallization will occur spontaneously. This is shown in Figure 2.2a.

The chemical potential difference, $\Delta\mu$, in the volume term is responsible for driving crystallization, and it can be defined as

$$\Delta\mu = \frac{\Delta H \Delta T}{T_m} \quad (2.2)$$

where ΔH is the enthalpy of crystallization, T_m is the melting temperature and ΔT is the temperature difference between the melting temperature and the temperature at which crystallization occurs. This equation shows that as the system is cooled below the melting point, the magnitude of $\Delta\mu$ will increase and will favour crystallization.

The fatty acid chains on triglyceride molecules are very flexible and can explore many different conformations in the liquid phase. However, in order to form crystals they must adopt certain specific conformations [58]. The process of aligning the triglyceride chains takes a finite amount of time which leads to the presence of a metastable zone, within which the system is

no longer stable but crystallization is not instantaneous. When the system is below its freezing point, but has not yet crystallized, it is said to be supercooled. The width of the metastable region is sensitive to many different factors such as impurities, seeding and shear stress [59–61]. In particular, seeding can induce crystallization in supercooled systems, reducing the width of the metastable zone [62]. Seeding is also a useful technique to control crystal size, size distribution and polymorphic form. Note that the classification into metastable and unstable zones here is different from the terminology used for fluid-fluid phase separation [63].

The classical nucleation model assumes isothermal nucleation, where the decrease in temperature is instantaneous. However, this is experimentally very difficult to achieve. A more realistic approach is non-isothermal crystallization where a constant cooling rate, ϕ , is applied between a high temperature in the stable region down to a lower temperature in the unstable region. This is a better model for industrial processes and therefore we use non-isothermal crystallization for the formation of the fat crystal networks.

For non-isothermal crystallization, it has been shown that it is not only the temperature difference but also the amount of time that a system is exposed to supercooling that affects the crystallization process [64]. Figure 2.2b describes a non-isothermal crystallization process with a constant cooling rate, which is defined as

$$\phi = \frac{\Delta T}{t_c} \quad (2.3)$$

with t_c the time between the temperature passing the melting point and reaching the crystallization point. The supercooling-time parameter, β , is given as the area under the cooling curve as shown in Figure 2.2b.

$$\beta = \frac{1}{2} \Delta T t_c \quad (2.4)$$

Equations 2.3 and 2.4 can both be rewritten in terms of ΔT , allowing us to rewrite the chemical potential difference in terms of the cooling rate and the supercooling-time parameter.

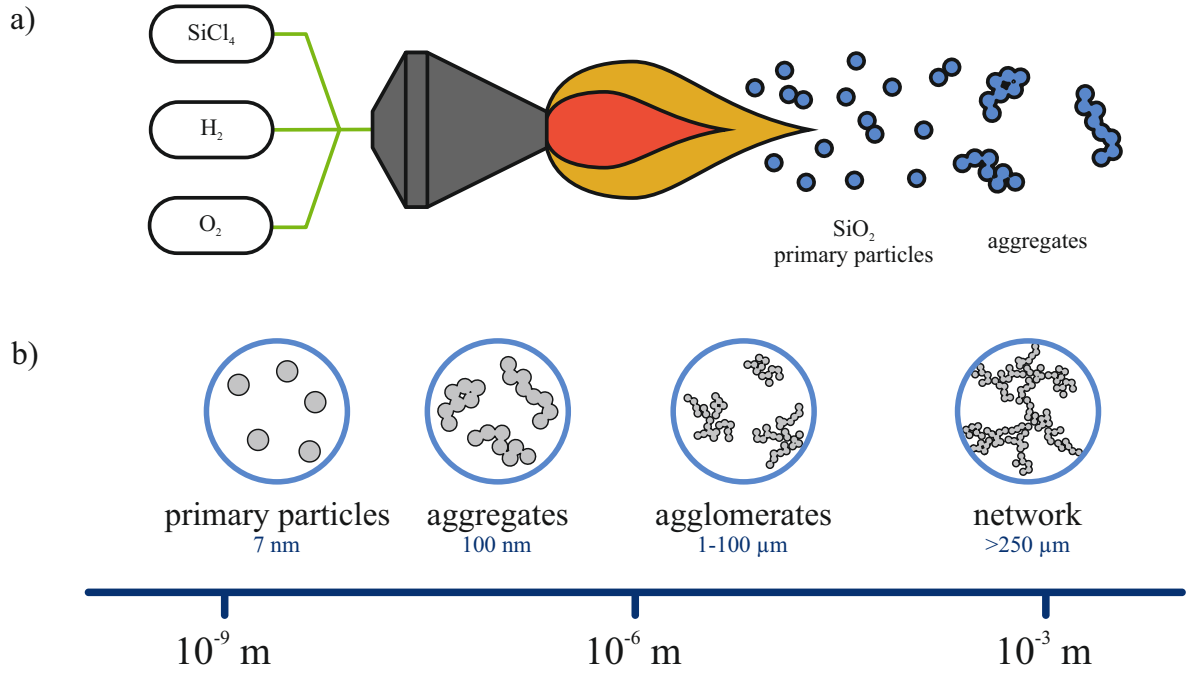


Figure 2.3: a) An illustration of the production of silica aggregates via the flame hydrolysis process. b) The different levels of structure in present in silica networks [67].

$$\Delta\mu = \frac{\Delta H \sqrt{2\phi\beta}}{T_m} \quad (2.5)$$

This equation shows that, for non-isothermal nucleation, the cooling rate plays a major role in determining the properties of the fat crystal network, a result that is well-known experimentally [65, 66]. Higher cooling rates drive crystallization and the system moves through the metastable region faster giving the triglyceride chains less time to efficiently pack into large crystals. This leads to crystallization into the least stable, α polymorph, which is closest in nature to the liquid form and a large number of small crystals are observed. At slower cooling rates, it is possible to crystallize directly into the more stable β' and β polymorphs and the typical crystal size increases whilst the number of crystals decreases.

2.1.2 Fumed Silica Aggregates

Fumed silica is a type of colloidal silicon dioxide (SiO_2), which is used in the food industry as a food-grade anti-caking and anti-foaming agent (E551). Fumed silica is formed by a flame hydrolysis process using vapourized silicon tetrachloride (SiCl_4) with hydrogen and oxygen [67],

see Figure 2.3a. This process produces non-porous, spherical primary particles which then, due to the residual heat from the production process, fuse together irreversibly to form fractal aggregates [68]. These aggregates have silanol ($-\text{Si-OH}$) groups on their surface and therefore they are able to form hydrogen bonds. In weakly hydrogen bonding solvents, such as soybean oil, the aggregates flocculate together via hydrogen bonds to form larger agglomerates and finally a network spanning the entire system [69–72], see Figure 2.3b. Unlike fat, the silica network does not melt or break down with heat at the temperatures used in our experiments, but it is affected by shear which can break down the network back to the aggregate level [67, 73].

2.2 Experimental Methods

2.2.1 Rheology

Our model system of a fat crystal network in oil is a good example of a colloidal gel; ‘a semi-solid system consisting of a solid dispersed in a liquid’ as defined by the Oxford English Dictionary [74]. This system is viscoelastic, which means that it has both liquid-like (viscous) and solid-like (elastic) properties. It is predominantly solid-like at rest, but will flow like a liquid under certain conditions. Rheology is the study of the deformation and flow of matter. It is a powerful tool to allow us to measure and understand this complex behaviour by quantifying the amounts of solid-like and liquid-like behaviours in a sample [1, 75].

In our experiments we apply a shear stress (σ) to the sample, which is a force (F) applied over an area (A) causing deformation along the planes parallel to the imposed force. This is shown schematically in Figure 2.4a for a simplified one-dimensional shear model. After a known stress ($\sigma = F/A$) is applied, the rheometer measures the displacement (Δx), which is then divided through by the thickness (l) of the sample to give the strain ($\gamma = \Delta x/l$).

In practice we apply a rotational shear stress, but the underlying principle is the same. We use an AR-G2 stress controlled rheometer from TA Instruments with a 60 mm aluminium plate geometry, illustrated in Figure 2.4b. The bottom plate is a stationary Peltier plate used to control the temperature of the sample. The top plate is fixed to a rotating spindle which is also attached to a motor, an optical encoder and a transparent disc. The transparent disc is marked with radial lines which the optical encoder can detect in order to accurately measure

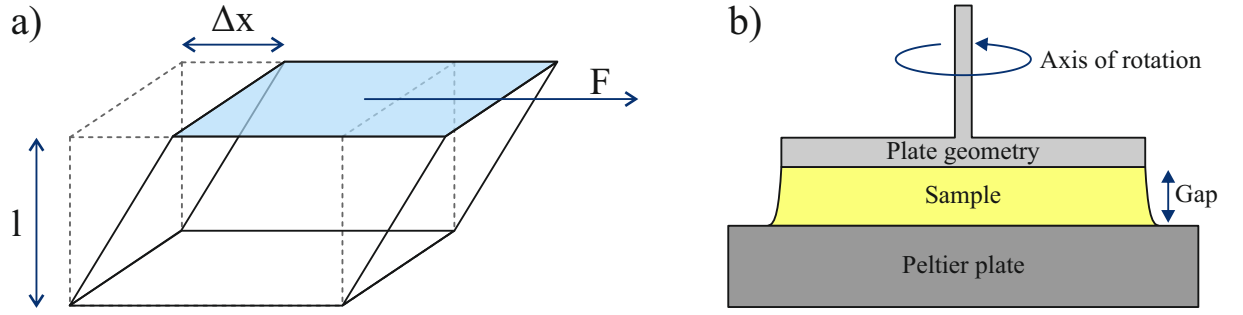


Figure 2.4: a) A simplified one dimensional model of shear. b) A schematic diagram of a rotational rheometer.

the angular position of the spindle as a function of time.

There are two modes in which the rheometer can be operated, rotational and oscillatory, which describe the force applied by the geometry to the sample. The rotational mode is typical for liquids and is used to extract a viscosity. The strain is measured as a function of time and converted into a strain rate ($\dot{\gamma} = d\gamma/dt$), which is related to the dynamic shear viscosity ($\eta = \sigma/\dot{\gamma}$).

The oscillatory mode is generally used for solid-like samples such as colloidal gels as it offers a way to gently probe the structure without damaging it under the applied force. In this case, a sinusoidal stress (σ) is applied and a sinusoidal strain (γ) response is measured.

$$\sigma = \sigma_0 \sin(\omega t) \quad (2.6)$$

$$\gamma = \gamma_0 \sin(\omega t + \delta) \quad (2.7)$$

In these equations σ_0 is the stress amplitude, γ_0 is the strain amplitude, ω is the frequency, t is time and δ is the phase difference between the applied stress and measured strain. Figure 2.5a shows the case where the input stress and the measured strain are exactly in phase. This is a solid-like response and the material is behaving as a classical Hookean spring, where the stress causes an immediate deformation. In this case, all of the energy being applied is stored, ready to be released once the applied stress is removed. Therefore, this solid-like behaviour is described by the ‘storage modulus’, G' :

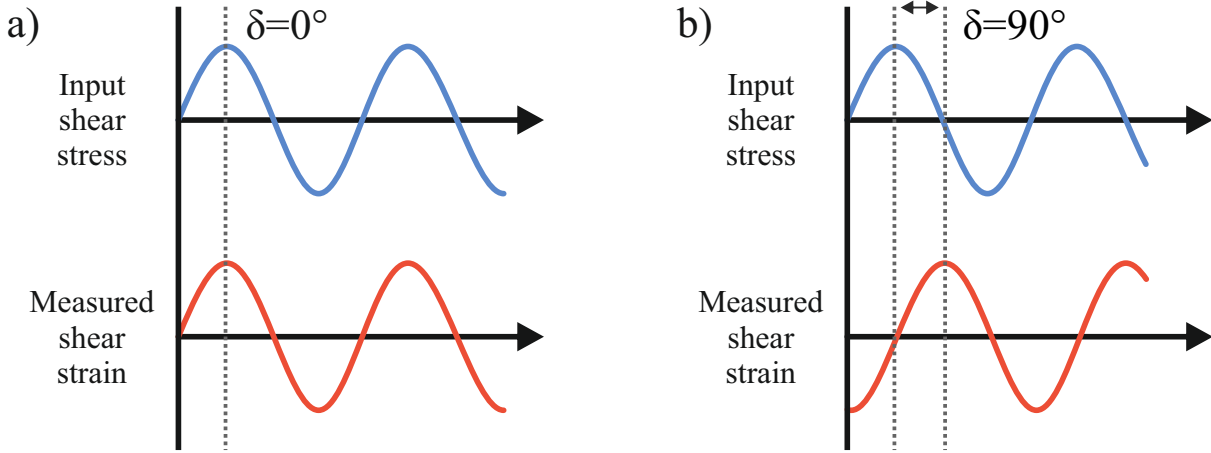


Figure 2.5: The oscillatory input and output values measured by controlled-stress rheology for a) A solid-like material. b) A liquid-like material. δ is the phase difference between the applied stress and the measured strain.

$$G' = \frac{\sigma_0}{\gamma_0} \cos \delta \quad (2.8)$$

Figure 2.5b illustrates the other extreme case where the input stress and the measured strain are 90° out of phase which corresponds to liquid-like behaviour. Here, the material is behaving as a dashpot and there is a delay between the applied stress and the measured deformation. In this case, all of the applied energy is dissipated and therefore this liquid-like behaviour is described by the ‘loss modulus’, G'' :

$$G'' = \frac{\sigma_0}{\gamma_0} \sin \delta \quad (2.9)$$

For soft materials, like colloidal gels, the phase angle will have an intermediate value and so a combination of solid-like and liquid-like behaviour will be measured. It is important to note here that both G' and G'' are derived from the phase angle and when one is much smaller than the other, it is less significant and more error is likely in its measurement [76].

We use oscillatory experiments to measure the shear storage and loss moduli, G' and G'' respectively. In particular, we use time sweeps, frequency sweeps and stress sweeps. The input shear stress signals for these tests are illustrated schematically in Figure 2.6. A time sweep

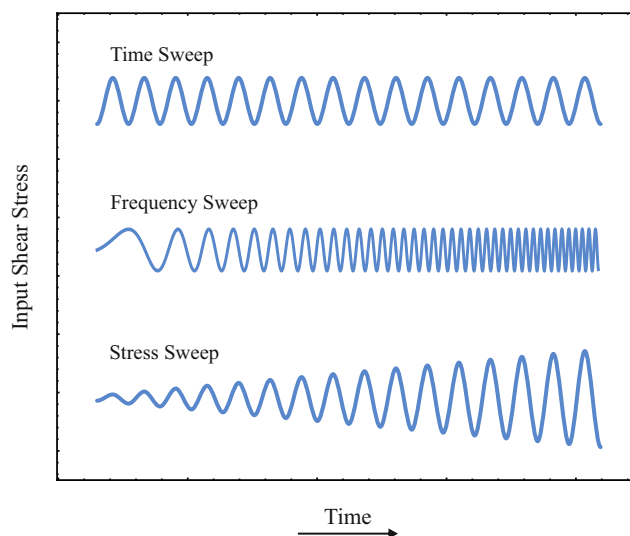


Figure 2.6: Schematic input shear stress signals for a time sweep, a frequency sweep and a stress sweep.

test has a fixed stress amplitude and frequency for the duration of the test. It is used here to study network strength as a function of time. A frequency sweep has a fixed stress amplitude and starts at very low frequencies working up to much higher frequencies. This test is used to probe the structure at different timescales, where low frequencies correspond to long timescales. Stress sweeps have a fixed frequency and start at small amplitude stresses and gradually sweep up to larger values. This allows for the determination of the linear viscoelastic region (LVR), the range of stresses within which the structure has a linear response to the applied stress. This method means we are able to probe the networks present in the samples without damaging them under the applied stresses [75, 77]. For all of the experimental techniques, we will describe the protocols and data analysis in the relevant chapters.

2.2.2 Differential Scanning Calorimetry

Differential scanning calorimetry (DSC) is used here to study the exothermic crystallization and endothermic melting processes of fat crystals. The principle works on precisely measuring the difference in temperature of two pans contained in the same furnace [78], shown schematically in Figure 2.7a. We use a TZero Q20 heat flux DSC with a RCS40 refrigeration system from TA Instruments, which has very accurate thermocouples in each of the platforms as well as a thermocouple in the centre of the furnace. One pan contains the sample of interest and the other pan is empty and serves as a reference sample. The output is the temperature difference between

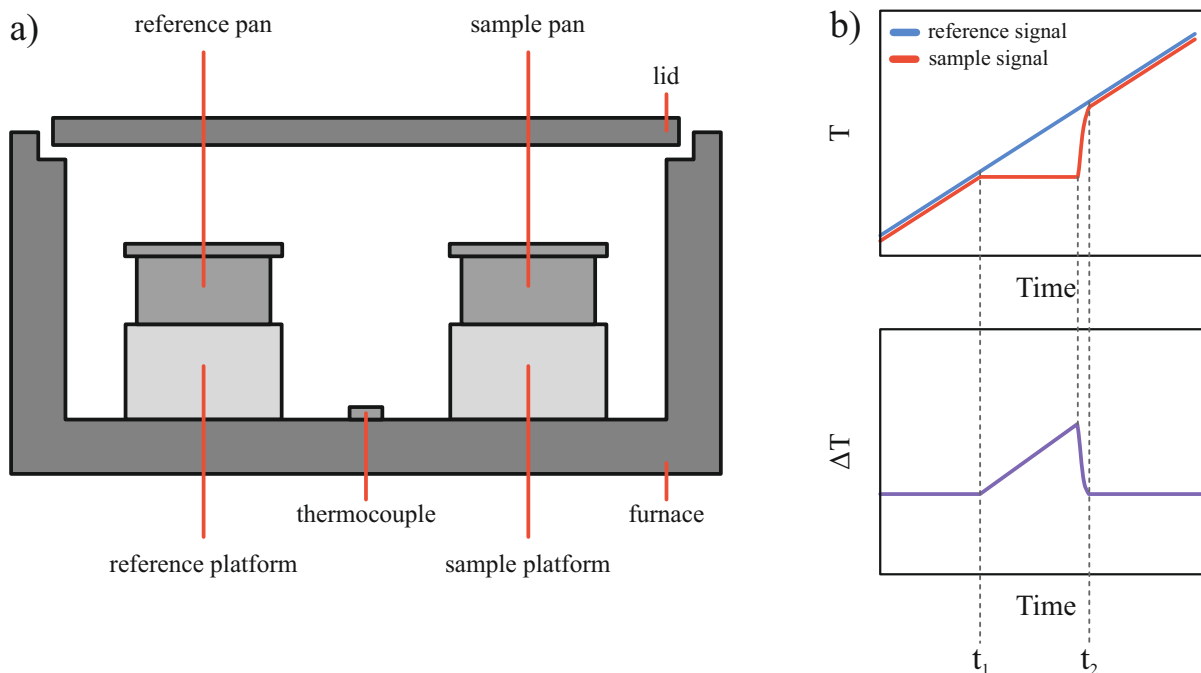


Figure 2.7: a) Illustration of a differential scanning calorimeter furnace. b) A schematic to show how melting peaks are calculated.

the pans which is converted to a heat flow rate (\dot{q}) after considering the thermal resistances and heat capacities of the two pans and the furnace [79]. As the temperature increases the sample will melt, which is an endothermic process causing it to take in energy. This means that the measured temperature of the sample pan will be lower than the reference pan and this difference will translate into a signal in the heat flow rate, which is shown in Figure 2.7b. In this work we present endothermic signals as peaks and exothermic processes as troughs.

2.2.3 Polarized Light Microscopy

Fat and oil are both made up of triglycerides and therefore they have very similar refractive indices. This means that it is very difficult to distinguish the two materials using brightfield microscopy. Instead, polarized light microscopy exploits the fact that fat crystals are birefringent, which arises from molecular order within the crystals [80].

In Figure 2.8a we illustrate how perpendicular polarizers interact with unpolarized light [81]. Electromagnetic waves oscillate at right angles to the direction of travel in unpolarized light, with equal probability in all orientations. As the light passes through the first polarizer, only one orientation is able to propagate through. The second polarizer is placed at 90° to the first

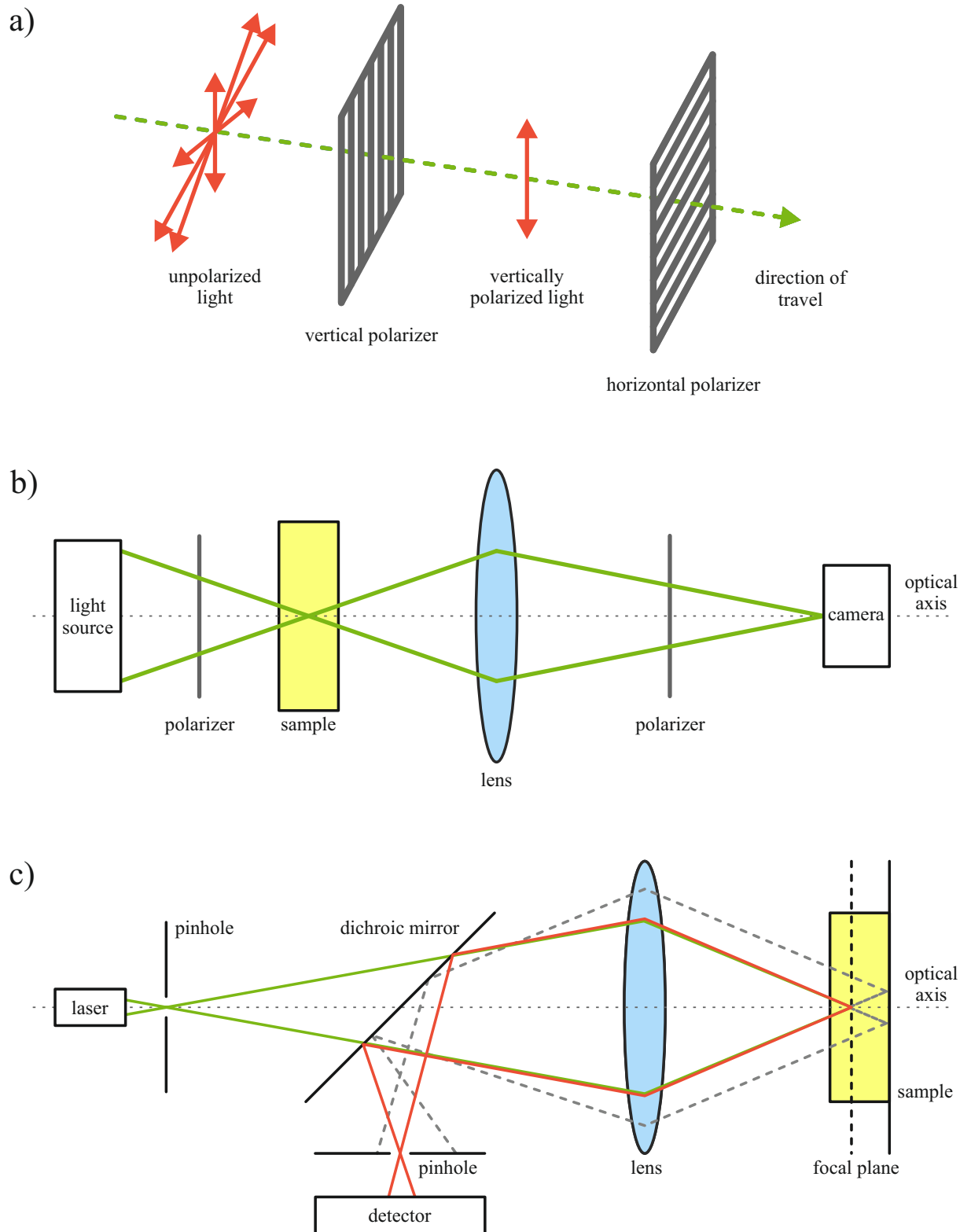


Figure 2.8: a) An illustration showing unpolarized light passing through a pair of polarizers that are held at 90° , with respect to one another. b) A schematic diagram of a polarized light microscope. c) A schematic diagram of a inverted confocal microscope.

which means that the polarized light will not pass through the second polarizer. In polarized light microscopy, the sample is placed between the two polarizers, shown schematically in Figure 2.8b. Birefringent samples are optically anisotropic and will split the light into orthogonal Ordinary and Extraordinary rays which have different orientations compared to the incident polarized light. Therefore, only electromagnetic waves which have been affected by the sample will be able to pass through the second polarizer and be detected by the camera. This leads to the birefringent material being shown as bright features on a dark background, offering much higher contrast imaging. In this study we use a Zeiss Axio Observer inverted microscope with a $10\times$ objective, crossed polarizers and a monochrome PixeLINK camera.

2.2.4 Confocal Scanning Laser Microscopy

In this study we use fluorescent confocal scanning laser microscopy to obtain a three-dimensional representation of the fat crystal networks. In Figure 2.8c we schematically illustrate the optical setup for an inverted confocal microscope [82]. In our experiments we use a Zeiss Axio Observer inverted microscope with a $63\times$ oil immersion objective. A 532 nm laser is focussed through an objective lens onto the sample which has been dyed with fluorescent Nile red dye. Only a very small amount of dye was added and so we assumed that it had a negligible effect on the physical properties of our system, such as the crystallization behaviour and the surface tension of the oil phase. The excited fluorophores then emit light which is focussed by the same objective lens on to a dichroic mirror which reflects the fluorescent light and transmits the laser light. A pinhole is placed between the mirror and the photomultiplier detector which prevents any light which has not come from the focal point in the sample. The use of a pinhole increases the resolution of the images but means that only light from a very small part of the sample is detected. In order to build up a larger two-dimensional image, the laser scans across the sample in the x - y plane. Subsequently, a three-dimensional image can be obtained by taking images at successive focal depths through the sample.

2.2.5 Infrared Spectroscopy

Infrared (IR) spectroscopy measures the interaction of matter with electromagnetic waves in the infrared region, with wavelengths ranging from 1mm to 750 nm. Molecular bonds can be

modelled as harmonic oscillators which vibrate at particular, characteristic frequencies. Therefore, when a sample is exposed to IR radiation, certain frequencies are absorbed, which can be directly related to the molecular bonds present [83].

Typically, IR spectroscopy is used to identify specific chemical bonds in organic molecules. It can also be used to detect hydrogen bonding between molecules [84]. We use this technique to determine the presence of inter-molecular hydrogen bonding between the components of our model system. In particular, we are interested in the carbonyl moieties on the triglycerides and the silanol groups on the silica aggregates.

All samples were analysed with a Bruker Vertex 80 FTIR spectrometer using a DuraSamplIR diamond ATR. The raw output of the measurement is a plot of energy absorbance as a function of wavenumber. A comparison of light transmission through the sample with the background transmission of the instrument provides transmittance data. We present transmittance as the percentage intensity of light transmitted through the sample relative to the measured intensity of the source radiation.

Chapter 3

The Structure of Fat Crystal Networks with Colloidal Aggregates

ABSTRACT

In this chapter we look at the influence of different solid fat concentrations and fumed silica concentrations on the resulting gel network. Oscillatory rheology shows that the addition of silica, at certain concentrations, to fat-in-oil gels does not significantly affect the magnitude of the storage modulus within the linear viscoelastic region. Interestingly, the range of this region is increased. Differential scanning calorimetry shows that the presence of silica leads to slightly earlier crystallization, though no significant effect on the melting profile of the formed network is found. Based on these observations, we propose that composite gel network structures have been formed. These results show that we have created reduced solid fat alternatives with similar rheological behaviour and thermal properties as the full-fat systems through the addition of colloidal silica.

3.1 Introduction

This study looks at lowering the overall amount of solid fat in a simplified model food system through the use of added colloidal particles. The model system used here is comprised of a fat crystal network in a continuous oil phase, and resembles foods such as chocolate and butter. The added colloidal particles are fumed silica aggregates which are food grade and are widely used to control the rheological properties of many different materials [85]. The microscopic fat crystal networks in foods are responsible for the macroscopic mechanical and thermal properties, such as the mouthfeel and the melting point. Therefore, a reduction of fat naturally leads to a change in the overall behaviour of the final food product. This chapter aims to understand the microstructure of these networks and how they are affected by added silica aggregates, in an attempt to lower the overall fat content whilst retaining the desirable macroscopic properties.

Research into models for understanding the mechanical properties of fat networks in oil has been carried out since the early 1960s, with eminent work coming from the Unilever Research Laboratory in Vlaardingen [46, 86]. Originally, the networks were modelled as straight chains of solid particles which transmitted stress through a system. However these models had limited success when compared with experimental data [47, 86–88]. Significant progress was made once the concept of fractal aggregates had been introduced by Mandelbrot and Meakin in the 1980s [89, 90] and gel networks were considered as collections of fractal objects [91]. This was then extended explicitly to fat crystal networks in 1992 [92, 93], where fat crystal clusters were considered as fractal aggregates of nanoplatelets. Note that the term ‘fractal’ is used here to quantify the way in which the mass, M , of a crystal cluster increases with its size, R , following the relation $M \sim R^{D_f}$, where D_f is the fractal dimension.

In the fractal model for fat crystal networks there are two types of interactions present; intra- and inter-crystal cluster interactions. Although both of these interactions are assumed to stem from Van der Waals interactions, the difference arises due to a higher number of interactions within the crystals. This leads to two scenarios once the system is submitted to an applied stress depending on which of these two interactions are weaker and will break first. Some early evidence [94] and good agreement with fractal models [93, 95] has shown that fat crystal networks belong in the ‘weak-link’ regime where the inter-cluster bonds are the ones that break first under an applied deformation to leave an unconnected collection of crystal clusters. In this

limit $G' \sim \phi^{(d-2)/(d-D_f)}$, where G' is the storage modulus within the linear viscoelastic region and d is the Euclidean dimension ($d = 3$ in rheology experiments). This relation was derived for semi-dilute polymers [96] and shown to hold for colloidal particle gels [97]. The fractal dimension does not vary with the fat concentration and so it can be considered as an underlying fundamental constant of the network and provides a way of relating the complex structure to the physical properties.

Oscillatory rheology is an effective tool for studying gel networks as it allows us to measure structure without damaging it. We begin by studying the fat and the silica aggregates separately via oscillatory rheology to probe the structures they form in oil at different concentrations. We then move on to mixed systems to develop an understanding of the interplay between these two components. In particular, we measure a range of samples prepared at different fat-silica ratios to determine the effect of hydrophilic silica on the fat crystal networks. This is coupled with differential scanning calorimetry which offers information about the crystallization and melting of the fat crystal networks in the presence of silica.

This chapter is organised as follows. In the next section we will detail the materials and methods used in these experiments. In Section 3.3 we discuss the oscillatory rheology data which probes the network structures formed in oil. This is followed by the differential scanning calorimetry (DSC) results for the crystallization and melting behaviour of these systems. Finally, we use these results to identify the different types of gelled structures and to suggest a picture of how the colloidal silica interacts with the fat crystal networks in Section 3.4.

3.2 Experimental Methods

3.2.1 Chemicals

Tripalmitin fat ($\geq 85\%$ pure) and soybean oil were purchased from Sigma Aldrich and used without further purification. We used hydrophilic Aerosil 300 (A300) fumed silica from Evonik Industries AG.

3.2.2 Sample Preparation

Soybean oil and silica were mixed in the required proportions with an Ultra Turrax mixer at 13000 rpm for 5 minutes. Solid tripalmitin was then added and the samples were heated in an oven at 100°C for 40 minutes with regular shaking by hand to ensure the samples were properly mixed. All samples were then sealed and stored in a refrigerator at 8°C until use. Before each experiment the bulk samples were melted in an oven at 100°C until completely liquid.

A range of samples containing only fat in oil was prepared at 2.5 wt.%, 5 wt.%, 7.5 wt.%, 10 wt.%, 12.5 wt.%. In order to investigate the effect of the fat-silica ratio a second batch of samples was produced at the same fat concentrations, all containing 2 wt.% of silica. This produced samples with fat-silica ratios of 1.25:1, 2.5:1, 3.75:1, 5:1 and 6.25:1. We also prepared samples containing 1 wt.%, 2 wt.%, 3 wt.%, 4 wt.% and 5 wt.% silica in oil without fat. For all samples, the weight percentages (wt.%) are given with respect to the total sample.

We have chosen to use mass percentages here since the fractal silica aggregates are able to occlude large amounts of oil which leads to much higher effective volume fractions [69]. However it is possible to estimate the volume fractions of the components since their densities are known. The density of soybean oil at 25°C is reported by Sigma Aldrich as 0.92 g/mL and the density of fumed silica is 2.2 g/cm³ [67]. A study on the non-isothermal crystallization of tripalmitin mixtures [98] has shown that for cooling rates above 0.5°C/min the α polymorph is formed, which is consistent with our own calorimetry experiments. Although the density for the α polymorph of tripalmitin is unknown, the density for the more dense β polymorph is 1.047 g/mL and the density of the α polymorph of tristearin is 1.014 g/mL [99]. Therefore, for a typical sample of 5 wt.% fat and 2 wt.% silica in soybean oil, we have approximately 4.5 vol.% fat and 0.9 vol.% silica.

3.2.3 Rheology

Approximately 1.5 ml of melted sample was dispensed onto the peltier plate of the rheometer, which was held at 50°C. Once on the rheometer, the samples were heated to 100°C and sheared at 50 rad/s for 3 minutes to destroy both fat crystal memory and any structures formed by the silica during storage. For all experiments we use a gap size of 500 μ m. The samples were subsequently left to equilibrate for 2 minutes before taking a 5 minute oscillatory time sweep

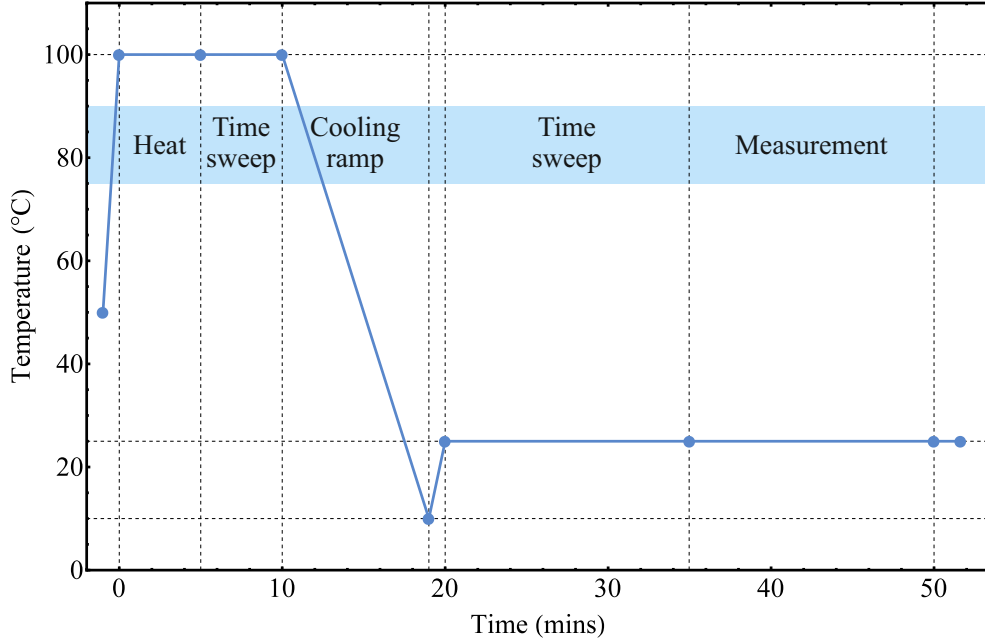


Figure 3.1: A typical experiment timeline.

to measure the amount of structure in the system. Figure A.1a in the appendix shows the time sweep data for typical samples at 100°C. A typical experiment timeline is shown in Figure 3.1.

Then they were cooled from 100°C to 10°C at a rate of 10°C/min with the geometry held static to avoid any shear-induced crystallization. Next, the samples were immediately brought to 25°C/min at a rate of approximately 28°C/min (the highest possible rate) and a second time sweep was done for 15 minutes to measure the formation of the network. These time sweeps confirmed that the system had stopped evolving before any measurements were taken and data for typical samples is shown in Figure A.1b of the appendix.

When taking the frequency sweep measurements, the oscillation frequency ranged from 0.005 to 628.3 rad/s, with a fixed oscillatory stress amplitude of 0.3 Pa. For the oscillatory stress sweep measurements, the oscillatory stress amplitude ranged from 0.01 Pa to 1000 Pa. For the temperature ramp measurements, we raised the temperature from 25°C to 100°C at 20°C/min with an oscillatory stress amplitude of 0.3 Pa. Once at 100°C, we carried out a time sweep measurement over 5 minutes. The frequency for all stress and time sweep experiments was held at 2π rad/s (1 Hz). Each experiment was repeated three times and the arithmetic mean is presented with the error bars corresponding to plus and minus one standard deviation.

3.2.4 Differential Scanning Calorimetry

The melted sample was sheared at 9600 rpm with an Ultra Turrax mixer for 5 minutes. Roughly 10 mg of the sample solutions was weighed out directly into stainless steel pans, which were then hermitically sealed. All the data was collected on a heat flux Q20 DSC from TA Instruments that was calibrated with an indium sample at 10°C/min.

The temperatures and cooling rates used were set to match those from the rheology experiments as closely as possible. The samples were heated to 100°C and held for 10 minutes to ensure that all crystal memory was destroyed before cooling at a rate of 10°C/min down to 10°C. The samples were brought to 25°C at a rate of 25°C/min and held isothermal for 15 minutes. DSC data confirmed that the system had stopped changing before we took the melting measurements and data for typical samples is shown in Figure A.2a of the appendix.

Melting was measured by ramping the temperature from 25°C to 100°C at a rate of 20°C/min. The sample was held at 100°C to destroy any remaining crystal memory and then crystallized for a second time at 10°C/min down to -20°C. We found that for some samples the first crystallization was not complete by 10°C and so the crystallization peak was not fully obtained. On the second crystallization we were able to collect the entire peak and we were also able to see if there were any effects of reheating the samples.

All experiments were repeated three times and the arithmetic mean is presented with the error bands corresponding to plus and minus one standard deviation. We use the TA Universal Analysis software to determine crystallization and melting temperatures.

3.3 Results

3.3.1 Rheology

We use oscillatory frequency sweeps as preliminary experiments to find suitable frequency values for further stress sweep experiments on the fat crystal networks. Figures 3.2a and b show the frequency sweep results for fat samples with 0 wt.% and 2 wt.% silica respectively. Samples that contain strong three-dimensional networks typically have storage modulus (G') values that are independent of frequency and much larger than the loss modulus (G'') values. For all samples we

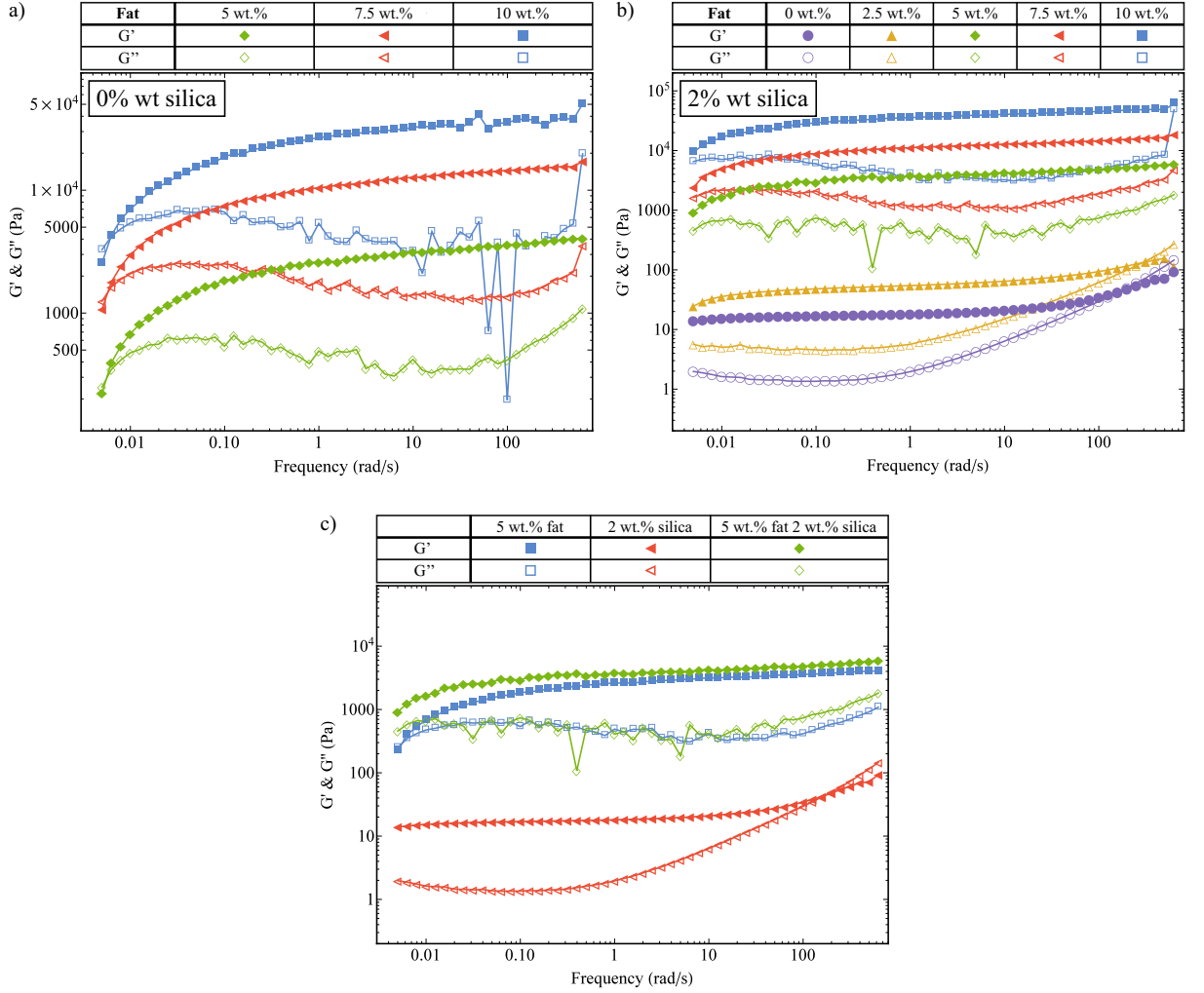


Figure 3.2: Frequency sweep data for a) Fat samples with 0 wt.% silica. b) Fat samples with 2 wt.% silica. c) A comparison of 5 wt.% fat in oil samples with and without silica present.

note that $G' > G''$ for the majority of the frequency range however, we also observe a frequency dependence which suggests that we are measuring weak networks. Nevertheless, in the range between 1 and 10 rad/s, the G' values are relatively constant. Therefore, we chose to use a frequency of 2π rad/s (1 Hz) for all stress sweep and time sweep experiments.

In Figure 3.2c we present a comparison between a 5 wt.% fat sample, a 2 wt.% silica sample and a composite sample containing 5 wt.% fat with 2 wt.% silica. We observe that the G' values for the samples containing fat are much higher than the silica-only sample, which indicates a stronger network is present. By comparison of the fat samples with and without silica present we see that at low frequencies G' is higher in the composite sample. Lower frequencies correspond to longer times between oscillations during which the samples can relax, which typically leads to a decrease in G' . Therefore, these results show that there is less relaxation in the presence of

silica at long timescales.

We use oscillatory stress sweeps to measure G' and G'' to characterize the solid- and liquid-like properties of the fat crystal networks. Figure 3.3a shows G' and G'' against the oscillatory stress, for samples with increasing fat concentration and 0 wt.% silica. There are clearly two different regimes: the high fat (≥ 5 wt.% fat) and the low fat (< 5 wt.% fat) regime. In the low fat regime we see that 2.5 wt.% fat is not enough to make a stress-transmitting network; G'' is greater than G' . For the samples with 5 wt.% fat and above, we see that a network is formed ($G' > G''$) and that G' increases with fat concentration, which means that a stronger network is formed. We also observe that the linear viscoelastic region (LVR) continues to higher stresses for higher fat concentrations, which means they can withstand greater amounts of stress before they are irreversibly deformed.

Figure 3.3b shows the stress sweep data for samples containing different concentrations of silica and 0 wt.% fat. As with the fat samples, this graph shows that there is a minimum required amount of silica necessary to create a network, which lies between 1 wt.% and 2 wt.%. Samples with more than 2 wt.% silica show an increase in G' and an increase in the range of the LVR as a function of silica concentration. This behaviour is similar to that seen in Figure 3.3a.

Figure 3.3c shows G' and G'' against oscillatory stress for samples of increasing fat concentration containing 2 wt.% silica. In the high fat regime, we observe that G' increases with the fat concentration which is similar to the samples without silica shown in Figure 3.3a. In the low fat regime, in the presence of 2 wt.% silica both 0 wt.% (\blacktriangledown) and 2.5 wt.% fat (\bullet) samples now form stress-transmitting networks, as demonstrated by the presence of a linear region. For all samples, we also see that the length of the LVR increases with the fat concentration.

In Figure 3.3d we replot the data from Figures 3.3a and 3.3c, showing only the G' values for samples with and without silica, to allow for easier comparison of the magnitudes of G' . In the high fat regime (≥ 5 wt.% fat), we observe that the silica does not have a significant effect on the magnitude of G' within the LVR. This is to be expected since at the higher fat concentrations the fat-silica ratio is the largest. However, the silica does significantly affect the range of the linear region, to the extent where the LVR is increased up to similar stresses as fat samples with higher fat concentrations. For example, the sample with 5 wt.% fat and 2 wt.% silica (Δ) has a similar LVR range as the sample with 7.5 wt.% fat and 0 wt.% silica (\blacklozenge). Similar results are also seen for the higher fat concentrations. This result is a key example of samples with less solid fat

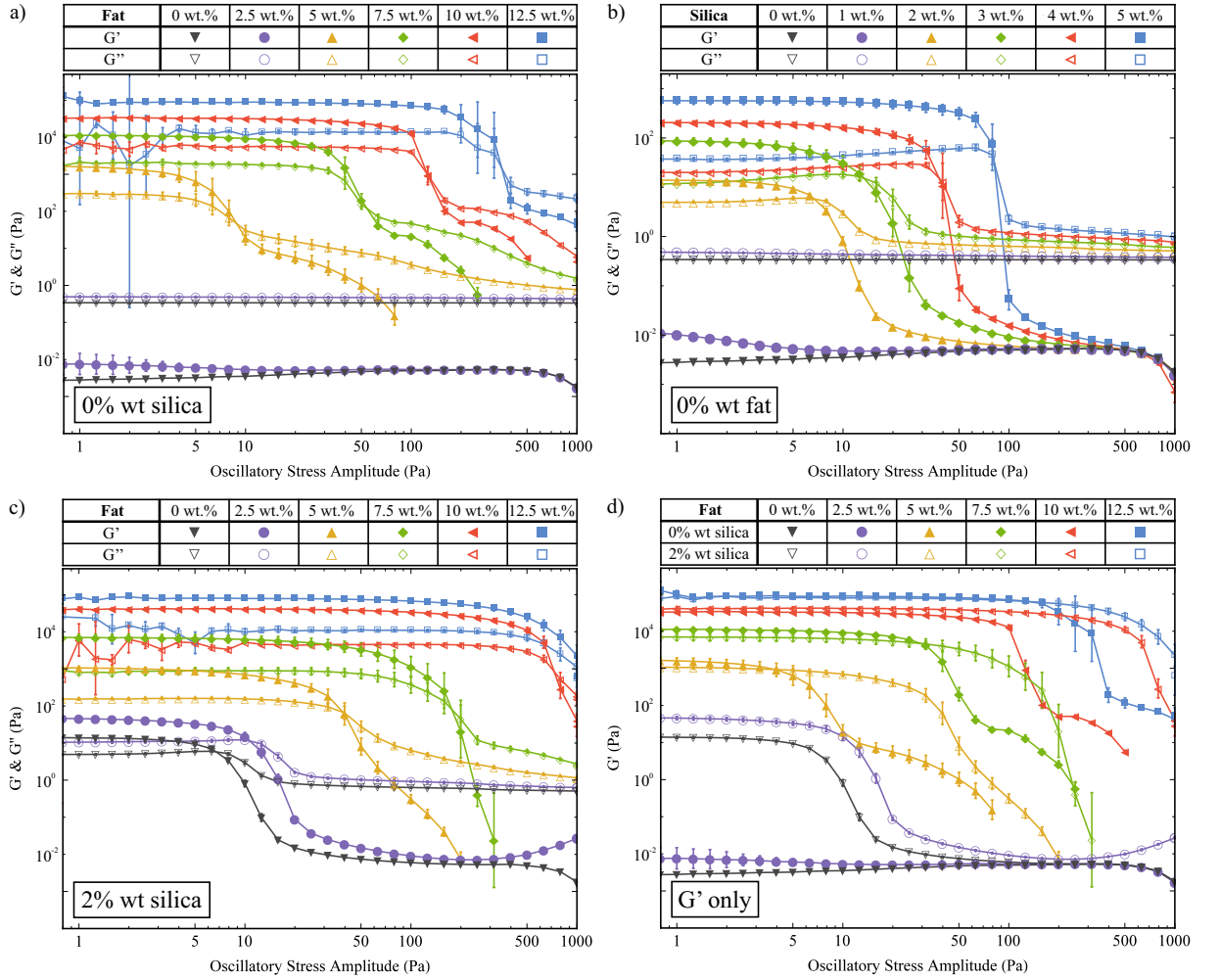


Figure 3.3: Stress sweep data for a) Fat samples with 0 wt.% silica. b) Silica samples with 0 wt.% fat. c) Fat samples with 2 wt.% silica. d) A comparison of G' values for fat in oil samples with and without silica present.

exhibiting macroscopic rheological properties similar to samples with higher fat contents due to the silica present. In the low fat regime (≤ 5 wt.%), we see that upon the addition of silica, the samples go from being liquid-like to viscoelastic gels. We believe that these are predominantly silica networks, since we know that both 0 wt.% fat and 2.5 wt.% fat are insufficient to create stress-transmitting fat networks as shown in Figure 3.3a. Therefore, in the remainder of this chapter we shall not consider the 2.5 wt.% fat samples, since our focus is on the manipulation of fat crystal networks.

We observed a strong power law relationship between the storage modulus and concentration for all systems studied. Plots of $\ln(G')$ against $\ln(\text{mass fraction})$ are given in Figure A.3 of the appendix and produced gradients of 4.22 ($R^2 = 0.999$) for the fat-only system, 3.92 ($R^2 = 0.994$) for the silica-only system, and 4.71 ($R^2 = 0.997$) for the mixed fat-silica system.

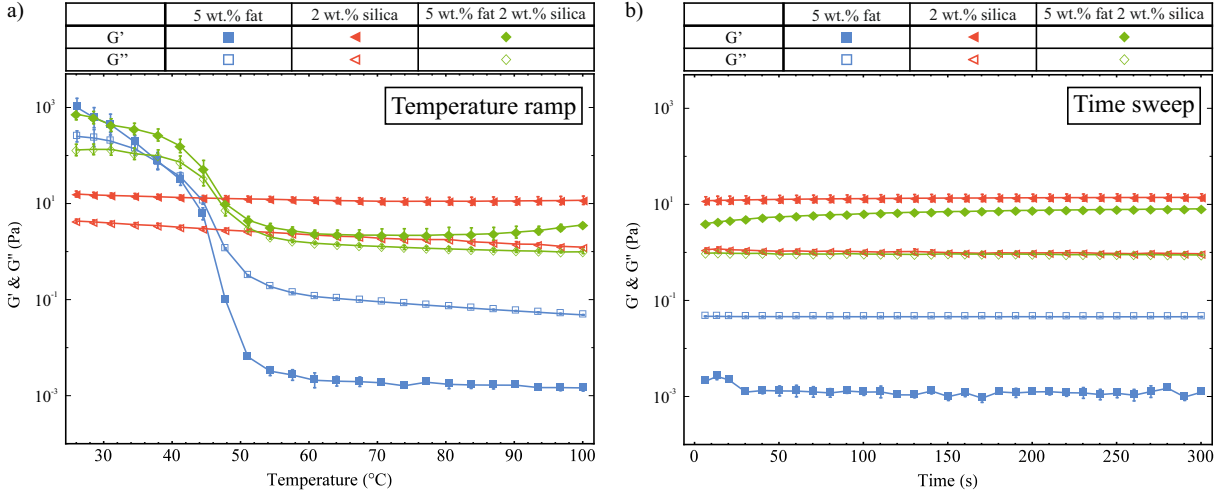


Figure 3.4: a) Temperature ramp data for 5 wt.% fat, 2 wt.% silica and 5 wt.% fat with 2wt.% silica. b) Time sweep data taken immediately after the temperature ramp.

Models of fat crystal networks describe this concentration dependence in terms of fractal dimensions and propose the relationship $G' \sim \phi^{(d-2)/(d-D_f)}$, where ϕ is the mass fraction, d is the Euclidean dimension ($d = 3$ in this case) and D_f is the fractal dimension [91–93,95]. These fractal dimensions offer insight into the density of the microstructure. A fractal dimension of 3 describes a homogeneous solid, and as this value decreases the structure becomes less densely packed and describes a collection of chains which percolate through the sample. Using this relationship, we extract fractal dimensions of 2.76 (fat-only), 2.74 (silica-only) and 2.79 (mixed fat-silica) illustrating that the networks are geometrically very similar and have comparable microstructures.

Within this fractal model, depending on which is stronger of the inter- and intra-fat crystal bonds, systems can be separated into two regimes, the strong-link and weak-link regime respectively. A characteristic of the weak-link regime is that the limit of linearity increases with increasing concentration, which we observe for the fat crystal networks both with and without silica. This is consistent with previous studies on fat crystal networks [93,95], and it means that as the fat crystal networks are deformed under the applied stress, the inter-fat crystal bonds break before the crystal clusters themselves are destroyed.

In Figure 3.4a we show G' and G'' as a function of temperature for samples with 5 wt.% fat, 2 wt.% silica and both 5 wt.% fat and 2 wt.% silica. The 5 wt.% fat sample (■) melts between 45°C and 50°C and we see a large decrease in G' which crosses over with G'' to give a liquid at higher temperatures. The 2 wt.% silica sample (◄) is solid-like over the whole temperature

range, with a small decrease in G' as a function of temperature. The storage and loss moduli values at 25°C for the 5 wt.% fat with 2 wt.% silica sample (◆) are very similar to those of the 5 wt.% fat sample, suggesting that they are made up of the same fat network. The decrease in G' due to melting also occurs at a similar temperature. However, unlike the pure fat sample, there is no crossover with G'' and the sample remains solid-like. This behaviour must be due to the silica present, but by comparison with the pure silica sample the measured G' value is 5 times lower (11.1Pa and 2.2Pa measured at 70°C). This indicates that it is not the same silica network present. Figure 3.4b shows G' and G'' as a function of time, for the same samples as in Figure 3.4a, which were collected immediately after the temperature ramp. This plot shows that the G' value for the 5 wt.% fat with 2 wt.% silica sample (◆) recovers over time to a similar value as the pure silica network (◄).

3.3.2 Differential Scanning Calorimetry

Next, we performed DSC experiments to collect crystallization and melting data, but also to determine whether there are any effects of reheating the samples. For these experiments, the samples were cooled, then heated and cooled a second time. For samples both with and without silica, the crystallization curves were not significantly different on the first and second crystallizations; this is shown for typical samples in Figure A.2b of the appendix. This confirms that we are starting each experiment from a valid reference point that is not affected by crystal memory or sample history.

Figure 3.5a shows the exothermic crystallization curves for samples both with and without silica for the second crystallization process. All curves have been rescaled with the fat concentrations and have been translated in the y-direction for clearer interpretation. Pure soybean oil and the 2 wt.% silica sample do not show any peaks for crystallization or melting (data not shown), which means that both soybean oil and silica do not go through any phase transitions at the temperatures of these experiments. In Figure 3.5a we can see that as the fat concentration increases the crystallization onset temperature increases; this is due to the amount of supercooling which is directly linked to concentration, and acts as a driving force for crystallization.

From the data in Figure 3.5a we also observe that crystallization occurs at slightly higher temperatures in the presence of silica. For heterogeneous nucleation, seeds or defects provide a surface to facilitate the nucleation of a substance. With a suitable surface present, the barrier

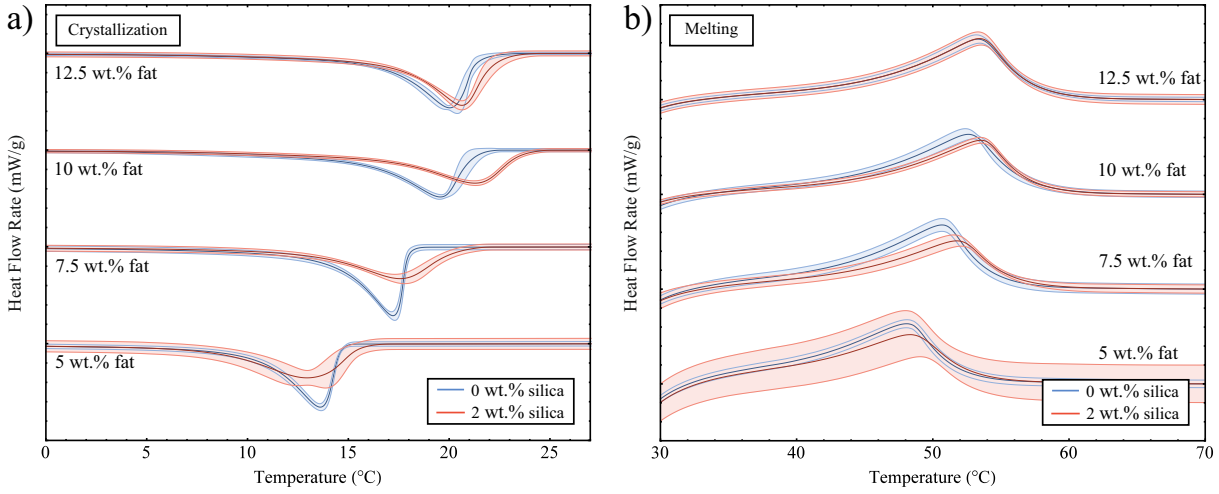


Figure 3.5: a) Crystallization curves for samples both with and without silica. b) Melting curves for samples both with and without silica. These curves have been rescaled with the fat concentrations.

to nucleation is decreased leading to earlier crystallization, reducing the amount of supercooling observed and bringing the crystallization temperature closer to the melting temperature. If the fat was nucleating on the surface of the silica, we would expect to see a larger effect due to the very large surface area of the silica aggregates ($300 \text{ m}^2/\text{g}$). The small shift we observe might be due to an excluded volume effect; the fat can not occupy the same space as the silica and so the volume available to the fat is reduced. This means that the effective concentration of the fat in the oil is increased.

In Figure 3.5b we show the endothermic melting peaks for samples both with and without silica. We see that the melting temperature is not notably different in the presence of 2 wt.% silica for all of the fat concentrations studied. The melting temperatures of the different tripalmitin polymorphs are reported as 44.7°C (α), 55.7°C (β') and 65.9°C (β) [54].

The α polymorph is known to form under non-isothermal conditions with cooling rates above $0.5^\circ\text{C}/\text{min}$ [98]. In Figure 3.5b we see that all of the peak melting temperatures occur below 55°C and therefore we can confirm that we form the α polymorph in our experiments, as opposed to the β' or β . Furthermore, this clearly shows that the presence of silica does not change the polymorphic form of the crystals.

3.4 Discussion

In this section we bring together the obtained results to elucidate the different types of structures we have produced. The simplest system in this study is pure soybean oil, which is a liquid. Below we shall discuss the remaining samples and the different behaviours between them.

3.4.1 Suspensions

For both pure fat and pure silica systems we found the minimum required amount of solid to form a stress-transmitting network. Below these threshold values the samples are suspensions of solids in a continuous liquid phase and show overall liquid-like behaviour ($G'' > G'$). For fat, this amount is found between 2.5 wt.% and 5 wt.% and for silica this lies between 1 wt.% and 2 wt.%. However, although the amount of solid present is insufficient to create a network, it does have a significant effect on the magnitudes of both G' and G'' . The loss modulus is equal to the product of the viscosity and the frequency of oscillations ($G'' = \eta\omega$), and since the frequency is fixed for these experiments, the presence of the solids increases the effective viscosity of these suspensions.

Einstein proposed a model relating the effective viscosity, $\hat{\eta}$, of a dispersion medium to the volume fraction, ϕ , of added particles, $\hat{\eta} \approx \eta(1 + 2.5\phi)$ [100, 101]. However, this model was derived for infinitely dilute, non-interacting hard spheres. Therefore, although we do see an increase in viscosity, we do not expect this relation to adequately describe our system since we know there are attractive interactions between the fat crystal clusters and we are not in the dilute limit.

3.4.2 Single Component Gels

The pure fat (5–12.5 wt.% fat) and pure silica samples (2–5 wt.% silica) both form gel networks within the oil. Both the fat networks and the silica networks show an increase in G' and the range of the LVR with increasing amounts of solids present. This means that the strength of the networks increases and they can be pushed further.

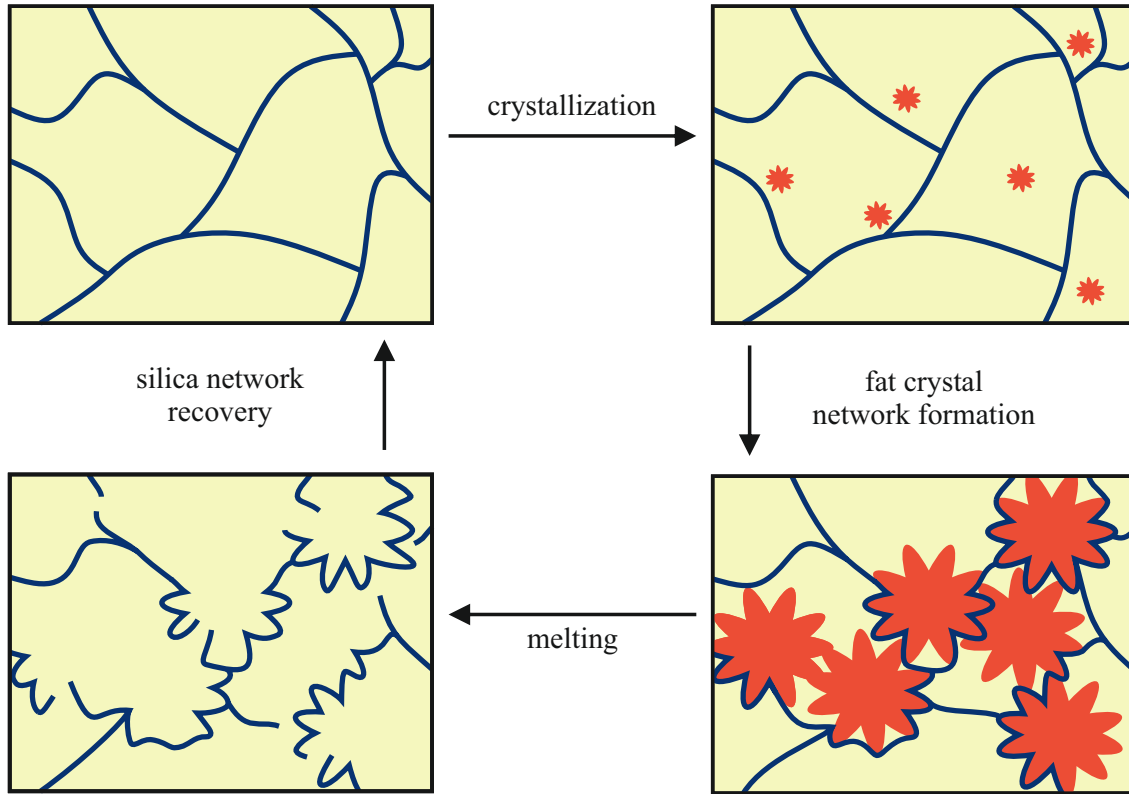


Figure 3.6: A schematic illustration for the formation of the composite fat-silica network. The silica network is shown in blue, the oil is yellow and the fat crystals are orange.

3.4.3 Composite Gels

Composite gel networks, made of both fat and silica, form in the high fat regime with 2 wt.% silica present. From the rheological data, shown in Figures 3.3a and 3.3b, we know that both the fat and the silica are capable of forming networks at these concentrations. The fat crystals form in the presence of a silica network; the initial rheological time sweep data taken at 100°C shows an increase in G' for samples containing 2 wt.% silica after the preshearing step. This data is presented in Figure A.1a of the appendix and means that before the experiments were carried out, the silica had already started to form a network.

There are various possible scenarios as the fat crystallizes within this silica network. One possibility is that, as the fat crystallizes, it encapsulates the silica within the crystals and clusters to form a mixed network. Another scenario is that they could form a bicontinuous, interpenetrating network structure where both networks co-exist within the sample volume unperturbed by the other. Alternatively, the silica network could be pushed out and rearranged by the fat crystal clusters as they grow.

From a comparison of the data with and without silica, we see that the magnitude of G' within the linear region is not significantly different in the presence of silica. This indicates that we are measuring the same fat crystal network structure in both cases made up of the same primary units and the same interactions between them. This then suggests that the silica has not been included into the fat crystal clusters to form a mixed network. The fact that the DSC melting endotherms are not significantly different in the presence of silica is also consistent with the formation of the same fat network.

A comparison from Figure 3.3d of G' values for the 5 wt.% fat sample (\blacktriangle), the lowest concentration to form a fat network, with the 0 wt.% fat 2 wt.% silica sample (∇) shows a difference of two orders of magnitude within the linear region. This means that the fat networks are significantly stronger than the network formed with 2 wt.% silica. Therefore, we believe that as the fat crystals grow, they move and rearrange the existing, weaker silica network. The fact that the G' values for the fat networks are almost unchanged by the presence of silica indicates that the fat networks grow unhindered by the silica network.

The temperature ramp data given in Figure 3.4a shows that as the fat network melts, we can measure the structure of the silica aggregates. We see that they give a lower storage modulus to the silica network formed in the absence of fat. This suggests that they have a different structure and the network has been rearranged by the fat. However, although the silica network has been rearranged and weakened, it is still solid-like ($G' > G''$). Therefore we believe that as the fat crystal clusters grow they push out and rearrange the silica network so that there is a layer of silica particles on the surface of the fat crystal cluster chains resulting in a composite gel network. This layer of silica is continuous and so once the fat melts, it is still possible to measure a solid-like response from the silica. This model is shown schematically in Figure 3.6.

The rheology data also shows that in the presence of silica the LVR is extended. This means that the silica is delaying the breakdown of the fat network under the applied shear. When higher stresses are applied to the fat network some chains will break forming weak points in the gel, from where the entire network will unzip. We believe that the added colloidal silica stabilizes these weak points by dissipating the energy around the weak spots over a much larger area, in a similar manner to that observed by Sun et al. [102]. In this model we do not expect a change in the G' value, but we do anticipate an increase in the linear region.

3.5 Conclusions

In this chapter we have identified the minimum amount of required solids for fat and silica networks to form in soybean oil. We have also identified some of the different types of structures seen. The rheology data has shown that as the fat crystallizes, it rearranges the existing silica network resulting in a composite gel network. These samples have almost the same G' values but an extended linear viscoelastic region. We have shown that it is possible to use fumed silica aggregates, at 2 wt.%, to create fat systems with 2.5 wt.% less fat and similar macroscopic thermal and rheological properties. In the food industry, a reduction by even 1 wt.% fat is regarded as a valuable improvement on a product. Therefore, we believe that the results presented here should be of significant industrial interest.

Acknowledgments

We thank Rob Style for many useful discussions.

Chapter 4

Exploring Concentration, Surface Area and Surface Chemistry Effects of Colloidal Aggregates on Fat Crystal Networks

ABSTRACT

We study the effects of concentration, surface area and surface chemistry of fumed silica aggregates on the model fat-structured food system. We use oscillatory stress sweep rheology to determine the storage modulus, the length of the linear viscoelastic region and the rate of network breakdown after the linear region. Differential scanning calorimetry shows that silica is not acting as a seed for crystal nucleation and that the melting profiles for samples with silica are not significantly different. We interpret these results in terms of hydrogen bonding between the silica aggregates and its role in strengthening the fat crystal networks. We use infrared spectroscopy in an attempt to measure and quantify the hydrogen bonding present.

4.1 Introduction

Our primary aim in this work is to reduce the amount of fat in a model fat-structured food system. Foods like chocolate and butter are composed of fat crystal networks which percolate through the sample and provide mechanical strength which corresponds to texture or mouthfeel. Low-fat food products are often poorly received by consumers due to the difference in their rheological properties. Therefore, we are investigating a method of reducing the fat content whilst retaining the desired macroscopic properties. In order to achieve this, we are using food-grade, colloidal silica aggregates.

The previous chapter has shown that it is possible to use colloidal aggregates to reduce the amount of solid fat whilst maintaining similar rheological and melting properties. We observed that the fat crystals grow within a network formed by the fumed silica aggregates and hypothesised that the fat crystals push out the silica aggregates, leaving silica on the surface of the fat crystal chains and forming a composite gel network. This chapter uses the same model system for fat-structured products to further investigate the effects of the fumed silica. In particular we focus on three different aspects of the silica: concentration, surface area and surface chemistry. Our overall aim is to use this model system to understand the role of the added colloidal aggregates on the fat networks and the resulting macroscopic properties. In the previous chapter, we held the silica concentration constant and varied the fat concentration. Here we hold the fat concentration constant and vary the silica concentration, in order to see the effect on the resulting fat crystal network and to determine which properties are silica concentration dependent. Also, from a financial and manufacturing point of view it is important to determine the minimum required amount of colloidal aggregates necessary to have a desired rheological effect.

In the next section, we describe how the different silica aggregates are produced and chemically modified. Then we give details on the materials and methods used in our experiments. Section 4.3 begins with the results for the experiments looking at silica concentration. This is followed by the results for the surface area and surface chemistry experiments. Next, we present results from the infrared spectroscopy experiments, which were used in order to measure the hydrogen bonding in the model system. Finally, we give our conclusions in Section 4.4.

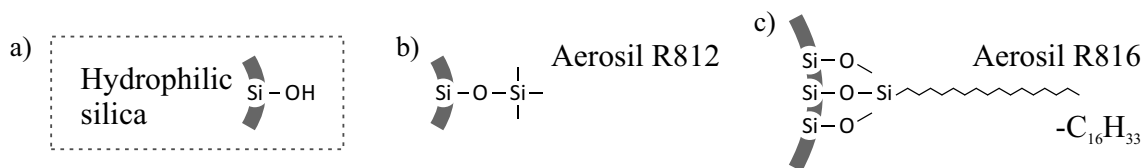


Figure 4.1: Surface functional groups for a) Untreated hydrophilic silica. b) R812 hydrophobic silica. c) R816 hydrophobic silica.

Fumed Silica Production and Modification

Fumed silica is made via flame hydrolysis of silicon tetrachloride (SiCl_4) which produces spherical primary particles [67]. Whilst they are still hot from the production process, they fuse together irreversibly to form branched, fractal aggregates. By varying the process conditions it is possible to vary the primary particle size, which causes a change in the surface area of the silica aggregates. Untreated fumed silica is naturally hydrophilic since the surface is covered with silanol ($-\text{Si}-\text{OH}$) functional groups. In oil, untreated silica aggregates bind to each other via hydrogen bonding rather than interacting with the non-polar solvent [69–72]. In this chapter, we conduct experiments with a range of different silicas both with and without solid fat to understand how the silica surface area, and in turn the number of silanol groups available for hydrogen bonding, can affect the resulting fat crystal networks.

Chemical after-treatment of hydrophilic fumed silica replaces a portion of the surface silanol groups with different chemical functional groups. This treatment is carried out directly after the flame pyrolysis process, before the silica leaves the system. The hydrophilic silica is treated with hexamethyldisilazane to form Aerosil R812 or hexadecylsilane to produce Aerosil R816, both of which are shown in Figure 4.1. The chemical treatment of hydrophilic silica means that it is no longer food grade, however we use it here to investigate the importance of hydrogen bonding via the silanol groups. Typically there are $2.5 \text{ silanol groups/nm}^2$ [67] and approximately 30-50% of these are substituted during the treatment [103].

Typically, in cases where there is a large mismatch between the functional groups on the surface of the particle and in the solvent, the particles will flocculate to form a gel [104,105]. The chemically modified silicas have a reduced mismatch with the oil in our model system, compared to the untreated silica, and so we expect to see a difference in the gelation behaviour. It has also been shown by Smith et al. [31] that additives with a similar chain length and number of double bonds to the fat are more likely to affect the nucleation and growth processes of the fat

Hydrophilic Silicas		
Name	1° Particle Size (nm)	Surface Area (m ² /g)
A300	7	300 ± 30
A255	-	255 ± 30
200F	12	200 ± 25
Hydrophobic Silicas		
Name	1° Particle Size (nm)	Surface Area (m ² /g)
R812	7	260 ± 30
R816	12	190 ± 20

Table 4.1: Data for the different types of fumed silica used in this study; data taken from reference 67.

crystals. In particular, we want to explore how this affects the fat crystal networks that are formed since the -C₁₆H₃₃ chain present in the hydrophobic R816 silica is the same as the fatty acid chain in tripalmitin, see Chapter 2 Figure 2.1b.

4.2 Experimental Methods

4.2.1 Chemicals

Tripalmitin fat ($\geq 85\%$ pure) and soybean oil were purchased from Sigma Aldrich and used without further purification. All fumed silica samples used in this study (A300, A255, 200F, R812 and R816) were provided by Evonik Industries AG.

4.2.2 Sample Preparation

The sample preparation protocol described in Chapter 3 was used to prepare the samples for the experiments in this chapter. A range of samples was prepared with A300 hydrophilic silica concentrations of 1 wt.%, 2 wt.%, 3 wt.% and 4 wt.% both with and without 5 wt.% fat. We prepared samples for the surface area and surface chemistry experiments using the five different types of silica, which are detailed in Table 4.1. For each type of silica, two samples were made, one with 5 wt.% fat and one without, both containing 2 wt.% silica.

4.2.3 Rheology

We used the same protocol described in Chapter 3 for the rheology experiments presented here. The only slight change is that, after the cooling ramp, we now bring the samples back to 25°C using a fixed heating rate of 20°C/min.

4.2.4 Differential Scanning Calorimetry

The DSC preparation protocol described in Chapter 3 was used for the DSC experiments in this chapter. As with the rheology, we bring the samples back to 25°C using a fixed heating rate of 20°C/min.

4.2.5 Infrared Spectroscopy

The spectrometer was configured for optimum performance in the Mid Infra-Red with a MidIR glow bar source and a liquid nitrogen cooled MCT detector. For the measurement of solids a very small amount of sample was placed onto the detector. In order to measure liquid-like samples we used a rubber O-ring and a small quartz disk to contain the sample and minimize solvent evaporation.

4.3 Results & Discussion

4.3.1 Silica Concentration

We use oscillatory stress sweeps to measure G' and G'' , which describe the solid- and liquid-like properties of the samples respectively. Figure 4.2a shows G' as a function of oscillatory stress (G'' is not shown), for samples with increasing hydrophilic silica (A300) concentrations both with and without 5 wt.% fat present. We note that without fat, 1 wt.% silica is not sufficient to form a stress transmitting network ($G' < G''$, G'' is not shown). We also saw this result in the previous chapter. For samples with no fat but 2 wt.% silica or more we observed stress transmitting networks ($G' > G''$, G'' is not shown). An interesting result to note here is that although 1 wt.% silica without fat (\square) is itself not enough to form a silica network, the stress

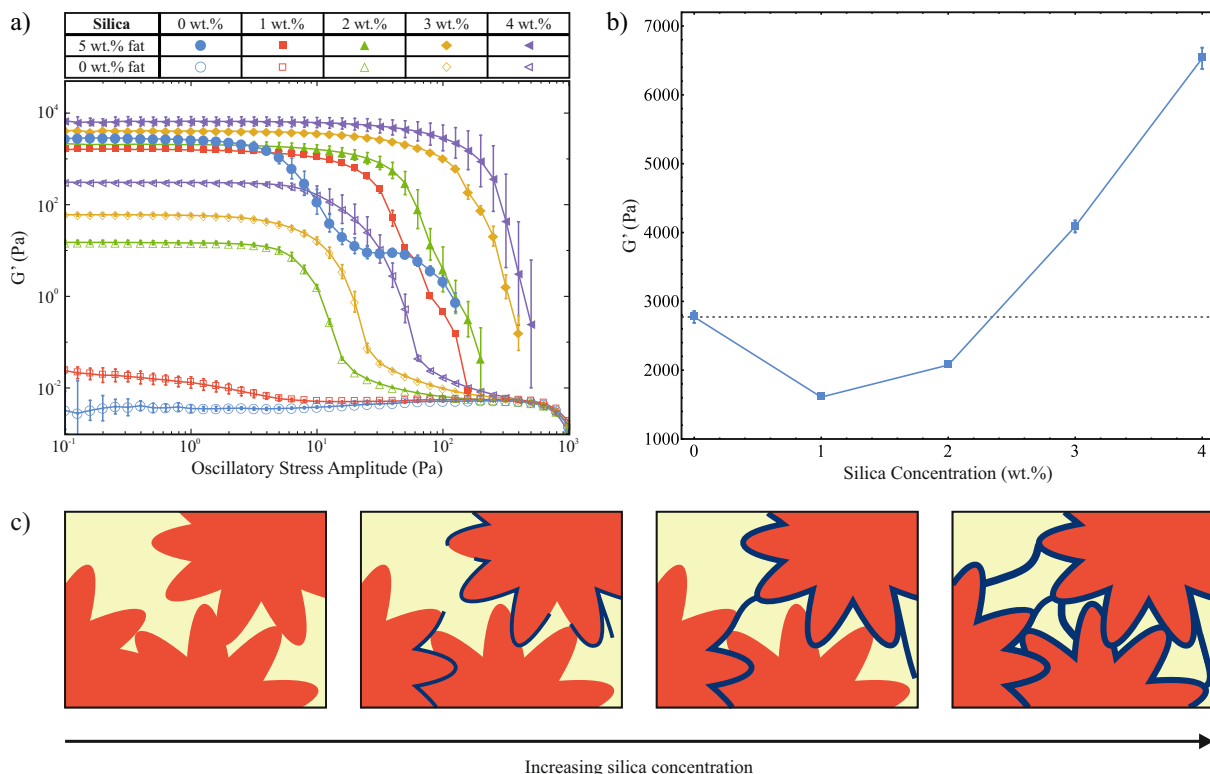


Figure 4.2: a) Stress sweep data for samples with a range of silica concentrations, both with and without 5 wt.% fat. b) A plot of the average G' magnitude within the LVR against silica concentration. c) A diagram to illustrate the effect of silica concentration on the strength of the fat crystal network. The silica network is shown in blue and the fat crystals are orange. Diagrams are not drawn to scale.

curve for the sample with 1 wt.% silica and 5 wt.% fat (■) has a similar shape to the other fat-silica samples, suggesting that the same stress-transmitting mechanism is at work. This potentially shows that the colloidal additives alone do not need to be able to form a network in order to strengthen the fat network.

We note here that the change in the heating protocol has led to a significant difference in the stress sweep curves presented in Figure 4.2a as compared to those in Figure 3.3d. After the cooling ramp, the temperature was brought up to 25°C at 20°C/min rather than ~28°C/min. This meant that the heating step took longer, allowing for more network growth and therefore stronger networks were measured. For example, the 5 wt.% fat 2 wt.% silica sample has a G' value of 2003 ± 158 Pa within the LVR as compared to 1089 ± 10 Pa at the same concentrations measured under the protocol from Chapter 3. Therefore, comparison of data between chapters should be done with some caution, but the data in each chapter is self-consistent.

In Figure 4.2a we see a variation in the magnitude of G' within the linear viscoelastic

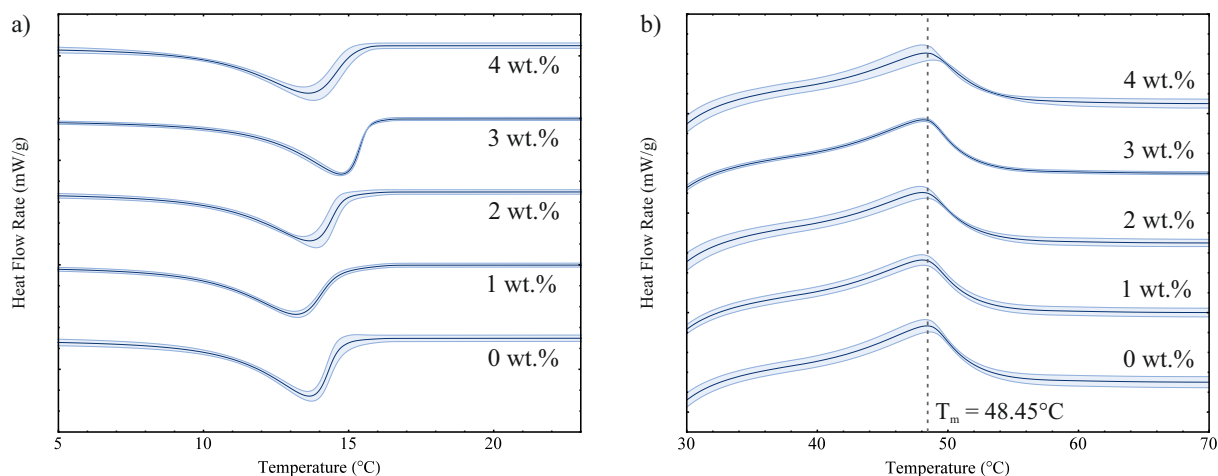


Figure 4.3: a) Crystallization curves for samples with different silica concentrations and 5 wt.% fat. c) Melting curves for samples with different silica concentrations and 5 wt.% fat.

region (LVR) for the samples containing 5 wt.% fat as a function of silica concentration. Figure 4.2b is a plot of the average G' magnitude for samples with 5 wt.% fat, between 0.1 Pa and 1 Pa which lies within the LVR for all samples, against silica concentration on a linear scale. We observe an initial decrease followed by an increase which can be explained by the balance of two opposing effects; as the fat crystals grow they will push out the silica aggregates which will lead to a higher concentration of silica around the fat crystals than in the bulk. As the fat crystals get larger some of the silica aggregates will become trapped between the fat crystals, weakening the fat crystal-fat crystal interactions. However, the silica surrounding the fat crystals will also form a continuous, protective layer which will increase the overall strength of the chains and the network. At lower concentrations, there is less silica to form an effective layer, but there are enough silica aggregates between the crystals to give an overall decrease in the strength of the network. At higher concentrations the second effect becomes dominant and we see an overall increase in G' . This is depicted schematically in Figure 4.2c. However, at both low and high silica concentrations we observe a large increase in the length of the LVR with the addition of silica, which means that the silica is able to help the fat network maintain its structure up to much larger applied stress levels.

Figure 4.3a shows the exothermic crystallization peak of the second crystallization process, for samples that contain 5 wt.% fat and a range of hydrophilic silica (A300) concentrations. All curves have been translated in the y-direction for clearer interpretation. There is a weak silica concentration dependence on the onset temperature for crystallization. This is a volume exclusion effect where the addition of silica slightly raises the effective fat concentration. We observed

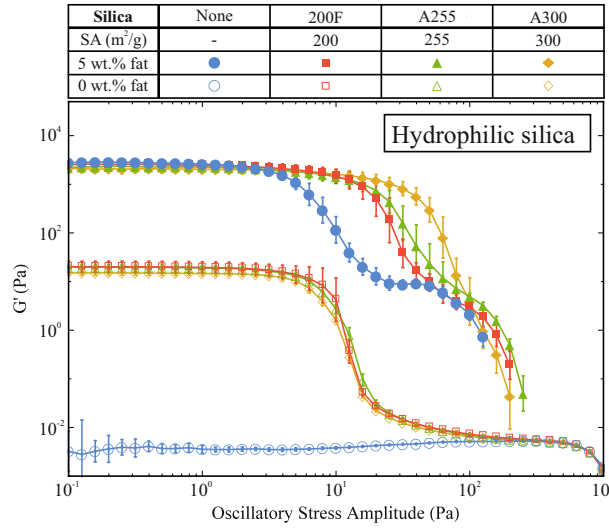


Figure 4.4: Stress sweep data for samples with 2 wt.% hydrophilic silica with different surface areas.

in the previous chapter that higher fat concentrations lead to increased onset temperatures, due to an increase in the amount of supercooling which is a driving force for crystallization.

Figure 4.3b shows the endothermic melting curves for the same samples as shown in Figure 4.3a. We observe that the curves for samples with and without silica are almost identical, which means that the added colloidal particles do not have a significant effect on the melting of these samples and that we form similar fat networks with comparable interactions between the fat crystals.

4.3.2 Silica Surface Area

Figure 4.4 shows G' against oscillatory stress for three hydrophilic silicas with different surface areas (SA) both with and without 5 wt.% fat and all containing 2 wt.% silica. In this set of results all samples showed solid-like behaviour except pure soybean oil (\circ). For all of the silica samples without fat, the G' curves are almost identical in shape and magnitude. This indicates that the surface area does not significantly affect the type of pure silica network that forms in oil, with regard to strength or breakdown under an applied stress.

The samples containing 5 wt.% fat and 2 wt.% silica all have a similar G' value within the LVR to the 5 wt.% fat sample, which indicates that we have the same fat network and that the silica is acting as an auxiliary component supporting the fat network. However, these samples

also have an extended LVR compared to the sample with only 5 wt.% fat. The length of the LVR does not significantly change with the surface area; instead it is the rate at which G' decreases after the linear region which varies. Samples containing silica with a higher surface area have G' curves that decline more slowly after the end of the region of linearity.

This decline in G' after the LVR describes the structural breakdown of the fat network and specifically the breaking of the connections between fat crystal clusters. As the silica surface area increases, the number of silanol groups available for hydrogen bonding increases and so the silica is able to form more bonds and it becomes easier to rearrange under the applied stress; when one hydrogen bond breaks it is more able to rearrange and form a new bond. This means that the silica is able to help the fat crystal chains to remain connected, or partially connected, and break down more slowly as higher stress levels are applied. The silica network is formed prior to the fat network and is disrupted during the crystallization of the fat, see Chapter 3 Figure 3.6. This means that the arrangement of the silica around the fat crystals is much more dense compared to that of the open, fractal structure of the pure silica network and possibly explains why we do not see this behaviour in the silica-only samples.

In Figure 4.4a we show the exothermic crystallization curves of the second crystallization process for the hydrophilic silica samples with 5 wt.% fat. For these experiments, the effective fat concentrations are held constant and so we do not see an effect on the crystallization onset temperature due to increased effective fat concentrations. There is no strong trend of surface area with the crystallization of the fat. The crystallization onset temperatures for the A300, A255, 200F and fat only samples were $15.52 \pm 0.73^\circ\text{C}$, $15.52 \pm 0.08^\circ\text{C}$, $14.94 \pm 0.08^\circ\text{C}$ and $14.75 \pm 0.21^\circ\text{C}$ respectively. This result suggests that the hydrophilic silica aggregates are not acting as seeds for nucleation; heterogeneous nucleation is a surface effect and so we would expect to see a clear trend of higher surface areas leading to earlier crystallization. Figure 4.4b shows the melting of the fat crystal networks in the presence of the different types of hydrophilic silica. From this data, it is clear that the silica surface area does not affect the melting temperature of the fat.

4.3.3 Silica Surface Chemistry

In this section we study two pairs of different silica samples, with the same silica concentrations and closely matched silica surface areas, and so the dominant variable is the surface chemistry.

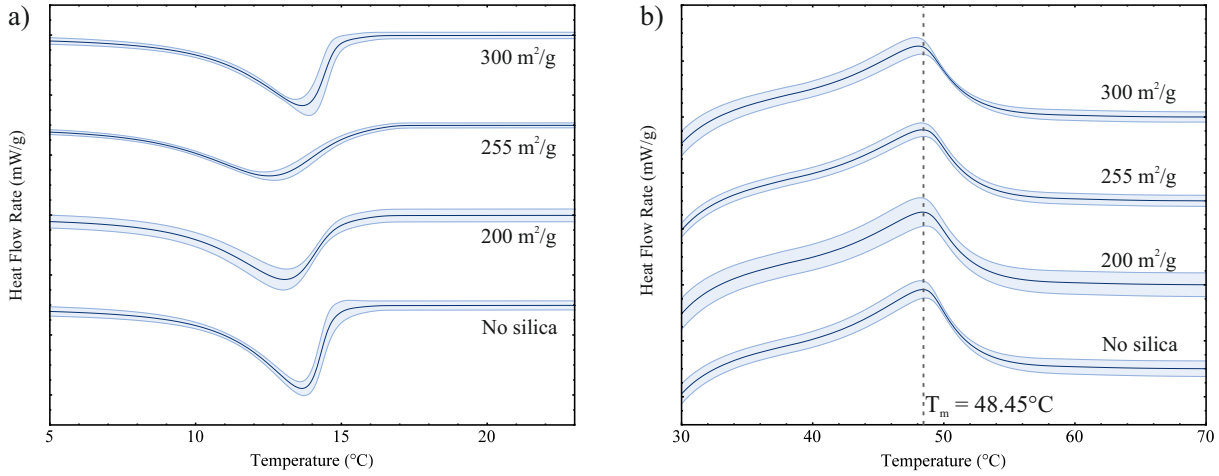


Figure 4.5: a) Crystallization curves for samples with different silica surface areas and 5 wt.% fat. b) Melting curves for samples with different silica surface areas and 5 wt.% fat.

The first pair is the hydrophilic 200F and hydrophobic R816 silicas, which have surface area values of $200 \text{ m}^2/\text{g}$ and $190 \text{ m}^2/\text{g}$ respectively. The second pair is the hydrophilic A255 and hydrophobic R812 silicas which have surface area values of $255 \text{ m}^2/\text{g}$ and $260 \text{ m}^2/\text{g}$ respectively. The hydrophobic silicas have been chemically modified so that a portion of the surface silanol groups were replaced with hydrophobic functional groups. For R816, some silanol groups were replaced with hexadecylsilyl ($-\text{SiC}_{16}\text{H}_{33}$) groups and for R812 the trimethylsilyl ($-\text{Si}(\text{Me})_3$) group was used, see Figure 4.1. Titration with LiAlH_4 has been used to determine the fraction of surface silanol groups that have been substituted during the chemical modification of similar fumed silicas [103]. Based on these results we estimate that for R812 and R816 approximately 30-50% of the surface silanol groups have been substituted.

Figure 4.6a shows the stress sweep data for the hydrophilic 200F and hydrophobic R816 silicas and Figure 4.6b shows the corresponding data for the hydrophilic A255 and hydrophobic R812 silicas. In both cases, the stress sweep data for the samples without silica present are also shown for reference (\blacklozenge and \blacklozenge). We note that the hydrophobic silica samples without fat do not form a network within the oil ($G' < G''$, G'' is not shown). This result is consistent with a combination of factors; less silanol groups available for hydrogen bonding, increased steric hindrance between aggregates and reduced mismatch in chemical nature between the hydrophobic silica and the non-polar soybean oil. Collectively, this means that it is easier for the silica to disperse in the solvent rather than agglomerating to form a gel. However, they are not completely liquid-like which can be seen by comparison with the pure soybean oil (\blacklozenge), which means that there is still a considerable amount of hydrogen bonding present, especially

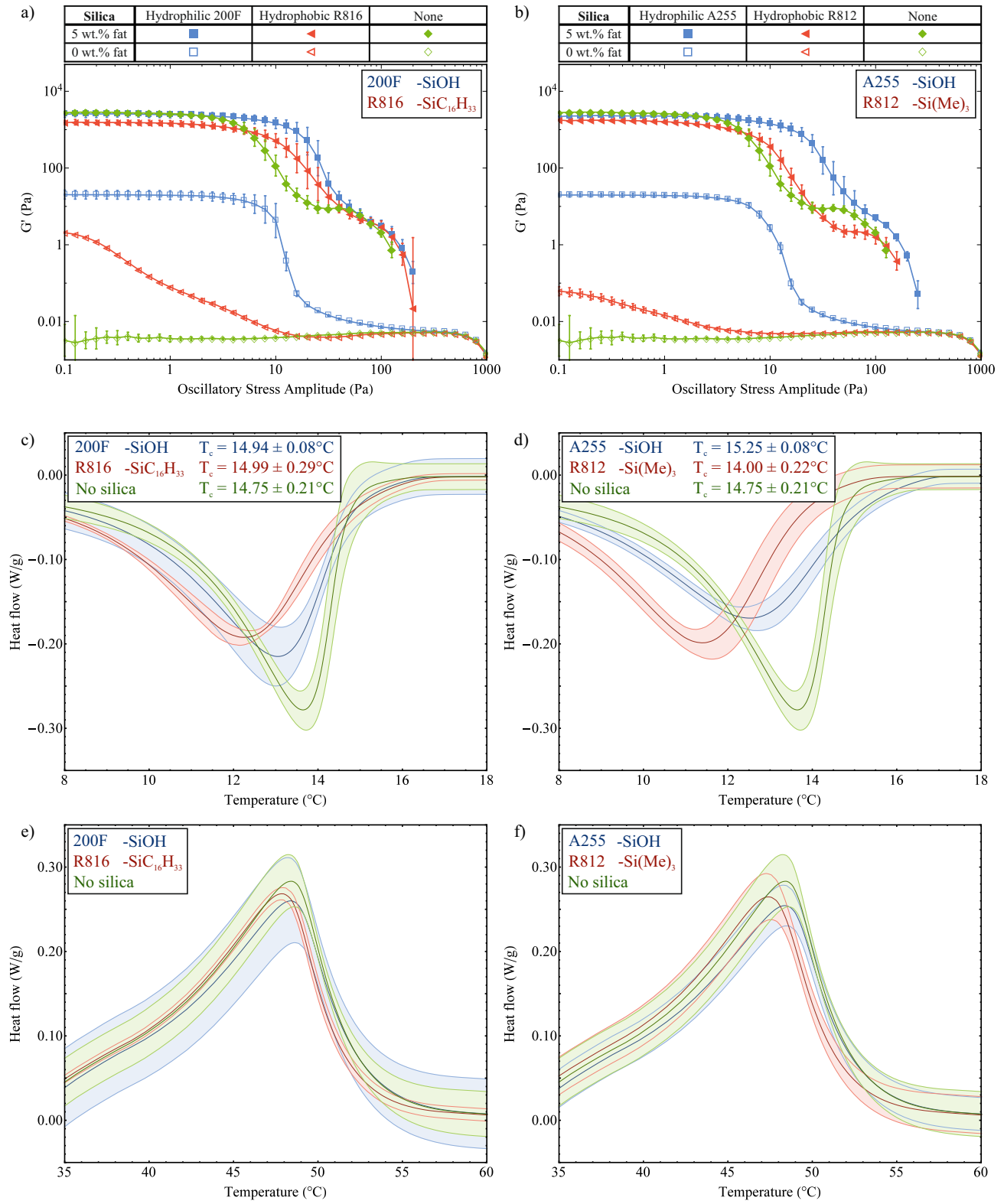


Figure 4.6: Stress sweep data for a) Hydrophilic 200F and hydrophobic R816 silicas. b) Hydrophilic A255 and hydrophobic R812 silicas. Crystallization curves for c) 200F and R816 silicas. d) A255 and R812 silicas. Melting curves for e) 200F and R816 silicas. f) A255 and R812 silicas.

in the R816 case.

With 5 wt.% fat present, we see a small but significant drop in the G' magnitude within the LVR for both of the hydrophobic samples. Without silica present this G' value was measured at 2773 ± 85 Pa and with R816 this was reduced to 1526 ± 27 Pa and 1721 ± 51 Pa for R812. This could be due to the modified functional groups providing increased steric hindrance and weakening the interactions between the fat crystal crystals in the stress-transmitting chains. The hydrophobic silicas do not greatly increase the length of the LVR; the curves start to decrease at roughly the same point as the fat-only sample (\blacklozenge), however the gradient of the breakdown is less steep. The hydrophobic silica present is still able to form some hydrogen bonds and to support the fat network as it breaks down, resulting in a slower decline in G' moving towards higher oscillatory stress levels. These hydrophobic silicas provide another example where the colloidal particles do not form a gel when present on their own in the oil, but they are able to provide some support to the fat crystal network.

Overall, these experiments have reiterated the important role of hydrogen bonds between the silica aggregates in reinforcing the fat network. This synergistic effect can be described by a simple example. A stack of Jenga[®] blocks is wobbled sinusoidally by moving only the top layer of bricks. Starting at small amplitudes and slowly increasing, the stack will eventually fall over. If this were repeated with the stack wrapped in cling film, the cling film would not add any additional strength to the stack when it is at rest. This is analogous to the storage modulus within the linear viscoelastic region. However, it would mean that the pile would be able to withstand larger amplitudes, corresponding to an extension of the linear viscoelastic region. Finally, the way in which the stack eventually falls would be different to the original case, which relates to the decrease in the storage modulus after the linear region. This example neatly captures the central idea of how a weaker material can reinforce another structure and qualitatively describes the measured rheological behaviour. However, we note that this is a simplistic model and there are limitations to this example such as the measurement of the at-rest structure and the role of gravity.

Figures 4.6c and 4.6d show the exothermic crystallization curves of the second crystallization process for the two pairs of silicas all with 5 wt.% fat present. From these plots we determined the crystallization onset temperatures to be $14.94 \pm 0.08^\circ\text{C}$ and $14.99 \pm 0.29^\circ\text{C}$ for the 200F and R816 silica respectively, relative to $14.75 \pm 0.21^\circ\text{C}$ for the 5 wt.% fat sample.

Similarly we measured onset temperatures of $15.25 \pm 0.08^\circ\text{C}$ and $14.00 \pm 0.22^\circ\text{C}$ for the A255 and R812 silicas. This shows that the crystallization of fat is not sensitive to the presence of the different types of silica. Furthermore, it shows that the silicas are not acting as seeds for the nucleation process. This experiment was important as we wanted to investigate whether or not the R816 in particular would act as a seed since it has the same carbon chains as the fatty acid chains of the tripalmitin molecules. Although the crystallization onset temperature is not affected by the different silicas, we see that the width of the peaks is broader for the hydrophobic silicas which indicates a slower growth rate. This might be due to disruption in the packing of the fat molecules into lamellae caused by the bulky functional groups on the silica aggregates. Figures 4.6e and 4.6f show the melting curves for the two pairs of silica. All of these curves lie within the measured variation of each other and so they are not considered to be significantly different.

4.3.4 Infrared Spectroscopy

Earlier in this chapter we have seen indirect evidence for hydrogen bonding. In this section, we attempt to establish this hydrogen bonding and determine whether it is responsible for the reinforcement effects measured via rheology. More specifically, we are looking to discern whether the silanol groups on the silica aggregates form hydrogen bonds with the carbonyl moieties on the triglyceride molecules. Since soybean oil is a complex mixture of different components, we start by studying fat in toluene, which gives spectra that are easier to interpret.

Figure 4.7a shows the IR spectra for toluene followed by 10 wt.% fat in toluene samples containing 0 wt.%, 1 wt.% and 3 wt.% ethylene glycol (EG). The spectra have been translated in the y-direction for clearer interpretation. When the fat is present we see a peak appear at 1745 cm^{-1} which corresponds to the carbonyl groups on the triglyceride molecule. In these experiments we add small amounts of ethylene glycol, which is a small molecule that is capable of forming hydrogen bonds. As ethylene glycol is added, we observe a broad peak around 3300 cm^{-1} which indicates hydrogen bonding is present. However, in order to differentiate the hydrogen bonding between the ethylene glycol to itself and between the ethylene glycol to the fat molecules we focus on the carbonyl region, which is shown more closely in Figure 4.7b. In this plot, the IR data for the toluene has been subtracted from the other samples. When ethylene glycol is present we see that a second peak appears at lower wavenumbers around 1700 cm^{-1}

and we attribute this to hydrogen bonding between the carbonyl group and a hydroxyl group on ethylene glycol. The shift to lower wavenumbers signals a weakening of the carbonyl bond via hydrogen bonding [106], and demonstrates the behaviour to look for in our more complex model system. Spectra for ethylene glycol in toluene were not collected since this experiment was primarily concerned with the carbonyl peak found at 1745 cm^{-1} and ethylene glycol does not have a peak in this region. The spectra for ethylene glycol in toluene at different concentrations could be added for completeness in future work.

Figure 4.7c shows the IR spectra for the separate individual components of our model system: soybean oil, fat and silica. Soybean oil and tripalmitin fat are both composed of triglycerides and so it is not surprising that their spectra are very similar. The main difference here is that the soybean oil is a liquid, which leads to a slight broadening of the peaks. The silica shows a peak around 1100 cm^{-1} which corresponds to Si-O bonds. In Figure 4.7d we present the data in the carbonyl region for samples in soybean oil, where the data for the oil has been subtracted. Relative to the data shown in Figure 4.7b these results are much more difficult to interpret. This stems from the fact that the soybean oil itself has a very strong carbonyl signal and so it effectively drowns out any signal from the fat. We carried out these experiments as an attempt to gain evidence for hydrogen bonding between the fat and the silica, but the results are inconclusive.

4.4 Conclusions

In this chapter, we have studied in detail three different aspects of fumed silica on the fat-structured model system: concentration, surface area and surface chemistry. We have observed that the silica affects the fat crystal networks response to stress in three distinct ways. The first is that the magnitude of G' within the LVR varies with both the silica concentration and the surface chemistry. We propose that silica aggregates between the fat crystal clusters can weaken the overall network, but at high enough concentrations a continuous layer of silica can form which is able to strengthen the network.

The second way in which the presence of silica affects the fat network is that it extends the linear viscoelastic region. This effect was greatest with higher concentrations of silica and hydrophilic, rather than hydrophobic silica. This effect shows that the silica aggregates, via

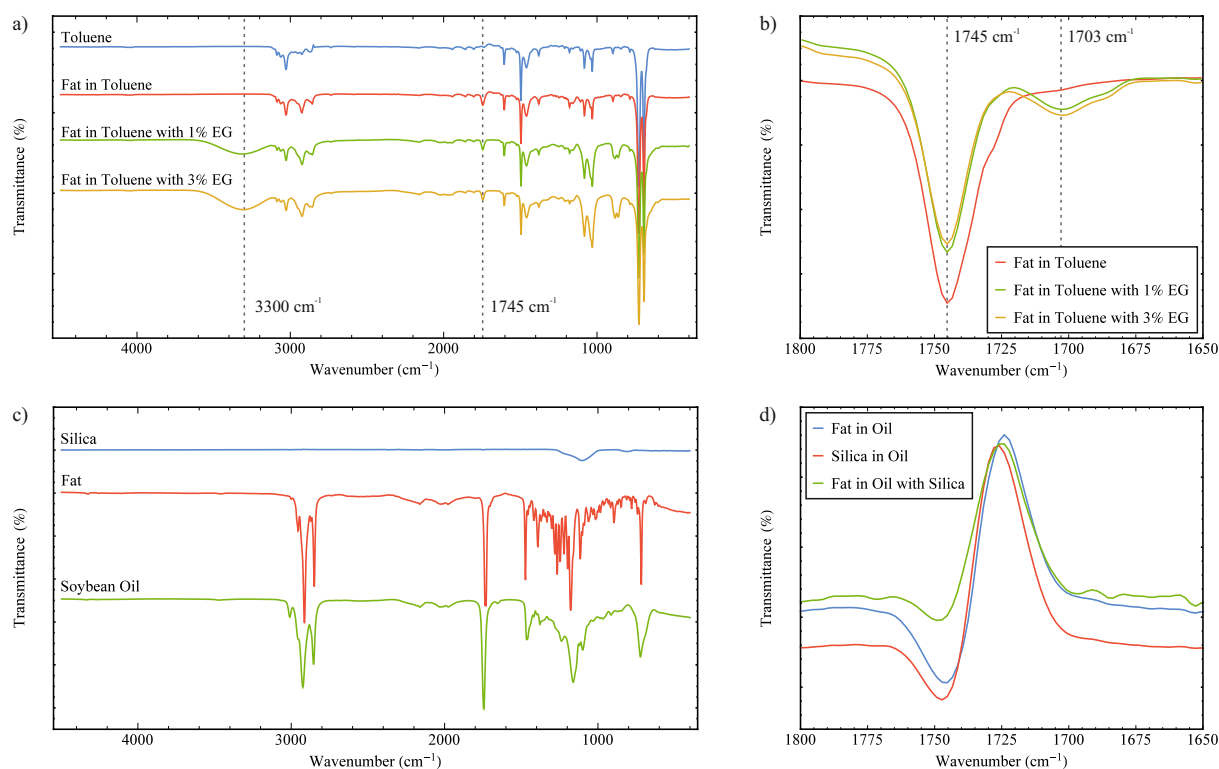


Figure 4.7: Infrared spectroscopy data for a) Fat in toluene with small amounts of ethylene glycol (EG). b) The carbonyl region for fat in toluene with EG. c) The individual components of the model system. d) The carbonyl region for samples of fat and silica in soybean oil.

hydrogen bonding, were able to help the fat crystals maintain their network structure up to higher stress levels. Finally, the silica also changed the breakdown of the fat network after the LVR. Both the surface area and surface chemistry experiments varied the number of available silanol groups, which are used to connect the silica aggregates. With more hydrogen bonds present the silica is able to rearrange and maintain connections for longer, slowing the overall rate of structural breakdown. This behaviour was described by the simple Jenga[®] and cling film analogy.

This chapter provides indirect evidence for hydrogen bonding, and we attempted to use IR spectroscopy as a more direct method for observing this bonding. We were able to measure hydrogen bonding between fat molecules and simple alcohol molecules in toluene, which shows that the fat is capable of forming hydrogen bonds. However, we were not able to observe the same effect in situ, since the fat and the oil in our model system are chemically very similar. This meant that we were not able to distinguish the signals from the different components. Therefore, these results were inconclusive but do we know that both the silica aggregates and the fat molecules can form hydrogen bonds. However, it is still unclear as to whether these

bonds form between the fat and the silica, or only between the silica aggregates.

This study also observed that the added particles do not need to be able to form a gel in oil in order to strengthen the fat crystal network. This further supports our previously proposed mechanism of a composite network rather than a double network structure comprised of two individual networks. We saw two examples of this situation in this chapter, first with hydrophilic silica at low concentrations (A300 at 1 wt.%) and then with both hydrophobic silicas (R816 and R812 at 2 wt.%).

The DSC crystallization data from all three experiments show that fumed silica does not act as a seed for heterogenous nucleation under these conditions. We did however see a weak dependence with silica concentration due to an increased effective fat concentration. The melting data also showed that despite observing large changes in the rheological behaviour upon the addition of silica, the way in which the fat network melts is left unchanged. From a consumer's standpoint this is a crucial result because the way fat-structured food products melt is a large part of the consumer experience; for example the way in which chocolate melts in the mouth or butter melts on hot toast.

Acknowledgments

We are very grateful to Martin Grossel and Robert Jacobs for their help with the design of the IR experiments and the acquisition and interpretation of the results.

Chapter 5

The Deformation and Recovery of Fat Crystal Networks with Colloidal Aggregates

ABSTRACT

In this chapter we use the step-wise three interval thixotropy test to study the rheological behaviour of the model fat-structured food system. We focus on the deformation under an applied rotational stress and the recovery of the oscillatory storage modulus once the applied stress is removed. We observe that stronger networks are deformed less and are able to recover more quickly once the stress is removed. We show that in our system, under certain conditions, both fat and silica networks are thixotropic, showing a full recovery after an applied deformation. Furthermore, when fat and silica are present together we observe a synergistic effect leading to much stronger composite gel networks. Through experiments with different silica surface areas and surface chemistries we attribute this synergistic effect to the ability of the silica aggregates to form hydrogen bonds.

5.1 Introduction

In this project, we focus on the reduction of solid fat in a model food system through the use of colloidal silica aggregates. Fat crystals form networks which structure foods like chocolate and butter, and are therefore vital to the overall mechanical behaviour of the food products. Typically, a reduction in fat leads to a loss of desirable properties such as thickness, texture or increased phase separation. The previous two chapters have shown that it is possible to use fumed silica to create mixed fat-silica systems which have reduced amounts of solid fat whilst also having similar rheological properties.

In the previous chapters we have focused on the at-rest structure of the fat crystal networks within the linear viscoelastic region. However, it is also important to understand how these samples deform under an applied stress and how they recover once the stress is removed. This cycle of breakdown and recovery, known as thixotropy, is central to the consumer experience of certain products. The classic example being toothpaste, which flows out of the tube like a liquid but almost immediately recovers its structure and sits on the bristles without oozing in [107].

In the stress sweep experiments presented in the previous chapters we saw destruction of the microstructure after the linear viscoelastic region, but since the stress was constantly increasing this was difficult to interpret. In the experiments here we apply a constant shear stress during the deformation which is easier to understand. We are looking to see the effect of silica on the amount of deformation and recovery and the strength of the final structure that is obtained. Our overall aim for this work is to understand fat-structured foods and to recreate the behaviour of higher-fat foods with less solid fat and the use of colloidal aggregates. Therefore, this chapter studies the deformation and recovery of systems containing different concentrations of fat and then looks at using different concentrations, surface areas and surface chemistries of silica to try and mimic these behaviours.

In the next section, we explain thixotropy and introduce the three interval thixotropy test. We then give details of our experimental protocol and analysis. In Section 5.3, we begin by presenting results from the thixotropy test for a fat sample at different stress values. We go on to present results for samples with different fat and silica concentrations followed by a comparison of fat samples with and without silica. Finally, we show results for fat samples containing silica with different surface areas and surface chemistries.

Thixotropy

The term ‘thixotropy’ has been widely debated, with Barnes [108] quoting 11 different definitions in his review paper. The definition we shall use is taken from Barnes, Hutton and Walters [109] and defines thixotropy as “a decrease of the apparent viscosity under constant shear stress or shear rate, followed by a gradual recovery when the stress or shear rate is removed”. It is also possible to have an increase in the viscosity under a constant stress, followed by a loss of structure when the stress is removed and this behaviour is termed ‘inverse-thixotropy’ or ‘rheopexy’. In many cases it is beneficial to have an increase in structure under an applied stress as a mechanism for shock-absorption, as is the case with the synovial fluid in our joints, which prevents joint surfaces from coming into contact during impact [110].

Thixotropy is often confused with shear-thinning (also known as pseudo-plasticity) which is defined as “a reduction in viscosity with increasing shear rate” [109]. Whilst most thixotropic materials are also shear thinning, the key difference is that thixotropy is a time-dependent effect and measured by a constant shear stress or shear rate, whereas shear-thinning is defined using an increasing shear stress or shear rate. Furthermore, thixotropy is defined as a completely reversible cycle of structural destruction and recovery, whereas shear-thinning only considers the deformation step. For example, mayonnaise is a shear-thinning and thixotropic material since it will become more liquid like under shaking or stirring, but it will also recover once the deformation stops [16].

Silica dispersions are well-known for being thixotropic under certain conditions and are commercially available for viscosity control, anti-sag and anti-settling behaviour [85]. They are also shear-thinning as shown by Chen et al. who carried out flow curves on both hydrophilic and hydrophobic fumed silicas in mineral oil [111]. Similarly, fat networks are both thixotropic and shear-thinning due to their three-dimensional crystal structure [112, 113].

Traditionally, thixotropy is measured by applying an increasing shear rate followed by a decreasing shear rate and observing a hysteresis loop. Hysteresis is present in thixotropic materials because the deformation and recovery processes occur at different rates; the recovery relies on thermal motion to rebuild the microstructure whereas an applied deformation typically occurs much faster. Moreover, under increasing shear rate the viscosity is decreasing and so flow is easier during deformation, but with a decreasing shear rate the viscosity is gradually increasing

and therefore making structural recovery under Brownian motion more difficult. Although this method is still widely used, especially within industry, it is considered “bad experimentation” [108] and “outdated” [114]. This is primarily because this experiment simultaneously varies shear rate and time, which is not suitable for measuring thixotropic samples which are time-dependent and sensitive to shear rate. Since thixotropy is a time-dependent phenomenon, it is best observed as a function of time under constant shear stress or shear rate values.

Therefore, step tests are preferred as a more direct measurement of both the deformation and recovery of a material. In particular, we shall use the three interval thixotropy test (3ITT) [114], which has already been applied to materials of interest within food research [25, 115]. In this test, the first interval is used to determine the at-rest structure of the material, the second interval is the deformation step and the third interval is the recovery step. The recovery seen in the third interval is compared with the at-rest structure in the first interval to determine the relative amount of recovery. These tests can be done using either rotational or oscillatory rheometry [114]. For our experiments we have chosen to use a combination of both; the first and third intervals are oscillatory and the deformation step is rotational, as shown in Figure 5.1a. We have chosen to use oscillatory stress for the reference and recovery intervals because, if the amplitude is chosen to be within the LVR, the stress should not damage the structure of the sample. Moreover, we can obtain G' and G'' values, which are easily understood within the framework of the previous two chapters. We chose to use a rotational, constant value of stress for the deformation step as it is a better model for real-world deformations like pumping, mixing and spreading. In this interval, as the structure is being deformed and flows under the applied stress we can measure a viscosity (η) value as shown in Figure 5.1b.

5.2 Experimental Methods

5.2.1 Chemicals

Tripalmitin fat ($\geq 85\%$ pure) and soybean oil were purchased from Sigma Aldrich and used without further purification. All fumed silica samples used in this study (A300, A255, 200F, R812 and R816) were provided by Evonik Industries AG.

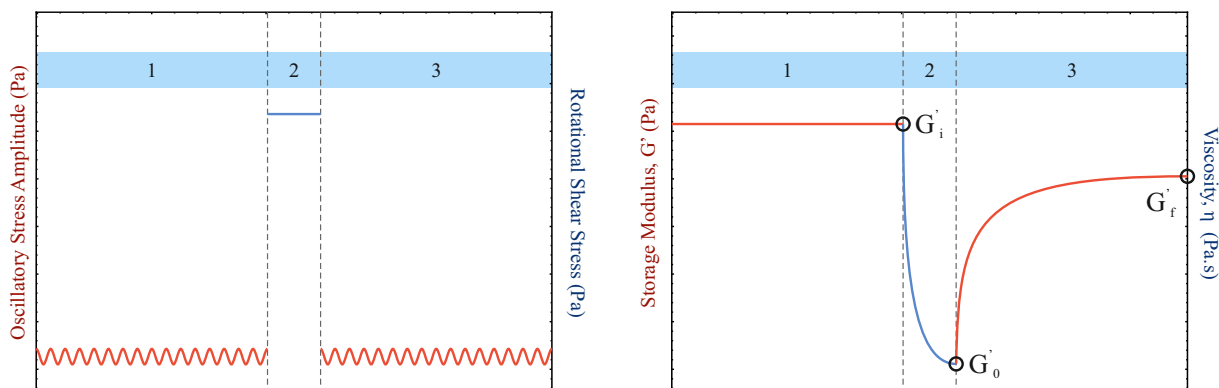


Figure 5.1: a) A schematic diagram of the 3 Interval Thixotropy Test (3ITT) showing both the oscillatory and rotational stresses used, shown in red and blue respectively. b) Example results from the 3ITT with the storage modulus (G') in red and the viscosity (η) in the second interval shown in blue.

5.2.2 Sample Preparation

The sample preparation protocol described in Chapter 3 was used to prepare the samples for the experiments in this chapter.

5.2.3 Rheology

Initially, the sample was melted and approximately 1.5 ml was placed on the rheometer with a gap size of 500 μm . The sample was heated to 100°C and sheared at 50 rad/s for 3 minutes in order to break down any fat crystal or silica structures, which was important for minimizing the effects of sample history. The sample was then allowed to equilibrate for 2 minutes before a 5 minute oscillatory time sweep, which quantified the amount of structure present in the system.

The sample was subsequently cooled down to 10°C at a rate of 10°C/min. During the cooling ramp the plate geometry was stationary in order to avoid shear-induced crystallization. The samples were then heated up to 25°C at a rate of 20°C/min where a second time sweep was conducted for 15 minutes. This time sweep acts as the first interval in our three interval thixotropic test (3ITT). The oscillatory stress amplitude used for the time sweeps was chosen to be within the LVR of the samples; typically between 0.5 and 5 Pa. The frequency was held at 2π rad/s (1 Hz) for all experiments. For the deformation interval, we applied a constant shear stress for 20 seconds and we measured the viscosity as a function of time. For the third interval, exactly the same conditions were used from the first interval, i.e. a 15 minute oscillatory time

sweep. Each experiment was repeated at least three times and we present the arithmetic mean with the error bars corresponding to plus minus one standard deviation.

The data from the three interval thixotropic test was then analysed by comparing the storage modulus, G' values at different points. The final value for G' within the initial interval was termed G'_i and was used as the reference value for the at-rest structure. The initial value for G' in the third interval was termed G'_0 and this was the point of maximum deformation. The final value of G' in the third interval was termed G'_f and gives the point of maximum recovery after the deformation. These are shown schematically in Figure 5.1b. From these values it was possible to calculate the amount of deformation and recovery as follows:

$$\%D = \frac{G'_i - G'_0}{G'_i} \times 100 \quad (5.1)$$

$$\%R = \frac{G'_f - G'_0}{G'_i - G'_0} \times 100 \quad (5.2)$$

5.3 Results & Discussion

5.3.1 Different Stress Values

This section looks at the effect of different stress values during the deformation step of the three interval thixotropic test (3ITT). For these experiments we studied a 5 wt.% fat sample and Figure 5.2a shows the storage modulus (G') values for the intervals 1 and 3, which are before and after the deformation. Figure 5.2b shows the viscosity of the samples during the deformation step. We note that for all deformation stress values, G' remains greater than G'' (G'' is not shown), even at the beginning of the 3rd interval. This indicates the presence of a stress-transmitting network throughout the test and means that the drop in G' at the beginning of the third interval is due to damage but not complete destruction of the fat crystal network.

In Figure 5.2b we observe different initial viscosities for the different stress levels. However, since we are measuring the same sample we expect to see the same initial viscosity values followed by different amounts of structural damage. This suggests that the majority of the damage to

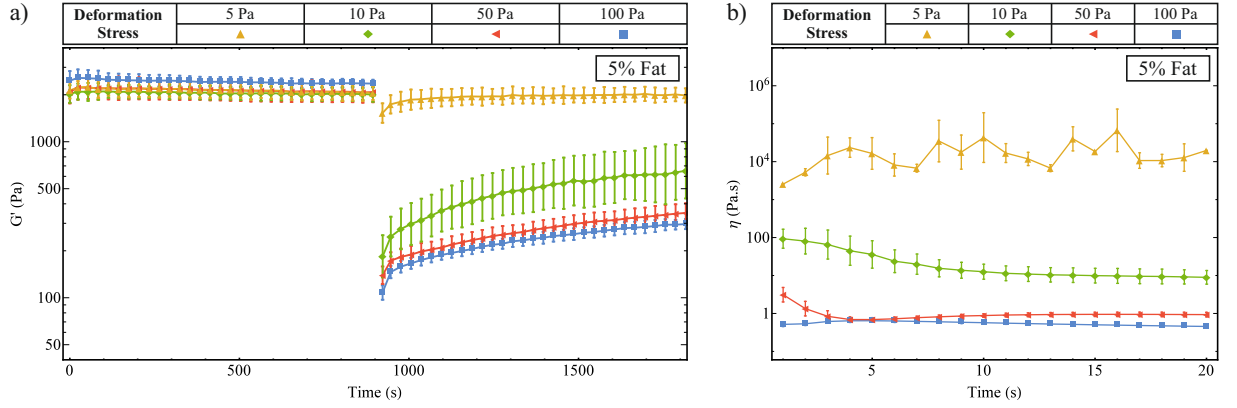


Figure 5.2: 3ITT results for a 5 wt.% fat sample at different deformation shear stress values. a) G' values for intervals 1 and 3 of the 3ITT. b) Viscosity for interval 2 of the 3ITT.

Deformation Stress (Pa)	G'_i (Pa)	G'_0 (Pa)	G'_f (Pa)	%D	%R
5	2053 ± 211	1527 ± 219	1981 ± 206	25.6 ± 15.0	86.4 ± 75.9
10	2009 ± 215	184 ± 57	651 ± 265	90.8 ± 14.7	25.6 ± 15.2
50	2081 ± 311	139 ± 18	350 ± 50	93.3 ± 20.5	10.8 ± 3.3
100	2359 ± 133	108 ± 11	297 ± 22	95.4 ± 7.8	8.4 ± 1.2

Table 5.1: Data showing the effect of deformation shear stress for 5 wt.% fat samples.

the fat crystal network is done in a very short time before the measurements begin in the second interval. Similar results have been seen in the literature where the duration of the deformation step did not significantly influence the destruction or regeneration, since the majority of the deformation caused by shearing occurs very soon after the stress is applied [115]. We noticed a time lag in the recording of measurements between the end of the first interval and the start of the second interval, which is on average 2.3 seconds but at least 1.9 seconds within which this breakdown could occur. For the remainder of the deformation interval there is a balance between breaking more stress-transmitting chains and the formation of new chains. The constant stress level and the strength of the network determine the extent of the damage and whether or not the chains are able to be rebuilt whilst under the applied deformation. These effects lead to either a further decrease in viscosity or a partial recovery of structure shown by an increase in viscosity as a function of time.

In Figure 5.2a we see that as the deformation stress value increases, the drop in G' after the rotational deformation step increases, which is also presented numerically in Table 5.1. In particular, for 10 Pa and above, we see a decrease of more than 90% in G' . This is coupled with a decrease in viscosity during the deformation step as shown in Figure 5.2b, which suggests

the breaking of more stress-transmitting chains under the applied stress after the large initial breakdown. In the case where a deformation stress of 5 Pa was applied we see a small increase in viscosity during the deformation step which is significantly different to the behaviour seen in the other experiments. However, although the viscosity increases, this is linked with a 26% decrease in G' after the deformation. This suggests that the initial damage to the network on going from oscillatory to rotational deformations was larger than 26% but that the deformation stress was low enough to allow for the formation of new stress-transmitting chains during the second interval and therefore an increase in the viscosity. This increase during the deformation stage could be misinterpreted as rheopexy or inverse-thixotropy. However, it is important to consider the large initial breakdown of the structure that occurs between the first and second intervals. Furthermore, for true rheopexy one would also expect to observe a higher G' value at the beginning of the third interval, which is not the case for this system. Nakai et al. also observed complex transient flow behaviour in silica suspensions, but attribute the apparent rheoplectic behaviour to the recovery and reformation of the silica network after the large breakdown of structure in the preshearing step [116].

For each of the deformation stress levels used here, we see the fat crystal networks recovering after the deformation step. At 5 Pa, although the calculated recovery is below 100%, the final G' value is within error of the initial structure, which can therefore be regarded as full structural recovery and so this sample can be considered as thixotropic under these conditions. For the samples exposed to more than 5 Pa, although we see a recovery in G' , they only recover up to 26% of the loss in structure during the 15 minutes after the deformation. Therefore these systems are not thixotropic under these experimental conditions, but at long enough timescales they could potentially make a full recovery. Although recovery on longer timescales is not relevant in the context of consumer experience at the point of consumption, e.g. squeezing ketchup from a bottle, it is still important since products are stored for very long periods of time in the supermarket and in the refrigerator.

5.3.2 Different Fat Concentrations

Here we applied a fixed deformation stress of 50 Pa to samples with different fat concentrations, in the absence of silica and the results can be seen in Figures 5.3a and b. As part of our wider aim for this project of creating low-fat samples with similar properties to higher-fat systems, these

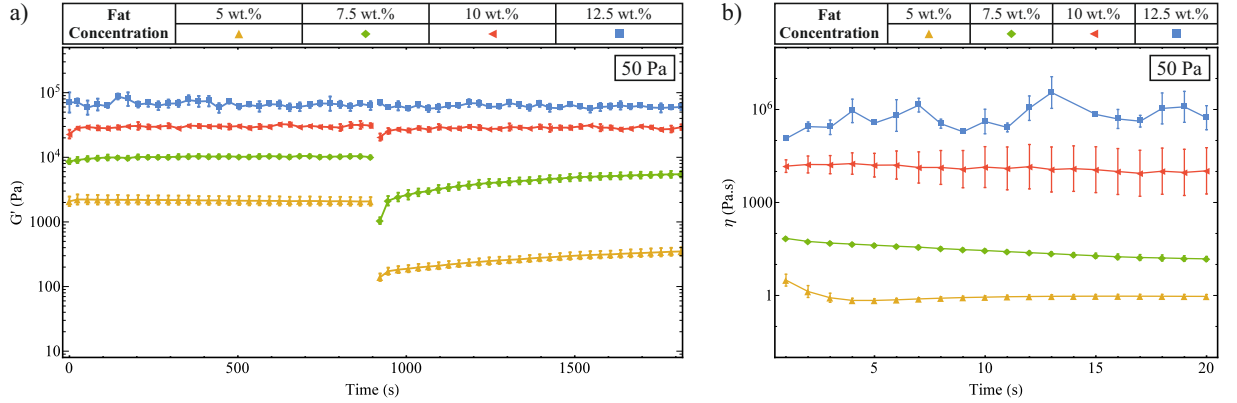


Figure 5.3: 3ITT results for different fat concentrations with a deformation stress of 50 Pa. a) G' values for intervals 1 and 3 of the 3ITT. b) Viscosity for interval 2 of the 3ITT.

Fat Conc. (wt.%)	G'_i (Pa)	G'_0 (Pa)	G'_f (Pa)	%D	%R
5	2081 ± 311	139 ± 18	350 ± 50	93.3 ± 20.5	10.8 ± 3.3
7.5	10074 ± 562	1046 ± 122	5463 ± 587	89.6 ± 7.6	48.9 ± 7.3
10	31087 ± 2440	20567 ± 2526	29237 ± 2840	33.8 ± 11.6	82.4 ± 45.4
12.5	63057 ± 9729	69753 ± 5888	60000 ± 6425	-10.6 ± 18.1	145.6 ± 279.6

Table 5.2: Data showing the effect of fat concentration with a deformation stress of 50 Pa.

experiments help us to understand how these properties, such as recovery after deformation, depend on the fat concentration.

The variation in the magnitude of G' in the first interval shows that stronger networks form at higher concentrations and is consistent with our results in Chapter 3. Therefore we use the relative values of deformation (%D) and recovery (%R) to describe the breakdown and rebuilding of these networks. As in the previous section, we observe that in all cases G' remains larger than G'' (G'' is not shown), so we are only considering structural damage to the fat crystal networks and not full breakdown into individual crystals. In Table 5.2 we see that the percentage deformation decreases with increasing concentration at a fixed deformation stress level. This intuitively makes sense, however it is difficult to know for certain the exact cause of this effect. It may be due to more stress-transmitting chains, stronger chains, more cross-linking, a decreased effective chain length or, more probably, a combination of these effects.

During the deformation step shown in Figure 5.3b, the 12.5 wt.% sample is notably more noisy than the other datasets but we do not measure a significant change in G' after the deformation. This means that this sample is strong enough to withstand the applied 50 Pa stress without significant damage. The 10 wt.% sample is almost constant throughout this interval

but we still measure a 34% deformation which suggests that this damage is done in the first few seconds of the deformation interval. The 5 wt.% and 7.5 wt.% samples show a decrease in viscosity, which means that following the breakdown before the start of the second interval, the networks continue to be broken down further by the applied stress. At lower concentrations there is less chance of finding other fat crystals to bond to and so we see less recovery for samples with lower fat concentrations.

5.3.3 Different Silica Concentrations

In Figures 5.4a and b we show the results of the 3ITT for samples containing 0 wt.% fat with different concentrations of hydrophilic A300 silica with a fixed deformation stress. This data is presented numerically in Table 5.3. From our previous work we know that silica networks are much weaker than fat networks and so a lower deformation stress of 5 Pa was used. Furthermore, at this stress level we were able to observe the full range of rheological responses under the applied deformation. 0 wt.% and 1 wt.% silica samples were liquid-like ($G' < G''$) and showed Newtonian behaviour; a constant viscosity as a function of time. From Chapter 3 we know that 1 wt.% is not enough to form a silica network, although we do see a slightly higher viscosity here, compared to pure soybean oil, due to the presence of the silica.

The 2 wt.% silica sample is solid-like in the first interval ($G' > G''$) but shows a decrease in viscosity under deformation, and at the beginning of the third interval the storage modulus is comparable in magnitude to the loss modulus ($G' \approx G''$), which means that enough of the structure has been damaged to take the network into the critical gel limit. In this limit the network is barely connected and the cleavage of only a few more stress-transmitting chains will result in the network no longer being able to span the gap of the rheometer and a liquid-like response being measured [117].

Interestingly, we do not observe any recovery of structure in the third interval for the 2 wt.% sample. This is surprising, since we observe silica recovery for this concentration at the very beginning of the experiment after the preshear step of rotational shear at 400rpm for 3 minutes. After the preshear step, we measure a G' value of 0.004 Pa at the start of the time sweep before the cooling ramp and this recovers to 11 Pa by the start of the first interval of the 3ITT after roughly 16 minutes and 20 seconds. In contrast, in the deformation step of the 3ITT there is a displacement of only 50 angular degrees over 20 seconds. However, in the third interval

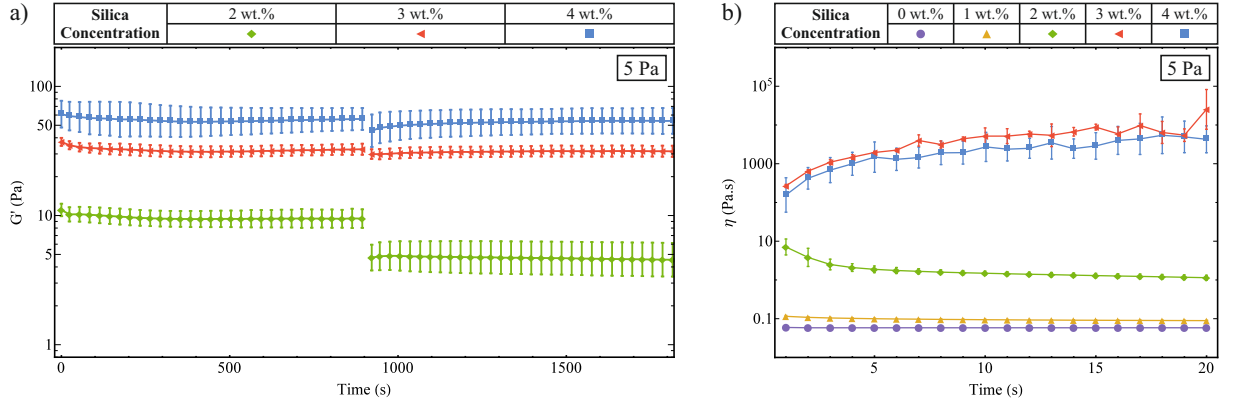


Figure 5.4: 3ITT results for different silica concentrations with a deformation stress of 5 Pa. a) G' values for intervals 1 and 3 of the 3ITT. b) Viscosity for interval 2 of the 3ITT.

Silica Conc. (wt.%)	G'_i (Pa)	G'_0 (Pa)	G'_f (Pa)	%D	%R
2	9.5 ± 1.6	4.7 ± 1.1	4.5 ± 1.4	50.1 ± 22.1	-3.8 ± 37.4
3	32.6 ± 3.2	29.9 ± 2.6	31.4 ± 3.1	8.3 ± 12.7	56.3 ± 172.3
4	55.9 ± 10.9	45.3 ± 13.1	$54. \pm 12.3$	19.0 ± 30.8	$82. \pm 214.9$

Table 5.3: Data showing the effect of silica concentration with a deformation stress of 5 Pa.

of the 3ITT we observe no significant recovery over 14 minutes and 30 seconds. This could be for two reasons, one is that the starting conditions in the two cases are very different and therefore there are different recovery processes. Alternatively, the recovery might be influenced by the cooling and heating steps between the initial time sweep and the first interval of the 3ITT.

Both the 3 wt.% and 4 wt.% samples gave solid-like responses in both oscillatory intervals along with an increase in viscosity during the deformation step. However, we also measure a decrease in G' for both samples at the beginning of the third interval. Therefore we believe that this behaviour is similar to the behaviour of the 5 wt.% sample discussed in Section 5.3.1, where the systems have been broken down but are recovering during the deformation stage. Both samples make a full recovery and therefore they can be considered to be thixotropic under these conditions.

5.3.4 Fixed Stress Value

Here we compare the results for the individual component networks with the mixed fat-silica system in order to observe the effect of silica on the rheological response of the fat crystal networks. In Figures 5.5a-d we show the results of the 3ITT for two different deformation stress

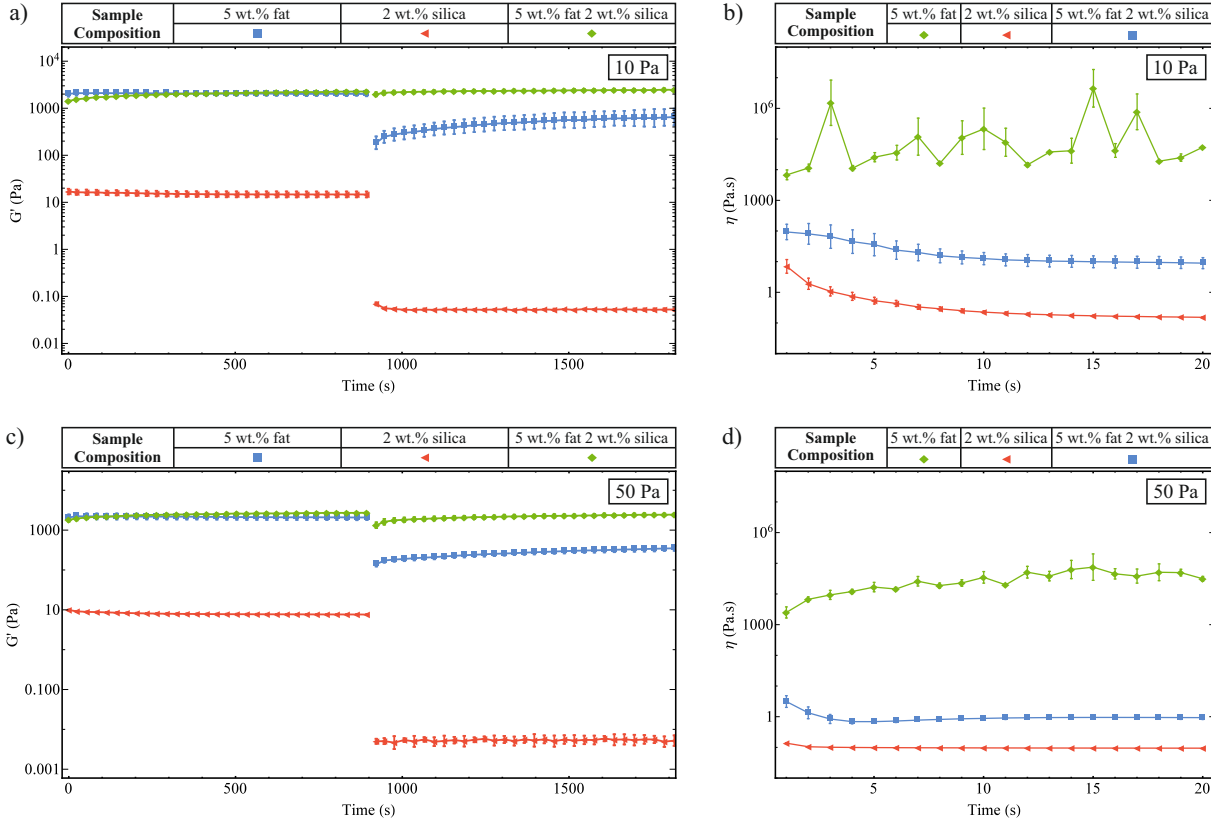


Figure 5.5: 3ITT results for samples with different compositions. a) G' values for intervals 1 and 3 of the 3ITT with a deformation stress of 10 Pa. b) Viscosity for interval 2 of the 3ITT with a deformation stress of 10 Pa. c) G' values for intervals 1 and 3 of the 3ITT with a deformation stress of 50 Pa. d) Viscosity for interval 2 of the 3ITT with a deformation stress of 50 Pa.

levels, 10 Pa and 50 Pa. The corresponding data is shown in Table 5.4.

These results show that the single component networks are deformed by over 90% at both deformation stress levels, but when the fat and silica are present together we see a much stronger network. This is demonstrated by much lower relative deformation values ($\%D$) and suggests a synergistic effect between the fat and the silica. In the silica-only samples we note that in both cases $G' < G''$ in the third interval and we see no recovery with G' over time, whereas the fat-only samples remain solid like after the deformation and show steady, but incomplete recovery. However for the composite, fat-silica system we see that G' remains larger than G'' and we see a full recovery of G' after the deformation.

The key result here is that when the silica is present at 2 wt.% there is no significant impact on the at-rest value of the storage modulus in the first interval, but the samples show less deformation under an applied stress and better recovery once the stress is removed. From Section 5.3.2 we know that both of these are properties of fat networks with higher fat concentrations.

a) Sample Composition	G'_i (Pa)	G'_0 (Pa)	G'_f (Pa)	%D	%R
5 wt.% fat	2009 ± 215	184 ± 57	651 ± 265	90.8 ± 14.7	25.6 ± 15.2
2 wt.% silica	14.7 ± 2.1	0.069 ± 0.005	0.053 ± 0.003	99.5 ± 20.1	$-0.1 \pm <0.1$
5 wt.% fat with 2 wt.% silica	2267 ± 117	1986 ± 200	2454 ± 124	12.4 ± 10.2	166.6 ± 160.8
b) Sample Composition	G'_i (Pa)	G'_0 (Pa)	G'_f (Pa)	%D	%R
5 wt.% fat	2081 ± 311	139 ± 18	350 ± 50	93.3 ± 20.5	10.8 ± 3.3
2 wt.% silica	7.6 ± 0.2	0.005 ± 0.001	0.005 ± 0.002	99.9 ± 3.7	$0.0 \pm <0.1$
5 wt.% fat with 2 wt.% silica	2726 ± 93	1329 ± 221	2447 ± 168	51.2 ± 9.0	80.0 ± 24.1

Table 5.4: Data for samples with different compositions under a deformation stress of a) 10 Pa and b) 50 Pa.

Furthermore this result can be compared to those in Chapter 3 where we saw that 2 wt.% hydrophilic silica did not significantly change the G' values within the LVR, but it did extend the length of the LVR. In the proposed composite gel network model, the silica aggregates form a continuous layer on the surface of the fat crystal chains. During the deformation, some of the fat crystal chains are broken but the presence of silica restricts and reduces the displacement of the fat crystals, making rearrangement and reconnection much easier, thereby reducing the amount of deformation and improving the amount of recovery.

5.3.5 5 wt.% Fat with Different Silica Concentrations

In this section we present the results for samples containing 5 wt.% fat with different concentrations of hydrophilic A300 silica, all with a deformation stress of 50 Pa. In the first interval of the 3ITT, shown in Figure 5.6a, we see a similar variation in G' as seen in Chapter 4, Figure 4.2b, which was explained by the balance of two opposing effects. This is also reflected in the numerical data presented in Table 5.5. Firstly, silica becoming trapped between fat crystals weakens the fat crystal-fat crystal interactions and secondly the silica forming a continuous layer at the surface of the fat crystal chains which increases the overall strength of the network.

We note that for all samples, $G' > G''$ at the beginning of the third interval, which means that the samples remain solid-like for the duration of the test, but are damaged by the deformation step. From the information in the deformation step, shown in Figure 5.6b, we see that there are clearly two different types of behaviour present. Below 2 wt.% silica we measure a

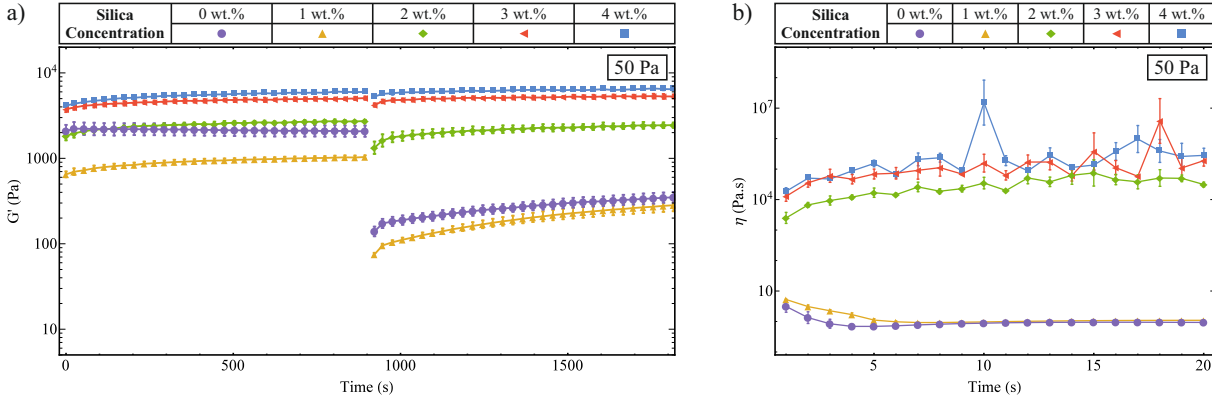


Figure 5.6: 3ITT results for samples containing 5 wt.% fat and different silica concentrations with a deformation stress of 50 Pa. a) G' values for intervals 1 and 3 of the 3ITT. b) Viscosity for interval 2 of the 3ITT.

drop in viscosity during the deformation step, which means that the system is being broken down further after the large initial breakdown discussed in Section 5.3.1, whereas at 2 wt.% and above we see an increase in the viscosity which means that connections between fat crystals are being recovered faster than they are being broken by the deformation.

It is interesting to note that concentrations below 2 wt.% silica are insufficient to form a network in the oil and this might be why we see a marked difference in the behaviour. We also see much lower relative recovery values (% R) for samples containing less than 2 wt.% silica. However, in Chapter 4 Figure 4.2a we saw that, although 1 wt.% was insufficient to form a stress-transmitting network, it had a similar rheological response to the other fat-silica samples, suggesting the same reinforcing mechanism was present. Therefore, the difference in behaviour of the 1 wt.% sample seen here may be due to the fact that the types of deformation being applied are very different in the two cases.

As the silica concentrations increase above 2 wt.% we see a decrease in the amount of deformation (% D) and an increase in the relative recovery (% R) to the point where we measure a recovery of above 100% for the 3 wt.% and 4 wt.% silica samples. This is due, in part, to the fact that these samples had not reached a steady value before the deformation step of the 3ITT. These experiments could be repeated over longer times to minimise this effect, but we chose to fix the duration of the intervals across all samples in this study in order to be able to compare the results directly to the data in the previous two chapters.

Silica Concentration (wt.%)	G'_i (Pa)	G'_0 (Pa)	G'_f (Pa)	%D	%R
0	2081 \pm 311	139 \pm 18	350 \pm 50	93.3 \pm 20.5	10.8 \pm 3.3
1	1036 \pm 45	75 \pm 3	283 \pm 45	92.8 \pm 5.9	21.6 \pm 4.8
2	2726 \pm 93	1329 \pm 221	2447 \pm 168	51.2 \pm 9.0	80.0 \pm 24.1
3	5071 \pm 216	4213 \pm 192	5305 \pm 274	16.9 \pm 5.7	127.3 \pm 58.0
4	5983 \pm 112	5279 \pm 94	6432 \pm 129	11.8 \pm 2.5	163.8 \pm 40.9

Table 5.5: Data for samples containing 5 wt.% fat and different silica concentrations with a deformation stress of 50 Pa.

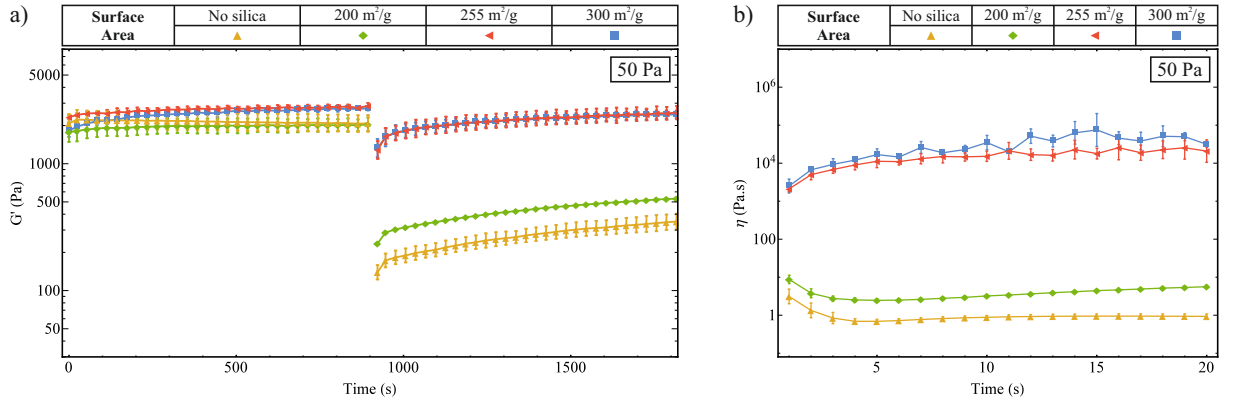


Figure 5.7: 3ITT results for samples containing 5 wt.% fat and 2 wt.% silica with different surface areas and a deformation stress of 50 Pa. a) G' values for intervals 1 and 3 of the 3ITT. b) Viscosity for interval 2 of the 3ITT.

5.3.6 5 wt.% Fat with Different Silica Surface Areas

In Figures 5.7a and b we present the 3ITT results for samples containing 5 wt.% fat and 2 wt.% hydrophilic silica with different surface area values, all with a deformation stress of 50 Pa. We note that G' was larger than G'' for all samples at the beginning of the third interval. In both Figures 5.7a and b we see a change of behaviour going from 200 m²/g to 255 m²/g. For A255 and A300 we see an increase in the viscosity due to structural regeneration after the large initial breakdown as the deformation stress is applied. For these samples we measured smaller deformation values and much higher recovery values, both of which are properties of stronger

Surface Area. (m²/g)	G'_i (Pa)	G'_0 (Pa)	G'_f (Pa)	%D	%R
No silica	2081 \pm 311	139 \pm 18	350 \pm 50	93.3 \pm 20.5	10.8 \pm 3.3
200F	2043 \pm 252	234 \pm 3	531 \pm 7	88.5 \pm 16.5	16.4 \pm 2.3
A255	2855 \pm 150	1284 \pm 207	2526 \pm 301	55.0 \pm 9.4	79.1 \pm 26.6
A300	2726 \pm 93	1329 \pm 221	2447 \pm 168	51.2 \pm 9.0	80.0 \pm 24.1

Table 5.6: Data for samples containing 5 wt.% fat and 2 wt.% silica with different surface areas and a deformation stress of 50 Pa.

network structures.

The behaviour of the 200 m²/g sample is more similar to the sample without silica than to the silica samples with higher surface areas. We see a large drop in the storage modulus along with poor recovery once the deformation stress is removed. Interestingly, we observe a shallow minimum in the viscosity profile followed by a slight increase over time; this behaviour is also seen for the fat-only sample but to a lesser extent. The decrease in viscosity before the minimum suggests that after the large initial breakdown stress transmitting chains continue to be broken. But the minimum and the slight increase then suggest a balance between the rate at which these bonds are being broken and the rate at which they are being reformed, followed by bonds being made more quickly.

The most significant difference for samples with higher surface areas is the increased number of surface silanol groups available for hydrogen bonding. This allows the silica to better rearrange under an applied stress in the dense regions of silica surrounding the fat crystal chains. As the system is deformed and the stress-transmitting chains are broken, the silica can rearrange to remain partially connected and in doing so limit the displacement of the fat crystal clusters and reduce the amount of destruction and the time required for structural recovery.

5.3.7 5 wt.% Fat with Different Silica Surface Chemistries

In this section we present 3ITT data for two pairs of different silica samples, with silica concentrations of 2 wt.% and closely matched surface areas. The first pair is hydrophilic 200F and hydrophobic R816, with surface areas of approximately 200 m²/g. The second pair is hydrophilic A255 and hydrophobic R812, with surface areas of approximately 255 m²/g. From Chapter 4 we know that both of the hydrophobic silicas do not form a gel network in the oil. However we have seen that although they do not extend the length of the linear viscoelastic region to the same extent as the hydrophilic silicas, they are able to support the fat crystal network which results in a slower decline in G' after the LVR.

In Figure 5.8a we see that the presence of hydrophobic R816 silica leads to a much lower G'_i value than the hydrophilic silica, which was also seen in Chapter 4 and might be due to the bulky hexadecylsilyl (-SiC₁₆H₃₃) side chains reducing the packing efficiency of the fat crystals. Nevertheless, despite this difference in the first interval, this pair of silicas shows very similar

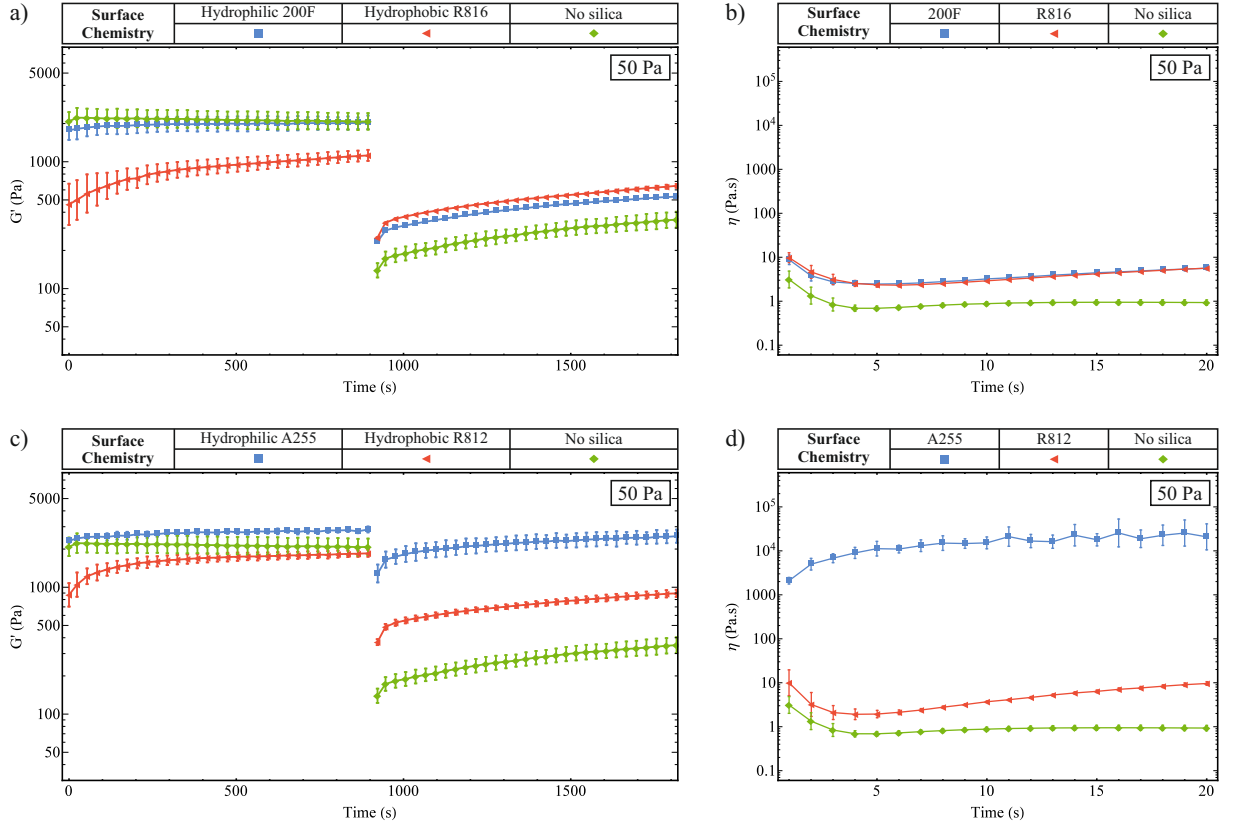


Figure 5.8: 3ITT results for samples containing 5 wt.% fat and 2 wt.% silica with different surface chemistries and a deformation stress of 50 Pa. a) G' values for intervals 1 and 3 of the 3ITT for 200F and R816. b) Viscosity for interval 2 of the 3ITT for 200F and R816. c) G' values for intervals 1 and 3 of the 3ITT for A255 and R812. d) Viscosity for interval 2 of the 3ITT for A255 and R812.

behaviour in the second and third intervals. This suggests that the responses being measured are predominantly from the fat clusters rather than the silica. This makes sense since both R816 and 200F have a reduced number of silanol groups compared to the hydrophilic A300 silica which was used for the majority of our experiments.

On comparison of Figures 5.8a and c, we observe that the R812 sample has a higher G'_i value than the R816 sample. This can be clearly seen in the numerical data shown in Table 5.7. The trimethylsilyl ($-\text{Si}(\text{Me})_3$) group used to modify R812 is much smaller than the one used for R816, which leads to less disruption of the packing of fat crystals. In the previous section we saw that A255 has very different behaviour to the 200F which could be attributed to the higher number of surface silanol groups available for hydrogen bonding. This explains the reduced deformation and improved recovery in Figure 5.8c along with the increase in viscosity in Figure 5.8d. For the sample containing R812 we see very similar behaviour to the 200F and R816, since there is a reduced number of hydrogen bonds available to support the fat crystal

Silica Surface Chemistry	G'_i (Pa)	G'_0 (Pa)	G'_f (Pa)	% D	% R
a) Hydrophilic 200F	2043 ± 252	234 ± 3	531 ± 7	88.5 ± 16.5	16.4 ± 2.3
Hydrophobic R816	1122 ± 112	252 ± 2	646 ± 22	77.6 ± 12.6	45.3 ± 6.4
b) Hydrophilic A255	2855 ± 150	1284 ± 207	2526 ± 301	55.0 ± 9.4	79.1 ± 26.6
Hydrophobic R812	1851 ± 115	369 ± 20	895 ± 59	80.0 ± 8.0	35.5 ± 5.0
No silica	2081 ± 311	139 ± 18	350 ± 50	93.3 ± 20.5	10.8 ± 3.3

Table 5.7: Data for samples containing 5 wt.% fat and 2 wt.% silica with different surface chemistries and a deformation stress of 50 Pa. Silicas with a surface area of a) 200 m²/g. b) 255 m²/g.

network. Notably, Figure 5.8c encapsulates the general idea that the hydrophobic silica is still able to support the fat crystal networks, but not as effectively as the hydrophilic silicas, above a certain surface area.

5.4 Conclusions

In this chapter we have used the three interval thixotropy test (3ITT) to investigate various different aspects of both the fat and the silica components in our model system. We observed that, in general, stronger networks were able to better withstand the applied stress and showed less deformation and better recovery. At high enough concentrations both the fat (>10 wt.%) and hydrophilic A300 silica networks (>2 wt.%) were thixotropic, making a full recovery after the deformation step. At 2 wt.% A300 silica was not thixotropic and did not show any recovery after the applied stress was removed, however it was able to improve the fat crystal network significantly via a synergistic effect, leading to smaller deformations and improved recovery. These are both properties of higher-fat concentration samples and therefore this is a significant result in the pursuit of mimicking higher fat systems.

When A300 silica was present at concentrations above 2 wt.% with 5 wt.% fat we saw that the samples were able to fully recover after the deformation and continue on to even higher G' values than those reached in the first interval, indicating that much stronger networks were formed. At different surface areas we observed a similar trend as in Chapter 4 Section 4.3.2, where higher silica surface areas lead to a slower rate of decline in G' after the LVR. Here we saw less deformation and more recovery with higher silica surface areas and we interpret these results in terms of a greater number of silanol groups available for hydrogen bonding. Likewise,

we describe the 3ITT results for different surface chemistries in terms of hydrogen bonding and we saw that, although hydrophobic silicas do not reinforce the fat crystal networks to the same extent as the hydrophilic silicas, they do still have a marked effect.

Due to experimental limitations we were not able to detect the initial breakdown of the networks, but we do see evidence of this large early breakdown. Therefore, although certain samples showed an increase in viscosity during the deformation step we believe this to be recovery rather than rheopexy.

Acknowledgments

We thank Arandeep Uppal for many useful discussions.

Chapter 6

Observing and Analysing Fat Crystal Networks

ABSTRACT

In this chapter we use polarized light microscopy and fluorescent confocal scanning laser microscopy to obtain a more direct insight into the effect of silica aggregates, and the gel networks they form, on the fat crystal microstructure. We focus on the effects of different fat concentrations, cooling rates, silica concentrations and silica surface chemistries. We capture images during the crystallization process and use these to obtain crystallization temperatures which are in good agreement with values measured via differential scanning calorimetry. We use various image analysis techniques to quantify the structure of the fat crystal networks after crystallization. We observe no significant difference in the fat microstructure, with silica present at low concentrations, as measured by the number and size of individual crystals and the structure factors obtained via discrete Fourier transforms. We also calculate two-dimensional fractal dimensions and discuss these values with regard to the fractal dimensions obtained by rheology. We use confocal scanning laser microscopy to create a three-dimensional reconstruction of the fat crystal networks. This data suggests a jammed structure of discrete fat crystals at low concentrations (≤ 10 wt.%).

6.1 Introduction

Foods such as butter and chocolate can be modelled by a fat crystal network in a continuous oil phase. The fat crystal network creates a rigid microstructure which dictates the macroscopic rheological properties, like the spreadability of butter or the snap of a chocolate bar. Food manufacturers are striving to make lower-fat, healthier food products, however a reduction in fat often results in a loss of these desirable mechanical properties. Our approach to this problem is to add food-grade colloidal silica aggregates. The previous results have shown that we are able to reduce the solid fat content whilst maintaining some rheological properties through the formation of a composite gel network between the fat crystals and the silica.

So far in this work we have relied on rheology and DSC to infer the composite gel network structure in our model system. In this chapter, we use polarized light microscopy (PLM) as a more direct tool for understanding the complex microstructure. We study four aspects of the fat crystallization process with PLM: fat concentration, cooling rate, silica concentration and silica surface chemistry.

We present time series experiments where we capture images to track crystal growth at regular time intervals during the crystallization process. From this data we are able to extract crystallization temperatures which are comparable to the DSC results. We then use various image analysis methods to study the final microstructure of the fat crystal networks. The first approach is counting and measuring the size of the individual fat crystals. The next approach uses two-dimensional discrete Fourier transforms to identify a typical lengthscale in the network structures. Finally, we calculate two-dimensional fractal dimensions using a particle counting method and compare these values to those obtained via rheology in Chapter 3. We use confocal scanning laser microscopy (CSLM) here to study the size, shape and morphology of the fat crystals. CSLM allows us to image thin slices at successive depths through our model system and we recombine these to form a three-dimensional representation of the fat crystal network.

In the next section we outline the experimental methods along with each of the image analysis procedures used. We then present the results of the time series experiments followed by a comparison of the data with DSC results. We then review the results of the different image analysis techniques on the final microstructure. At the end of this chapter we show a three-dimensional reconstruction of the model system and discuss the current limitations of fluorescent

confocal microscopy and the related image analysis for fat crystal networks.

6.2 Experimental Methods

6.2.1 Sample Preparation

The sample preparation protocol described in Chapter 3 was used to prepare the samples for the experiments in this chapter.

6.2.2 Differential Scanning Calorimetry

The data in this chapter was collected on a power compensated Perkin Elmer DSC 8000 following the protocol described in Chapter 3. The DSC was calibrated with an indium sample at 2°C/min, 5°C/min and 10°C/min. Samples were reused for successive experiments, and between experiments they were melted at 100°C for 3 minutes to destroy all crystal memory.

6.2.3 Polarized Light Microscopy

The melted sample was sheared at 9600 rpm with an Ultra Turrax mixer for 5 minutes, then 7.5 μl was pipetted directly onto a glass slide on a Linkam PE120 peltier stage at 100°C. The sample was covered with a second glass slide, which had also been heated on the peltier stage. The sample was held at 100°C for 4 minutes before being cooled down to 10°C. For the time series experiments we started recording images at the start of this cooling ramp. The images are 1280 x 1024 pixels where 1 pixel is equivalent to 0.652 μm . The silica aggregates are not birefringent which means that they can not be seen in the PLM images. Therefore, we can only comment on the fat crystal networks and any apparent change in the presence of silica. All experiments were repeated three times.

6.2.4 Confocal Scanning Laser Microscopy

A few grains of solid Nile red fluorescent dye were added to a melted sample of 10 wt.% fat in soybean oil with 4 wt.% hydrophobic R812 silica. Then approximately 0.5 ml of the resulting

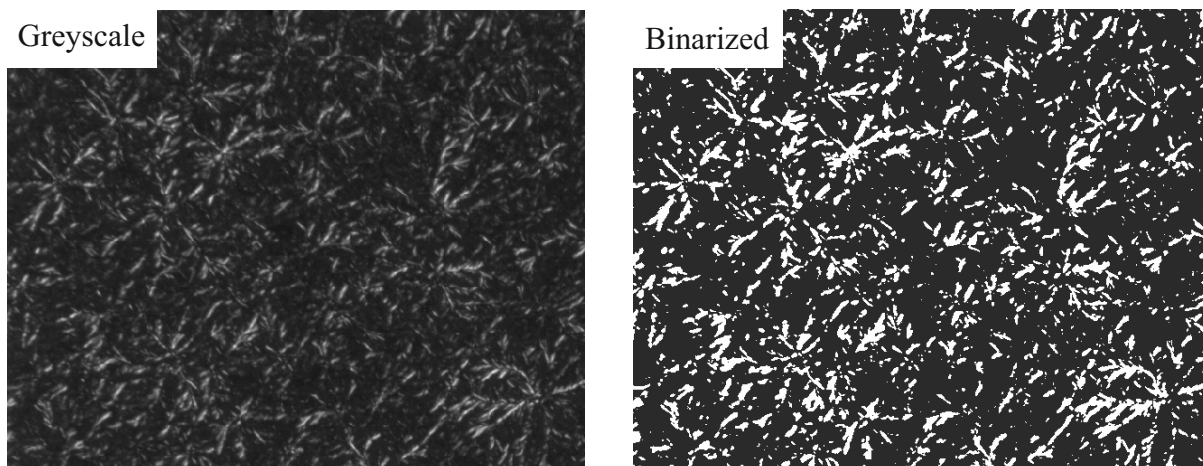


Figure 6.1: A comparison between a greyscale image and the corresponding binarized image for a 25 wt.% fat sample cooled at 10°C/min.

mixture was pipetted into a bespoke sample holder, made from a small glass vial with the bottom removed, glued onto a glass coverslip. The sample was held at 100°C for 10 minutes before being cooled at 10°C/min down to 10°C. The temperature was then raised to 25°C at 20°C/min before the images were captured at successive depths through the sample. We used a 532 nm laser with a HFT 543 dichroic beam splitter and a LP560 long pass filter.

6.2.5 Image Analysis

Binarization

Binarization is the process of converting a greyscale image into a black and white image. This is done by finding a suitable threshold value, above which all pixels are set to white and below which all pixels are set to black. The PLM images show the birefringent fat crystals as bright features on a dark background and so an optimal threshold value would set all of the crystal features as white on a black background. However, Figure 6.1 demonstrates that finding the optimal threshold value is not a trivial task. We use the Binarize function in Wolfram Mathematica to apply the well-established Otsu cluster variance maximization method [118] to systematically find threshold values for our images. For the time series experiments, a threshold value was found for the final image and it was used to binarize all of the images in the series. This was important in order to keep the intensity of the background constant throughout the series.

Feature Detection

In the binary images we count the total number of white pixels, which can be converted to give the total fat crystal cross-sectional area via a scale factor. By calculating the fat crystal area for each image in the time series experiments we are able to track the overall crystal growth as a function of time during the cooling process. We are also able to determine the number of fat crystals by counting the distinct white regions in the binary images. This meant we were able to determine the total crystal area along with individual crystal sizes. This analysis was done using the `ComponentMeasurements` function in Wolfram Mathematica, which counts and measures the size of these regions.

Fourier Transformation

To obtain a typical lengthscale, L , in the greyscale images we calculated the squared magnitude of the two dimensional discrete Fourier transform. This was then radially averaged to obtain the structure factor, $I(k)$, where I is the intensity of the image and k is the wavevector. The typical lengthscale in the system is given by $L = 2\pi/k_{max}$, where k_{max} is the wavevector at the point of maximum intensity. In order to improve the statistics, each image was partitioned into twenty 255×255 pixel tiles before the analysis; a lengthscale larger than the approximate fat crystal lengthscale.

Fractal Dimension

There has been a considerable amount of research into the extraction of fractal dimensions from PLM images [93, 119, 120]. However, this process has several notable challenges; the most significant being that the microscopy images are two-dimensional representations of a three-dimensional network. This is made more difficult by the need to binarize the images before they can be analysed, since crystal clusters that are out of the focal plane appear smaller. Therefore, traditional fractal dimension approaches, such as the Hausdorff or box-counting methods are not suitable since they would consider the crystal cluster size.

Most studies on fat crystal networks employ a particle counting method, which is described in detail by Marangoni [54]. The fractal dimension obtained gives a measure of order and the

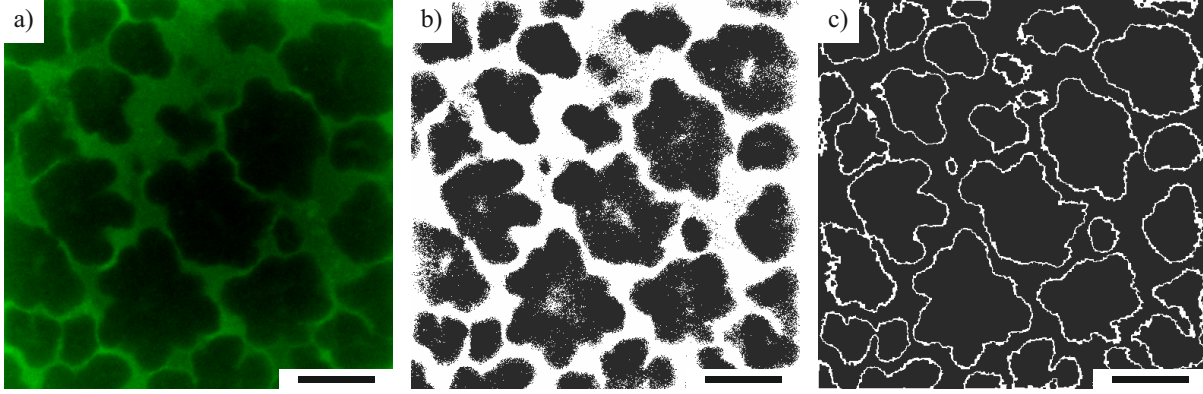


Figure 6.2: The different stages of image analysis for a confocal scanning laser microscopy image. a) The raw image. b) The corresponding image which has been binarized using the local adaptive binarization method. c) The outlines of the crystals. The scale bar represents 20 μm .

distribution of mass in a system. The number of particles (N_p) in a region of interest of size (R^2) is given by $N_p \sim R^{D_f}$, where D_f is the fractal dimension. Assuming that the typical crystal size is much smaller than the region of interest, this method is not affected by the crystal size. Starting with the full image and then reducing the area in 5% increments, the number of particles are counted for each region of interest. Regions below 30% of the original image are discarded since the number of particles in very small regions drops significantly and can lead to large changes in the fractal dimension. In order to minimise edge effects the average of two different fractal dimensions are taken; one which includes particles that are in contact with the edge of the region of interest, and one which excludes these particles. This method assumes all of the crystal clusters are represented in the final images and therefore it is only suitable for very thin samples.

CSLM Image Analysis

In Figure 6.2a we present a raw CSLM image of the fluorescent system, where the oil is shown in green and the fat crystals are shown as dark regions. The raw images are binarized using a local adaptive binarization algorithm, which determines the threshold value locally for each pixel. This algorithm is built in to Wolfram Mathematica and gives improved results for images that have a non-uniform background intensity. The result of this binarization is shown in Figure 6.2b. At this point, any features below 10 pixels are removed as they are considered to be noise. Next, we find the perimeter of the crystals using the in-built `MorphologicalPerimeter` function. Then we apply a dilation of 1 pixel followed by an erosion of 1 pixel, in order to ensure that the

perimeters are closed loops. Our approach is similar to that used by Singh et al. [121] and the final result is shown in Figure 6.2c.

6.3 Results & Discussion

6.3.1 Time Series Experiments

This section looks at the total crystal cross-sectional area as a function of time measured by sets of polarized light microscopy (PLM) images. We use this technique to look at four different aspects of the fat crystallization process: fat concentration, cooling rate, silica concentration and silica surface chemistry. Figure 6.3a shows the results for samples with different fat concentrations and a cooling rate of $10^{\circ}\text{C}/\text{min}$, where the error bands correspond to plus and minus one standard deviation. We observe that samples with higher fat concentrations crystallize earlier, which corresponds to a higher temperature. This is due to the increased amount of supercooling at higher concentrations which drives earlier crystallization and is consistent with our previous DSC results.

Figure 6.3b shows the crystal area curves for 10 wt.% fat samples at different cooling rates. We observe that crystallization occurs at very different times in this plot but the crystallization temperatures show a much smaller variation; 23.46°C , 21.62°C , 21.10°C and 20.43°C for the $2.5^{\circ}\text{C}/\text{min}$, $5^{\circ}\text{C}/\text{min}$, $7.5^{\circ}\text{C}/\text{min}$ and $10^{\circ}\text{C}/\text{min}$ cooling rates respectively. At higher cooling rates a slightly larger amount of supercooling is achieved before crystallization occurs, which means the sample reaches a lower temperature before it crystallizes.

In Figure 6.3c we present the results for 10 wt.% fat samples containing different amounts of hydrophilic A300 silica, which were crystallized at $10^{\circ}\text{C}/\text{min}$. We do not see any significant difference for the samples containing 0 wt.%, 2 wt.% and 4 wt.% silica; all of the crystal growth curves overlap within error and we measure crystallization temperatures of 20.43°C , 20.56°C and 20.50°C respectively. However, we do observe a distinct change in the growth curve for the sample containing 7 wt.% silica along with a small shift up to 21.93°C in the crystallization temperature. We observed similar behaviour in the DSC results shown in Chapter 3 Figure 3.5a and believe that this is due to an excluded volume effect caused by the silica which raises the effective concentration of the fat.

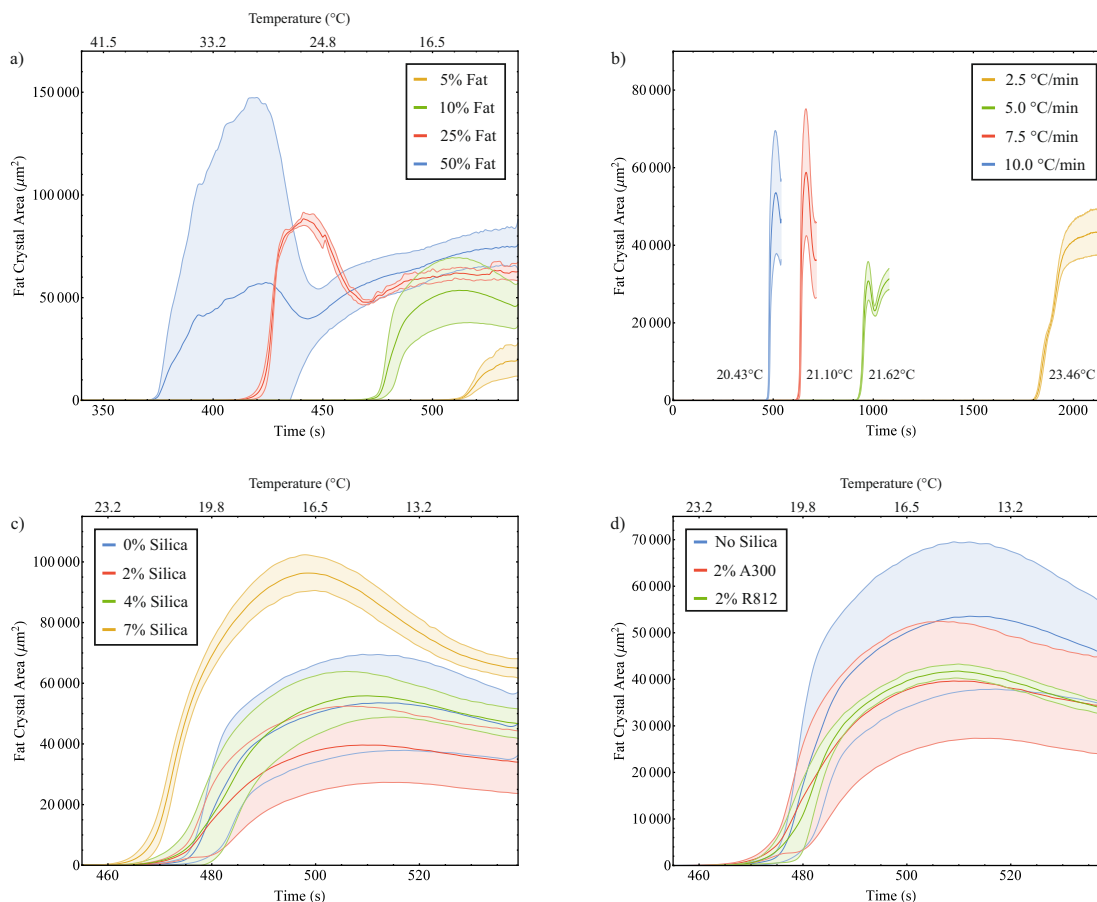


Figure 6.3: Total fat crystal area as a function of time for a) Different fat concentrations cooled at 10°C/min. b) 10 wt.% fat samples crystallized at different cooling rates. c) 10 wt.% fat samples with different concentrations of hydrophilic A300 silica cooled at 10°C/min. d) 10 wt.% fat samples containing 2 wt.% of different silica types cooled at 10°C/min.

Figure 6.3d compares the crystal area curves for 10 wt.% fat samples containing different silica types present at 2 wt.%, cooled at 10°C/min. In this experiment we use hydrophilic A300 and hydrophobic R812 silica, which is made via the chemical treatment of A300 with hexamethyldisilazane (HMDS). We do not observe any significant difference in the crystallization temperature or the crystal growth as a function of time. This is consistent with the DSC data presented in Chapter 4 and suggests that, at this concentration, the silica is neither acting as a seed nor affecting the way in which the fat crystals grow and form a network.

The majority of the crystal area curves have a characteristic shape; a sharp initial increase which reaches a maximum followed by a subsequent decrease in the measured fat crystal area. We present an example of this in Figure 6.4a along with the original greyscale and corresponding binarized images for times $t = 442$ s, $t = 470$ s and $t = 498$ s. We see that although there is a variation in intensity, there is no clear change in the overall crystal network morphology. We

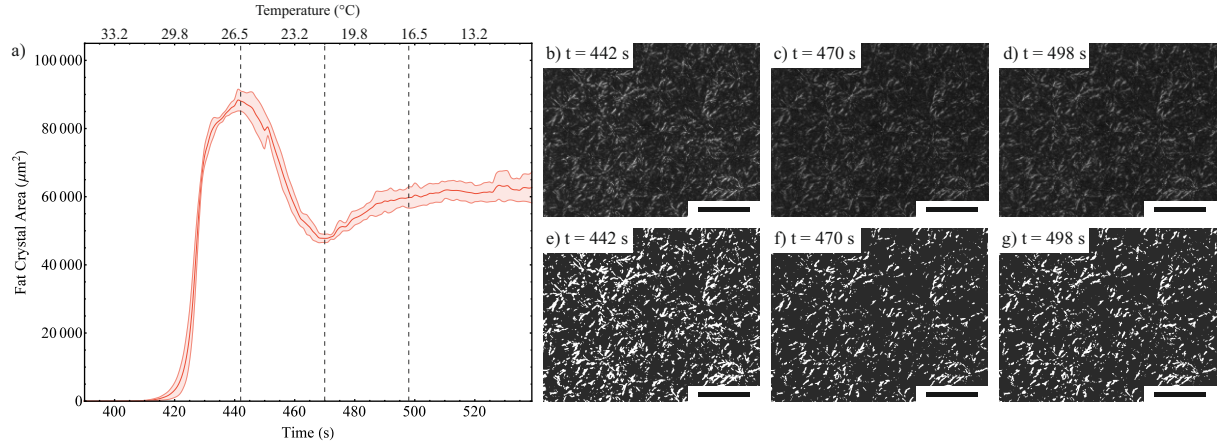


Figure 6.4: a) Fat crystal area data for the 25 wt.% fat sample crystallized at $10^{\circ}\text{C}/\text{min}$. The vertical dashed lines are plotted at 442 s, 470 s and 498 s after the beginning of the cooling ramp. b-d) Greyscale images at different points during the cooling process. e-g) Binarized images corresponding to the greyscale images above. The scale bar represents $100\text{ }\mu\text{m}$.

note that we also see this shape when analysing the greyscale images and therefore this is not a result of the binarization process.

This behaviour has been observed in similar experiments [64] and is thought to be caused by stepwise crystallization. Kellens et al. [122] have shown that, under certain conditions, transition between polymorphs can occur with almost no change in the microstructure. We believe that this effect is due to a combination of Ostwald ripening [123] and stepwise crystallization at higher fat concentrations ($>10\text{ wt.}\%$). However, since this data is difficult to interpret, we choose to focus only on the very beginning of these curves in the following section, which corresponds to the point at which the fat crystals become large enough to be detected.

6.3.2 Measuring Crystallization with Polarized Light Microscopy

In this section we use the crystal area curves to extract crystallization temperatures and compare them to values obtained by differential scanning calorimetry (DSC). Figure 6.5 shows the start of the crystal area curve, plotted (in red) as a function of temperature, for a $5\text{ wt.}\%$ fat sample cooled at $10^{\circ}\text{C}/\text{min}$. On the same axis we plot the corresponding DSC data in blue. The vertical dashed lines indicate the crystallization onset temperatures for the two techniques along with the crystallization peak temperature measured by DSC. The values for these temperatures are presented in Table 6.1. The onset temperatures are determined by finding the intersection between the baseline and the tangent to the data curve at the point of greatest slope.

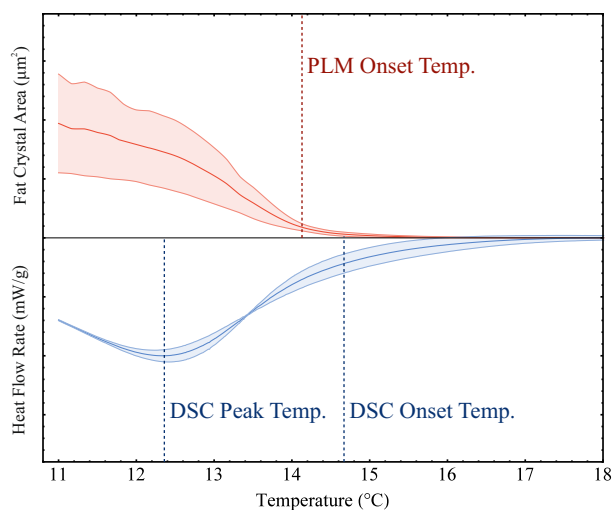


Table 6.1: The crystallization values for a 5 wt.% sample crystallized at 10°C/min measured by PLM and DSC.

	Mean (°C)	Error (°C)
PLM Onset Temp	14.13	0.31
DSC Onset Temp	14.67	0.38
DSC Peak Temp	12.36	0.10

Figure 6.5: A comparison between PLM (red) and DSC (blue) data for a 5 wt.% sample crystallized at 10°C/min. The curves have been normalised in order to aid comparison.

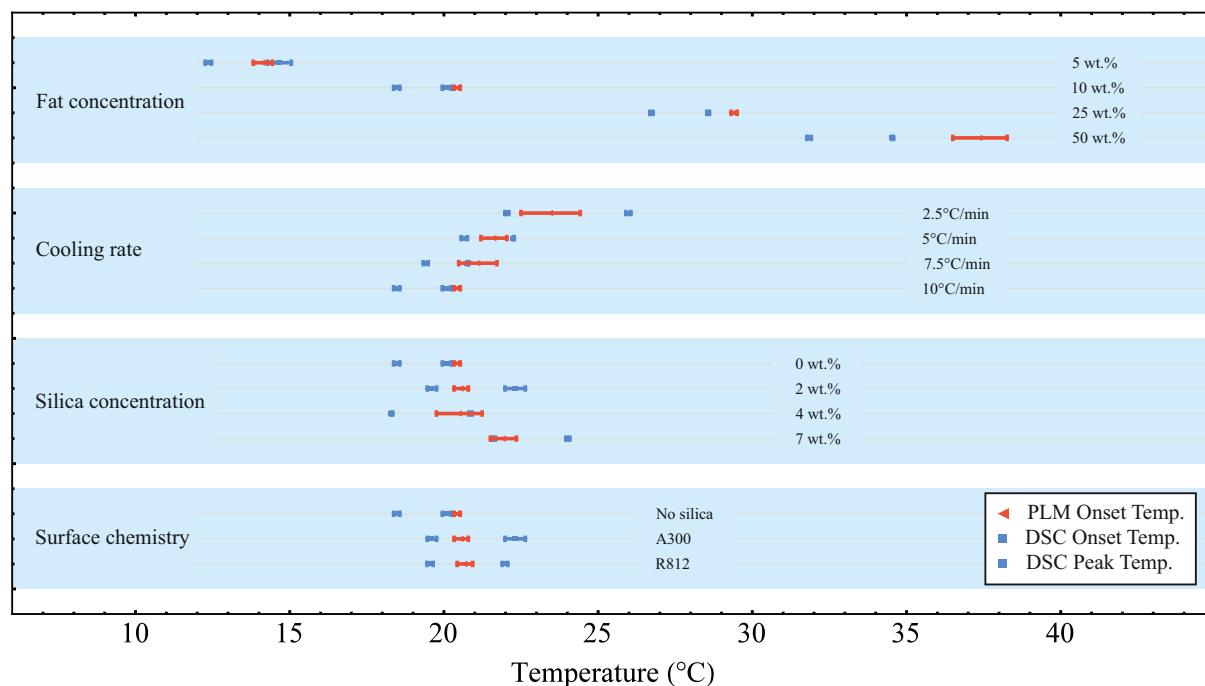


Figure 6.6: A plot showing the crystallization temperatures as measured by PLM (red) and DSC (blue) for four different aspects of fat crystallization: fat concentration, cooling rate, hydrophilic A300 silica concentration and silica surface chemistry.

The fat crystallization process begins on the molecular scale and therefore with PLM we are limited to the detection of early growth events as opposed to true nucleation events. However, we see in Figure 6.5 that there is only a small difference between the onset temperatures measured by PLM and DSC, which is a more sensitive technique. To further illustrate the agreement between the values obtained from the different techniques, we ran the same analysis on all of the crystal area curves shown in Figure 6.3 and show them in Figure 6.6 alongside the corresponding DSC values. This figure shows that PLM was able to detect the fat crystallization between the onset temperature and the peak temperature of the DSC, in almost all cases. Although, we do notice that in some cases, particularly at higher fat concentrations, the PLM data shows earlier crystallization. However, we believe that this is due to confinement effects in the microscope samples since it has been observed that crystallization can occur at higher temperatures in thinner samples. [122].

These results highlight the advantage and suitability of using both techniques to study this system. PLM offers a qualitative insight into the manner of fat crystal growth but the crystal growth curves can be difficult to interpret. DSC, on the other hand, offers a more quantitative and sensitive measure of the crystallization process but gives little information about the way the crystals grow.

6.3.3 Polarized Light Microscopy Image Analysis

In this section we present and analyse the final images from the time series experiments discussed in the previous sections. These images show the final microstructure of the fat crystal networks at the end of the cooling ramp at 10°C. Figure 6.7a shows the binarized images for samples with different fat concentrations and a cooling rate of 10°C/min. All of the corresponding greyscale images are given in the appendix. Across the range of concentrations studied we see a large change in microstructure. At low concentrations (≤ 10 wt.%) we observe small, discrete crystals which appear as distinct white regions. At concentrations above 10 wt.% we no longer see discrete crystals but networks that span the entire image.

In Figure 6.8a we present a histogram of individual crystal sizes for the low fat concentration samples, where the bin size has been set to 1 μm^2 . The data shown in these histograms is the average of data taken from three repeat experiments and the error bars correspond to plus and minus one standard deviation. At 10 wt.% fat we measure an overall increase in the number of

crystals as well as a greater number of larger crystals compared with the 5 wt.% fat sample. For higher concentrations (≥ 10 wt.%), it is not possible to count the individual crystal areas since dense, continuous networks form rather than discrete particles.

We note that for samples with low fat concentrations (≤ 10 wt.%) crystallized at $10^\circ\text{C}/\text{min}$ we measured gel networks ($G' > G''$) via rheology in Chapter 3, but we observe discrete crystals here. Comparison of the binary images with the greyscale images shows that binarization can artificially segment crystals or chains, potentially overestimating the presence of discrete particles. Nevertheless, the rheology data presented in Chapter 3 Figure 3.3a shows that higher fat concentrations create stronger networks, which is measured by a larger storage modulus within the linear viscoelastic region. The images shown here in Figure 6.7a suggest that this result may be due to both a larger number of fat crystals and an increase in crystal size.

In Figure 6.7b we show the images for 10 wt.% fat samples which have been crystallized at different cooling rates. We see that at higher cooling rates there is an increase in the number of crystals and a decrease in the typical crystal size. At higher cooling rates the samples are able to reach lower temperatures before they crystallize. At lower temperatures, there is a larger amount of supercooling which decreases the size of the energy barrier for crystallization and this leads to a greater number of nucleation sites [64, 124]. This result is reflected in Figure 6.8b which shows an increase in the number of smaller crystals at higher cooling rates.

Figure 6.7c compares samples with different concentrations of hydrophilic A300 silica and Figure 6.8c shows the corresponding histogram for the individual crystal sizes. It is difficult to identify a trend on inspection of these images and we also do not see a silica concentration dependence in the histogram, where the results all coincide within experimental error. Figure 6.7d shows samples containing 2 wt.% hydrophilic A300 silica with 2 wt.% hydrophobic R812 silica and similarly we find it difficult to extract any obvious changes with the silica surface chemistry. We do measure a slight drop in the number of small crystals when silica is present, however this result is within experiment error and so it is difficult to make any conclusions here. From this data it is also difficult to differentiate between the hydrophilic and hydrophobic silicas.

It is important to mention that binarization leads to a loss of information and can split individual crystals into multiple, smaller regions. This can be seen in Figures 6.1 and 6.7, and could explain the high number of very small crystals. Therefore, although binarization is a necessary process in order to be able to count and measure individual crystals, we note that

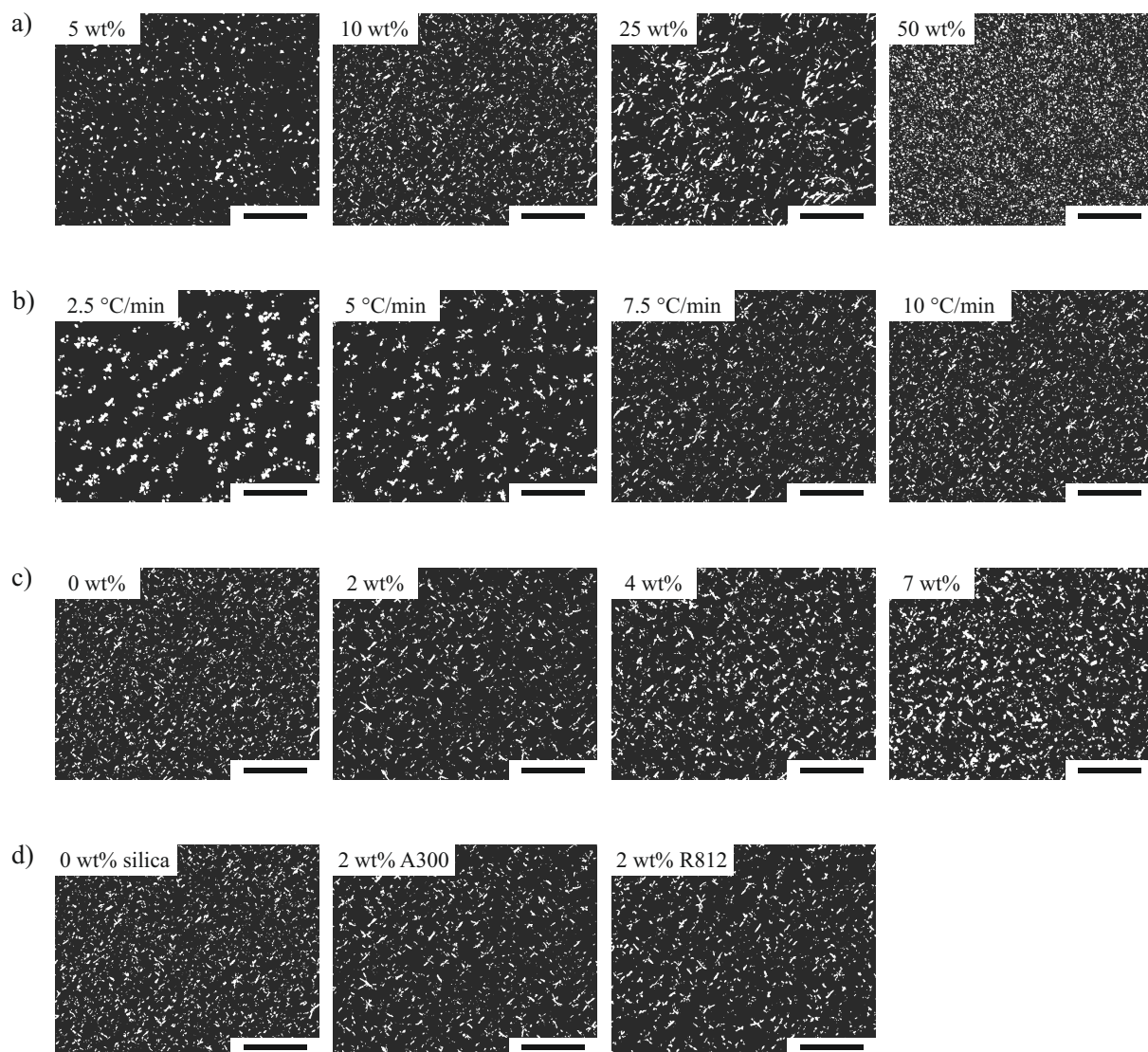


Figure 6.7: Binarized images for a) Samples with different fat concentrations crystallized at $10^\circ\text{C}/\text{min}$. b) 10 wt.% fat samples crystallized at different cooling rates. c) 10 wt.% fat samples containing different amounts of hydrophilic A300 silica, crystallized at $10^\circ\text{C}/\text{min}$. d) 10 wt.% fat samples containing different types of silica, crystallized at $10^\circ\text{C}/\text{min}$. The images are taken at the end of the cooling ramp and the scale bars represent 100 μm .

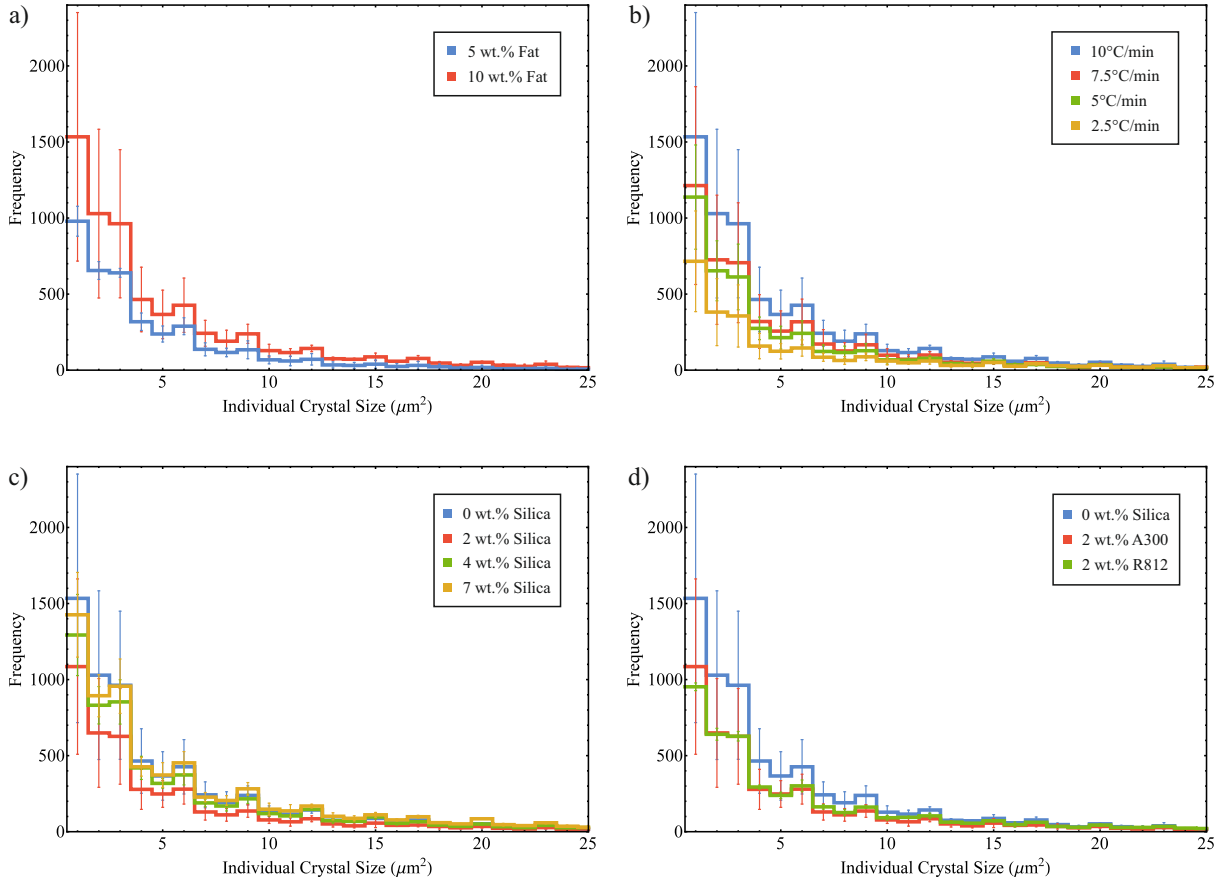


Figure 6.8: Histograms of individual crystal sizes for a) Samples with different fat concentrations crystallized at $10^\circ\text{C}/\text{min}$. b) 10 wt.% fat samples crystallized at different cooling rates. c) 10 wt.% fat samples containing different amounts of hydrophilic A300 silica, crystallized at $10^\circ\text{C}/\text{min}$. d) 10 wt.% fat samples containing different types of silica, crystallized at $10^\circ\text{C}/\text{min}$. The data is taken from images at the end of the cooling ramp and the bin size has been set to $1 \mu\text{m}^2$.

it introduces a significant error in these measurements. In the following sections we use two different quantitative techniques in a further attempt to extract information from these images.

Fourier Transform

We use two-dimensional discrete Fourier transforms in order to identify typical lengthscales in the greyscale versions of the final time series images, which are presented in the appendix. The structure factor data from this analysis is shown in Figure 6.9 and the inset plots offer a closer look at the region for small k values.

Figure 6.9a shows the structure factors for samples with different fat concentrations crystallized at $10^\circ\text{C}/\text{min}$. We observe a small amount of structure for the 5 wt.% and 10 wt.%

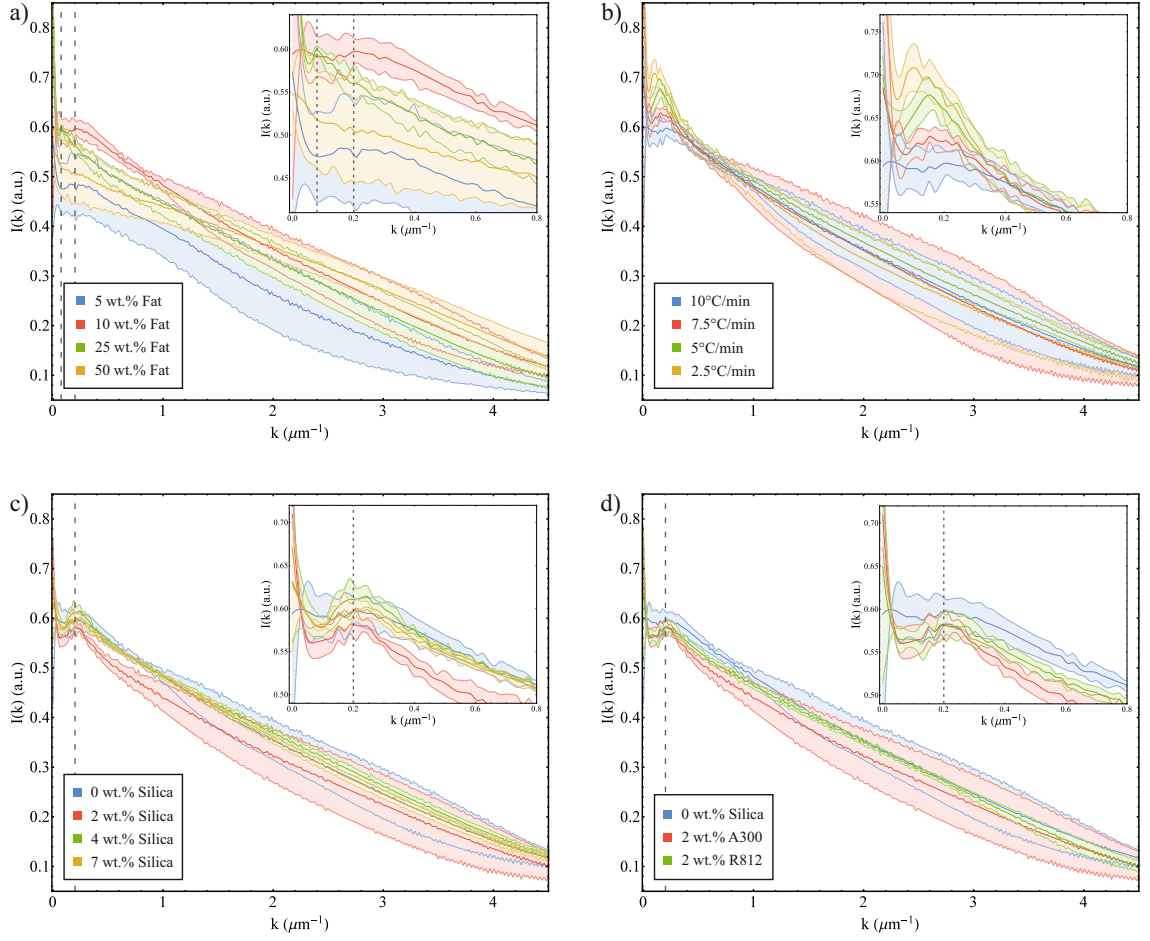


Figure 6.9: Structure factors for a) Samples with different fat concentrations crystallized at 10°C/min. b) 10 wt.% fat samples crystallized at different cooling rates. c) 10 wt.% fat samples containing different amounts of hydrophilic A300 silica, crystallized at 10°C/min. d) 10 wt.% fat samples containing different types of silica, crystallized at 10°C/min. The structure factors, $I(k)$, are presented in arbitrary units (a.u.).

samples at approximately $0.2 \mu\text{m}^{-1}$, which corresponds to a typical lengthscale of $30 \mu\text{m}$. We also see a small peak at $0.08 \mu\text{m}^{-1}$ for the 25 wt.% fat sample corresponding to $80 \mu\text{m}$. However, we do not observe any sharp peaks in the 50 wt.% sample data, but instead we see a smaller gradient relative to the other samples at higher k values. This indicates a larger range of smaller crystals, which can be seen in the greyscale and binary images.

The data shown in Figure 6.9b is from samples containing 10 wt.% fat crystallized at different cooling rates. In this data we see more defined peaks appear at smaller k values for lower cooling rates. This corresponds to larger crystals being formed and is consistent with the crystals observed in Figure 6.7b.

Figure 6.9c shows the Fourier transform results for 10 wt.% fat samples with different

concentrations of hydrophilic A300 silica, crystallized at 10°C/min. We see a distinct peak at approximately $0.2 \mu\text{m}^{-1}$, corresponding to a lengthscale of 30 μm , but this peak does not significantly vary with the amount of silica present. Similarly in Figure 6.9d we compare the results for 10 wt.% fat samples containing 2 wt.% silica with different surface chemistries. For both hydrophilic A300 and hydrophobic R812 silica we observe the same peak at $0.2\mu\text{m}^{-1}$, and all of the structure factors overlap within experimental error. These results are consistent with the proposed composite gel network model from the previous chapters. We see that the presence of silica does not significantly affect the at-rest microstructure of the fat crystal network.

Particle Counting Fractal Dimension

We calculate the two-dimensional fractal dimension of the fat crystal networks using a particle counting algorithm as a way to quantify the amount of order in the microstructure. The results of this analysis are presented in Table 6.2. We do not expect to see any variation of the fractal dimension with different fat concentration and this is in good agreement with the data. However, the fractal dimension has been shown to be sensitive to process conditions like the crystallization rate [93]. In Figure 6.7b we see that slower cooling rates lead to larger, more organised crystals and we would expect this trend to be reflected in the measured fractal dimensions, with higher values at lower cooling rates. However, we do not observe any significant variation as a function of the cooling rate, which indicates that this quantitative analysis might not be sensitive enough to the microstructural changes in our model system.

We do not observe any clear trend with silica concentration and all of the fractal dimension values lie within experimental error of each other. This is consistent with the other results showing that the silica does not change the microstructure but, in light of the previous results, we feel that we should avoid putting too much emphasis on these results. We do see a more substantial decrease in the fractal dimensions in the presence of hydrophobic R812 silica. This might be explained by a reduced packing efficiency caused by the bulky trimethylsilyl groups on the modified silica aggregates. However, we also treat these results with some caution.

Since these fractal dimensions were extracted from two-dimensional images they belong to two-dimensional Euclidean space. In order to compare them to fractal dimensions obtained from three-dimensional techniques, such as rheology, one approach is to simply add ‘1’ to these values [89]. This assumes that the distribution of mass is homogeneous in the third dimension,

a) Fat Concentration	Fractal Dimension	b) Cooling Rate	Fractal Dimension
5 wt.%	1.97 ± 0.05	10°C/min	1.97 ± 0.03
10 wt.%	1.97 ± 0.03	7.5°C/min	1.97 ± 0.03
25 wt.%	1.97 ± 0.02	5°C/min	1.99 ± 0.05
50 wt.%	1.92 ± 0.04	2.5°C/min	1.98 ± 0.05
c) Silica Concentration	Fractal Dimension	d) Silica Type	Fractal Dimension
0 wt.%	1.97 ± 0.03	No silica	1.97 ± 0.03
2 wt.%	1.95 ± 0.02	A300	1.95 ± 0.02
4 wt.%	1.94 ± 0.09	R812	1.88 ± 0.12
7 wt.%	1.97 ± 0.05		

Table 6.2: Fractal dimensions calculated by the particle counting method for a) Samples with different fat concentrations crystallized at 10°C/min. b) 10 wt.% fat samples crystallized at different cooling rates. c) 10 wt.% fat samples containing different amounts of hydrophilic A300 silica, crystallized at 10°C/min. d) 10 wt.% fat samples containing different types of silica, crystallized at 10°C/min.

however this is an approximation and actually lies closer to 0.79 for fat crystal networks measured by particle counting methods [120]. Therefore if we add this value to the fractal dimensions measured here we get good agreement with the values (~ 2.8) extracted from rheology in Chapter 3.

However, we would like to note that within the fractal model described in Chapter 3, the range of lengthscales considered to be fractal spans only from the size of a nanoplatelet up to the size of a single crystal cluster. At the magnifications used, these microscopy images do not offer any information from within the crystal clusters, but only from their arrangement in space. The distribution of these crystals may well also have a fractal nature, but this is distinctly different to the fractality being discussed in this model. Therefore, we feel that it is inappropriate to link the fractal dimensions measured by PLM and rheology in this way. However, this type of analysis is typically done in the literature [93, 119, 125] and so we have followed this protocol for completeness.

6.3.4 Confocal Scanning Laser Microscopy

In this section we explore the use of fluorescent confocal scanning laser microscopy (CSLM) for the study of fat crystal networks. In Figure 6.10a we present a three-dimensional reconstruction of 80 raw CSLM images for a 10 wt.% fat sample containing 4 wt.% hydrophobic R812. The sample volume shown here is $101.9 \times 101.9 \times 40 \mu\text{m}$, with each voxel corresponding to $0.199 \times 0.199 \times 0.5 \mu\text{m}$. The fluorescent dye was added into the soybean oil and so we see the fat

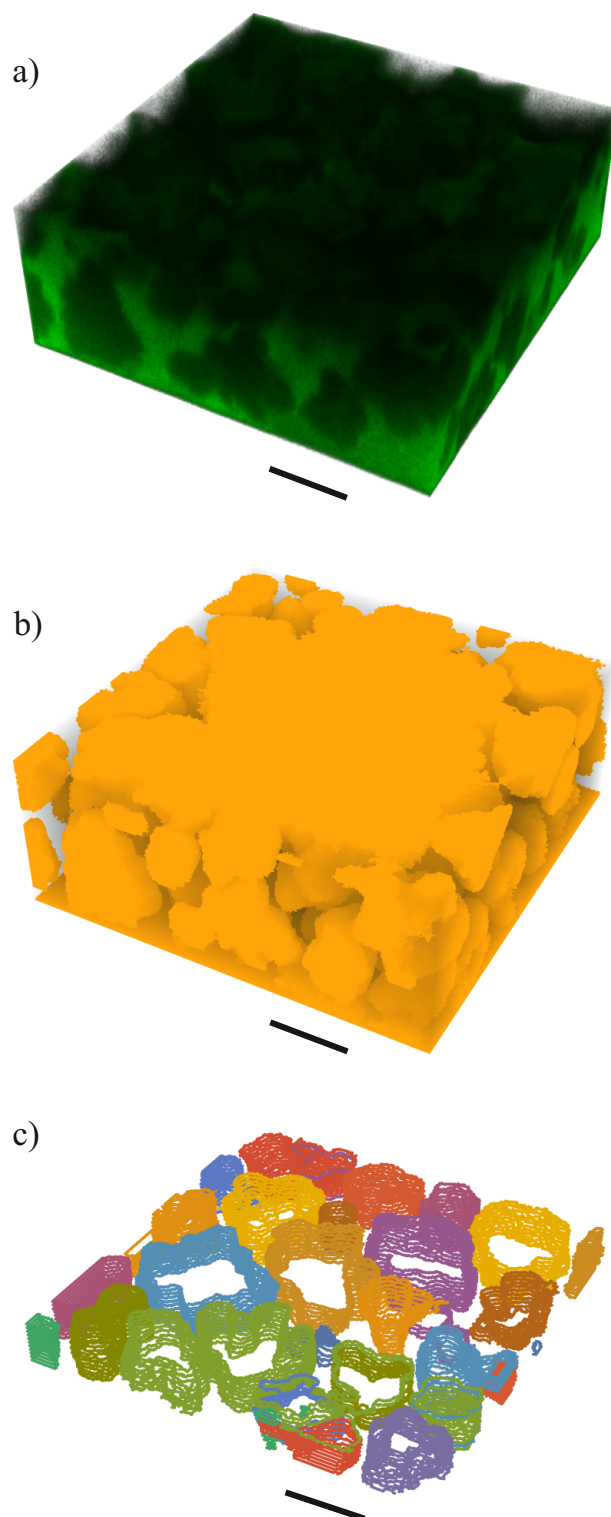


Figure 6.10: a) A 3D reconstruction of raw confocal scanning laser microscopy images for a 10 wt.% fat sample containing 4 wt.% hydrophobic R812 silica. The oil is shown in green and the fat crystals are shown as dark regions. The sample volume is $101.9 \times 101.9 \times 40 \mu\text{m}$. b) A 3D reconstruction of the image stack once the images have been analysed following the procedure give in Section 6.2.5. c) A $7.5 \mu\text{m}$ thick slice of the image stack showing the isolation of individual fat crystals. The scale bar represents $20 \mu\text{m}$.

crystals as dark regions in a bright green continuous phase. The silica was not fluorescently labelled and so we can not comment on the position of the silica in these images. At the base of Figure 6.10a we see the glass coverslip and we notice a distinct intensity gradient through the sample due to light scattering.

Figure 6.10b shows the same microscopy data once the analysis procedure described in Section 6.2.5 has been applied to each image. This analysis removes the noise in the raw images and differentiates the fat crystals from the oil. However, we can clearly see the effect of scattering at the top of the sample which means that we are no longer able to resolve individual crystals. When taking these images the microscope settings must be constant for the entire sample and so a compromise must be found to compensate for the increase in scattering at larger z-values. This provides a significant challenge and limits the sample thickness that can be observed with this technique.

In Figure 6.10c we present a thin slice through this image stack and we show that we are able to isolate individual crystals, shown here in different colours. This slice is taken 7.5 μm above the glass slide and is 5.5 μm thick. We are able to build three-dimensional reconstructions of individual crystals by comparing their centroid values in each analysed image. However, since these crystals have very irregular shapes this approach breaks down in various different cases which limits the slice thickness that can be accurately analysed using this approach.

Once the individual crystals have been isolated it is possible to extract sizes and we see that the typical lengthscale is approximately 30 μm , which corresponds well with the PLM measurements presented earlier in this chapter. We note that the fact that it is possible to isolate individual crystals means that we are not observing a continuous fat crystal network. Solid bridges are known to form between fat crystals during post-crystallization processes [94]. But their formation is dependent on the triglyceride composition, polymorphic form, fat concentration and crystallization conditions [123]. Here, we see that the fat crystals are discrete, disordered and slot into each other. This result suggests that the system is jammed [126], which could be responsible for the macroscopic solid-like properties measured by rheology. This was also observed in Section 6.3.3 for low fat concentrations (≤ 10 wt.%) but was more difficult to interpret because of the lower magnification and segmentation due to binarization.

This technique also gives insight into the shape and morphology of the fat crystals, however, due to the numerous challenges presented by this approach we did not pursue these experiments

any further. CSLM has been used to study food systems for many years [127–131], although the data is typically very qualitative and little use has been made of image analysis. We note that Singh et al. [121] have shown that it is possible to identify crystal polymorphs from three-dimensional reconstructions obtained via CSLM and image analysis for more regular crystal shapes and so this may be a potential area for future research.

6.4 Conclusions

In this chapter we used PLM and a range of image analysis techniques to investigate datasets looking at different aspects of fat crystallization. The time series experiments showed that, at low concentrations of silica (≤ 4 wt.%), the aggregates did not affect the nucleation or growth of the fat crystals. We also saw that crystallization temperatures can be extracted via PLM that are comparable to the DSC. This is a useful result for future studies of this system, since PLM offers more insight into the crystallization process. Furthermore, the experimental procedure and sample preparation are both much simpler.

On inspection of the final microstructures, we observed large changes at different fat concentrations and cooling rates. This was reflected in the individual crystal sizes and the structure factors extracted by Fourier transforms. However, it was more difficult to observe clear changes in the microstructure with different silica concentrations and types. The individual crystal sizes did show some variation with silica concentration, but there was no obvious trend here. Furthermore, the structure factors also showed no significant change with silica concentration. Similarly, for the different hydrophilic and hydrophobic silicas we observed a slight drop in the individual crystal sizes but the structure factors showed no significant difference.

We used a particle counting algorithm to calculate two-dimensional fractal dimensions for the fat crystal microstructures. However, we found that this approach was not sensitive enough to the observed changes in this system and so we do not place much significance on these results.

Finally, we used CSLM to build up a three-dimensional reconstruction of the fat crystal network. We were able to isolate individual fat crystals and reveal that the crystals slot together in a disordered arrangement. This result suggests a jammed structure made up of discrete crystal clusters, rather than clusters that have been mechanically sintered together. This technique is clearly very powerful for providing direct insight into the microstructure of these systems,

however we feel that more work must be done to optimize both the experimental procedure and analysis in order to maximize the quality of these results.

Acknowledgments

The differential scanning calorimetry data presented in this chapter was collected at Unilever's Research and Development facility in Vlaardingen, the Netherlands. In particular, we would like to thank Patricia Heussen and Ruud Adel den for training me and supervising the DSC experiments. We would also like to thank Lia Verhoeff and Arran Curran for many helpful discussions about microscopy.

Summary

In this thesis we studied the effect of colloidal silica aggregates on fat crystal networks in oil, which acts as a model system for fat-structured foods such as chocolate and butter. Our overall aim was to shine light on ways to reduce the amount of solid fat whilst maintaining similar mechanical and thermal properties.

Our approach to this challenge was to use silica aggregates to reinforce the fat crystal networks. We found that the silica was also capable of forming networks in oil, but these networks did not melt within the range of temperatures used in this study. This meant that in our system, since we started at temperatures above the melting point of the fat, the fat crystallized within a pre-existing silica structure. The rheological data presented in Chapter 3 showed that, at the concentrations of interest, the silica networks were much weaker than the fat networks. In Chapter 6 the polarized light microscopy images showed that the silica did not have a significant effect on the way in which the fat crystal networks formed or the final microstructure, at low concentrations. These results suggested that the initial silica structure was easily deformed and rearranged by the fat crystals as they grew. This led to the formation of a composite gel network, where the silica had been pushed out to form a dense layer of aggregates on the surface of the fat crystals.

We have used oscillatory rheology to show how the silica was able to affect the overall strength of this composite gel network. Firstly, at sufficiently high concentrations, the silica was able to increase the at-rest strength of the sample, as measured by the storage modulus within the linear viscoelastic region. Secondly, the silica was able to extend the length of the linear region, which meant that the composite gel networks could withstand larger deformations before being irreparably damaged. Finally, the addition of fumed silica changed the breakdown of the material after the linear region.

After characterizing the at-rest structure of the model system we looked at the time-dependent rheological behaviour in Chapter 5. We discussed the importance and desirability of thixotropy within the food industry and showed that both the fat and the silica networks possess thixotropic behaviour under certain conditions. We also showed that added silica reduced deformation and improved recovery which were both characteristics of samples with higher fat concentrations.

The differential scanning calorimetry results showed that the silica aggregates did not act as seeds for heterogeneous nucleation and therefore did not have a large effect on the fat crystallization process. We also showed that the silica did not change the melting temperature or the polymorphic form of the fat crystals, which is a very important result in terms of consumer experience.

Throughout this work we have considered various different types of fumed silica aggregates. We found the number of surface silanol groups available for hydrogen bonding to be the most important factor when considering the reinforcement of the fat networks. Silica varieties with lower surface areas and chemical modifications have fewer silanol bonds and they were less effective at providing support. We used infrared spectroscopy to show that fat was also able to form hydrogen bonds. However, we were unable to determine whether hydrogen bonds form between the two components or only between the silica aggregates.

It is worth noting here that the 200F hydrophilic silica is food grade and so this could be an immediately industrially viable option for creating reduced-fat food products. Food regulations vary across different regions and food categories and so it is difficult to quote the exact allowed amount of silica. However, as an example, 200F silica is currently allowed in grated cheese up to 2 wt.% in the USA and up to 3 wt.% in soups and condiments in Brazil. [30].

Based on the experiments and results presented in this thesis, several suggestions for future work can be made:

1. In Chapters 3 and 4 we relied on differential scanning calorimetry to determine the polymorphic form of the fat crystals. This data could be complemented and supported by X-ray diffraction which is also widely used to study polymorphism [39, 54]. Moreover, it is possible to determine the dimensions of the fat nanoplatelets from small angle X-ray scattering (SAXS) data [132]. This has been coupled with cryogenic transmission elec-

tron microscopy (cryo-TEM), allowing for quantitative visualization and characterization of these nanoplatelets [45]. Therefore, these techniques would enable us to examine the effects of the silica aggregates at the nanoscale.

2. The development of optical rheometers means that it is now possible to take rheological measurements with in-situ polarized light microscopy [133, 134]. This would allow for a much deeper understanding of the changes in microstructure under shear in our model system.
3. In Chapter 6, we saw the limitations of the current protocol and analysis for the study of fat crystal networks via fluorescent confocal scanning laser microscopy. This technique is very powerful and, if optimized, could produce considerable rewards in this line of study.
4. This work could now be developed by looking at different types of particles. Polysaccharides like inulin, cellulose and starch are potential candidates since they have multiple hydroxyl groups which are capable of hydrogen bonding. We carried out preliminary experiments with corn and rice starch along with spherical silica. These particles ranged from 1 to 10 μm and had similar surface chemistries to the fumed silica aggregates. However, instead of observing gelation of the oil phase, we saw sedimentation due to the size of these particles. This highlighted the importance of the large surface-to-volume ratio of the fractal aggregates and so future work should focus on creating smaller particles with larger surface areas.
5. Our model system of fat crystals in oil currently best represents shortening, which is typically used to create crumbly pastry. Margarine and butter are water-in-oil emulsions containing roughly 20 wt.% water as finely dispersed droplets [135]. This change in microstructure has a marked difference on the rheological behaviour and it would be interesting to study the effect of silica aggregates on a more complex food system. Moreover, there is growing interest in edible Pickering emulsions and fat crystals and nanoplatelets have been shown to stabilize water-in-oil emulsions [136].

Appendix

Rheology Time Sweeps

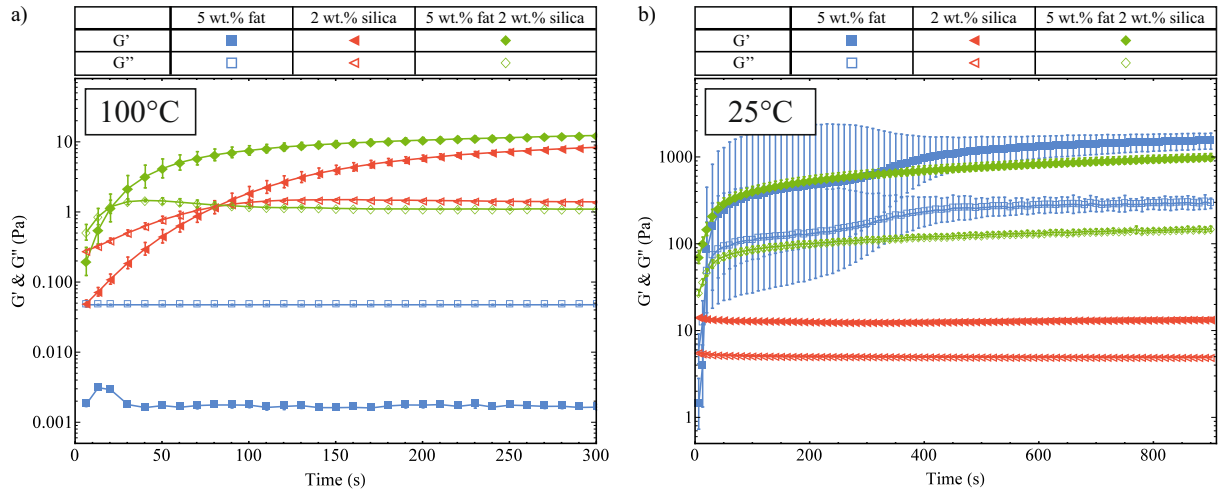


Figure A.1: Oscillatory time sweep data taken at a) 100°C before the cooling ramp. b) 25°C after the cooling ramp.

Figure A.1a shows the initial time sweep data taken at 100°C . It was obtained after preshearing the sample in order to quantify the amount of structure present. We see that the 5 wt.% fat sample is liquid-like ($G' < G''$) which shows that it is completely melted. The samples containing hydrophilic A300 silica show an increase in structure after the preshearing step and we observe a cross-over between the storage and loss moduli indicating recovery from liquid-like to solid-like behaviour. This data shows that a silica network can form at 100°C and is therefore present before the fat crystallizes during the cooling ramp.

In Figure A.1b we show the oscillatory time sweep data taken at 25°C after the cooling ramp. The fat crystallizes during the cooling ramp and so we measure strong networks ($G' > G''$) for the samples containing fat. This data was obtained to measure the formation of the fat

crystal networks and to confirm that the system had stopped evolving before any measurements were taken.

Differential Scanning Calorimetry

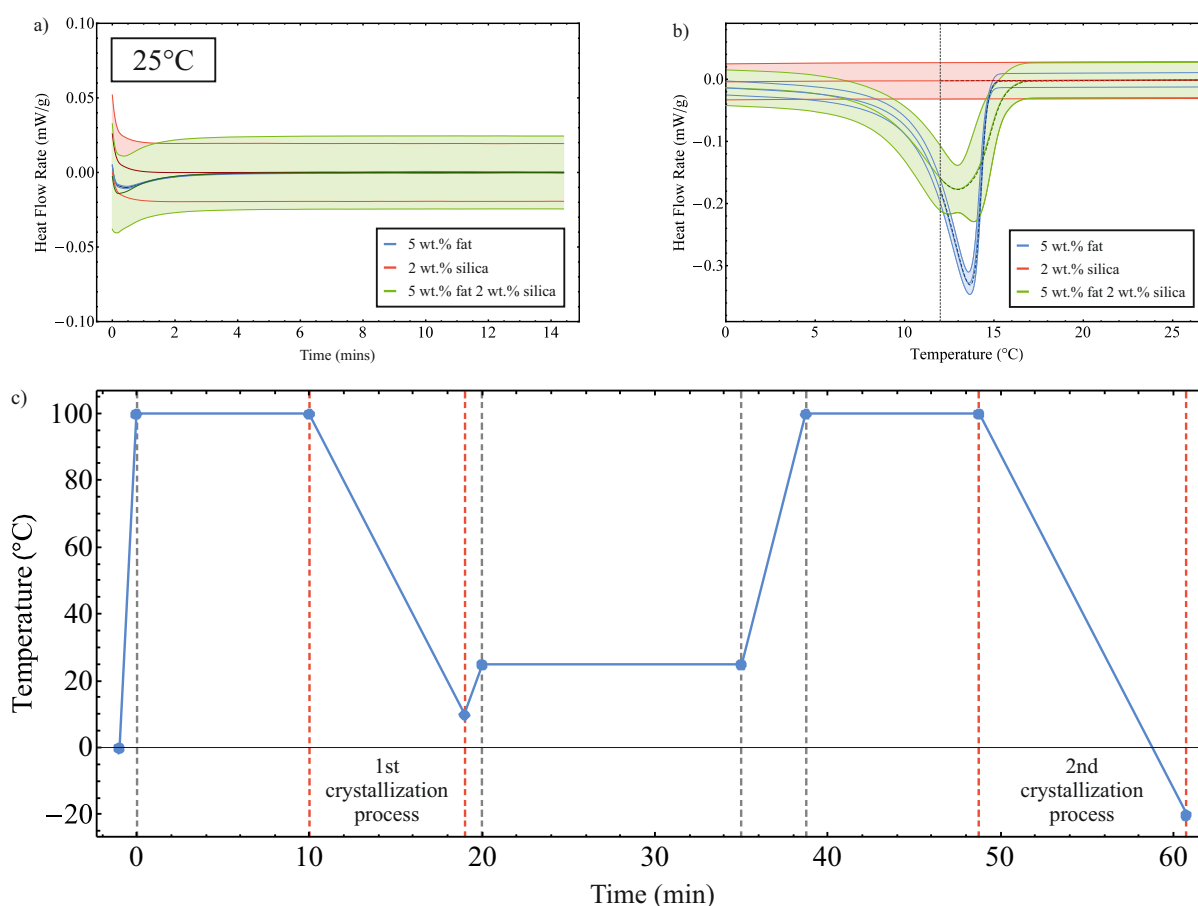


Figure A.2: a) Heat flow rate data taken after the cooling ramp. b) A comparison between the first and second crystallization peaks. The dashed vertical line shows the end of the first crystallization data. c) A timeline for a typical DSC experiment showing both crystallization processes.

The DSC data shown in Figure A.2a was collected after the cooling ramp and confirms that the system had stopped changing before we took any measurements. Figure A.2b compares the crystallization data for the first and second crystallization processes, which is shown by dashed and solid lines respectively. The vertical dashed line marks the end of the 1st crystallization data, which ranged from 100°C to 10°C, as shown in the DSC timeline given in Figure A.2c. The second crystallization process continued down to -20°C. For samples both with and without silica, the crystallization curves are not significantly different on the first and second crystallizations.

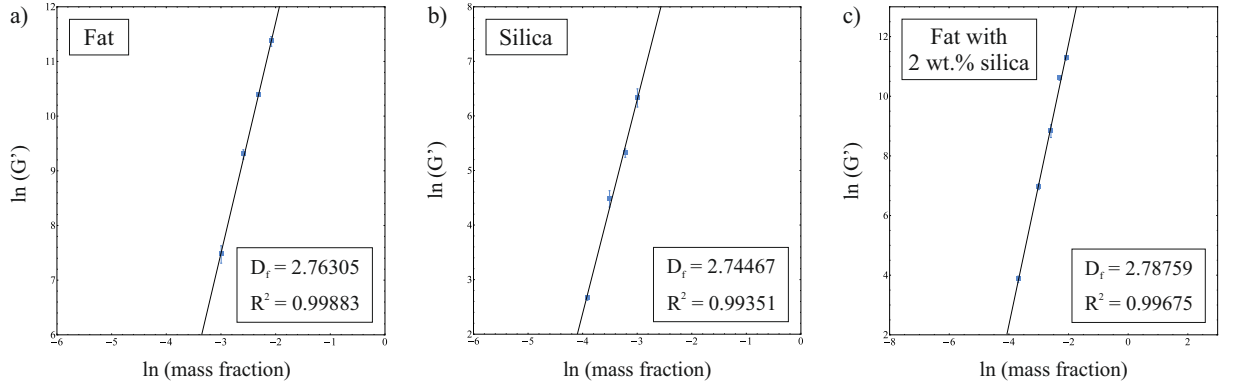


Figure A.3: Log-log plots of the mass fraction against the storage modulus for a) Fat samples. b) Silica samples. c) Fat samples containing 2 wt.% hydrophilic A300 silica.

This confirms that we are starting each experiment from a valid reference point that is not affected by crystal memory or sample history.

Fractal Dimension Calculations

The plots shown in Figure A.3 highlight a strong power law relationship between the storage modulus and mass fraction for all systems studied. The value for G' was taken from within the linear viscoelastic region in all cases. We are able to extract three-dimensional fractal dimensions from the stress sweep rheology data using the relationship $G' \sim \phi^{(d-2)/(d-D_f)}$, where ϕ is the mass fraction, d is the Euclidean dimension ($d = 3$ in this case) and D_f is the fractal dimension.

Greyscale Images

We present the final greyscale images from the time series experiments discussed in Chapter 6. These images show the final microstructure of the fat crystal networks at the end of the cooling ramp at 10°C . Figure A.4a shows the greyscale images for samples with different fat concentrations and a cooling rate of $10^\circ\text{C}/\text{min}$. In Figure A.4b we show the images for 10 wt.% fat samples which have been crystallized at different cooling rates. Figure A.4c compares samples with different concentrations of hydrophilic A300 silica which were crystallized at a cooling rate of $10^\circ\text{C}/\text{min}$. Figure A.4d shows samples containing 2 wt.% hydrophilic A300 silica with 2 wt.% hydrophobic R812 silica and a cooling rate of $10^\circ\text{C}/\text{min}$.

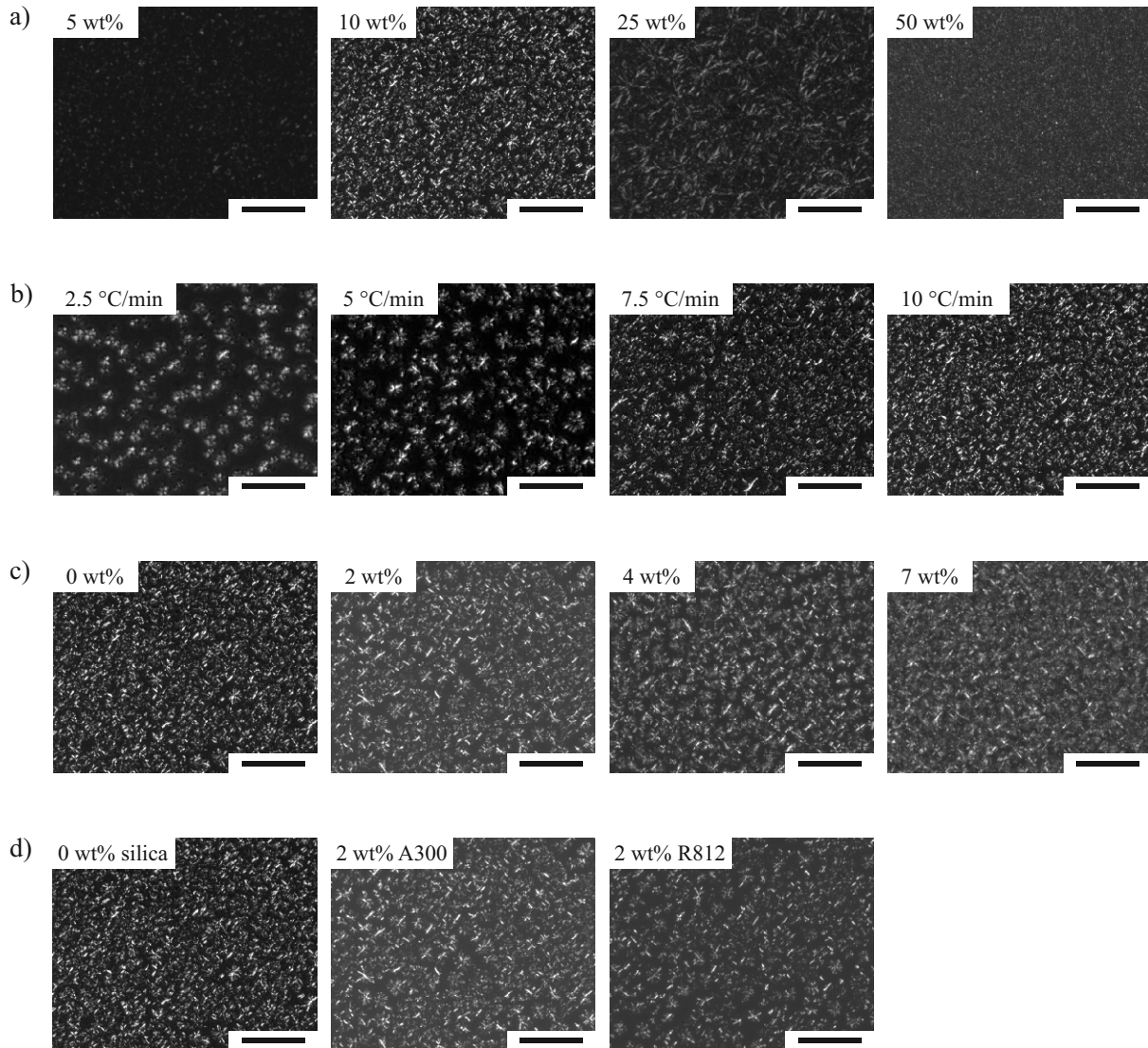


Figure A.4: Greyscale images for a) Samples with different fat concentrations crystallized at 10°C/min. b) 10 wt.% fat samples crystallized at different cooling rates. c) 10 wt.% fat samples containing different amounts of hydrophilic A300 silica, crystallized at 10°C/min. d) 10 wt.% fat samples containing different types of silica, crystallized at 10°C/min. The images are taken at the end of the cooling ramp and the scale bars represent 100 µm.

Bibliography

- [1] Howard A Barnes. *A handbook of elementary rheology*. University of Wales, Institute of Non-Newtonian Fluid Mechanics Aberystwyth, 2000.
- [2] MG Marudova-Zsivánovits. Thixotropic behaviour of ketchup. *Journal of Food Physics*, XIX:85–91, 2006.
- [3] Richard AL Jones. *Soft condensed matter*. Oxford University Press, 2002.
- [4] Ken Dill and Sarina Bromberg. *Molecular driving forces: statistical thermodynamics in biology, chemistry, physics, and nanoscience*. Garland Science, 2010.
- [5] Masao Doi. *Soft matter physics*. Oxford University Press, 2013.
- [6] Raffaele Mezzenga, Peter Schurtenberger, Adam Burbidge, and Martin Michel. Understanding foods as soft materials. *Nature Materials*, 4(10):729–740, 2005.
- [7] Job Ubbink, Adam Burbidge, and Raffaele Mezzenga. Food structure and functionality: a soft matter perspective. *Soft Matter*, 4(8):1569–1581, 2008.
- [8] RGM Van der Sman and AJ Van Der Goot. The science of food structuring. *Soft Matter*, 5(3):501–510, 2009.
- [9] Maud Langton, Elvy Jordansson, Annika Altskär, Charlotte Sørensen, and Anne-Marie Hermansson. Microstructure and image analysis of mayonnaises. *Food Hydrocolloids*, 13(2):113–125, 1999.
- [10] H Douglas Goff. Colloidal aspects of ice cream – a review. *International Dairy Journal*, 7(6–7):363–373, 1997.
- [11] F MacRitchie. Seventy years of research into breadmaking quality. *Journal of Cereal Science*, 70:123–131, 2016.
- [12] K Niranjana and SFJ Silva. Bubble-containing foods. In *Food Materials Science*, pages 281–303. Springer, 2008.
- [13] I Heertje. Structure and function of food products: a review. *Food Structure*, 1(1):3–23, 2014.

-
- [14] Suresh S Narine and Alejandro G Marangoni. Relating structure of fat crystal networks to mechanical properties: a review. *Food Research International*, 32(4):227–248, 1999.
- [15] P Corvisier, C Nouar, R Devienne, and M Lebouché. Development of a thixotropic fluid flow in a pipe. *Experiments in Fluids*, 31(5):579–587, 2001.
- [16] Basim Abu-Jdayil. Modelling the time-dependent rheological behavior of semisolid food-stuffs. *Journal of Food Engineering*, 57(1):97–102, 2003.
- [17] Philip C Calder. Functional roles of fatty acids and their effects on human health. *Journal of Parenteral and Enteral Nutrition*, 39(1 suppl):18S–32S, 2015.
- [18] Nozomu Kono and Hiroyuki Arai. Intracellular transport of fat-soluble vitamins A and E. *Traffic*, 16(1):19–34, 2015.
- [19] Seth J Baum, Penny M Kris-Etherton, Walter C Willett, Alice H Lichtenstein, Lawrence L Rudel, Kevin C Maki, Jay Whelan, Christopher E Ramsden, and Robert C Block. Fatty acids in cardiovascular health and disease: a comprehensive update. *Journal of Clinical Lipidology*, 6(3):216–234, 2012.
- [20] Michael A Rogers. Novel structuring strategies for unsaturated fats—meeting the zero-trans, zero-saturated fat challenge: a review. *Food Research International*, 42(7):747–753, 2009.
- [21] Mimma Perneti, Kees F van Malssen, Eckhard Flöter, and Arjen Bot. Structuring of edible oils by alternatives to crystalline fat. *Current Opinion in Colloid & Interface Science*, 12(4):221–231, 2007.
- [22] Ashok R Patel and Koen Dewettinck. Edible oil structuring: an overview and recent updates. *Food & Function*, 7(1):20–29, 2016.
- [23] Hong-Sik Hwang, Sanghoon Kim, Kervin O Evans, Clarissa Koga, and Youngsoo Lee. Morphology and networks of sunflower wax crystals in soybean oil organogel. *Food Structure*, 5:10–20, 2015.
- [24] Chi Diem Doan, Davy Van de Walle, Koen Dewettinck, and Ashok R Patel. Evaluating the oil-gelling properties of natural waxes in rice bran oil: rheological, thermal, and microstructural study. *Journal of the American Oil Chemists’ Society*, 92(6):801–811, 2015.
- [25] Ashok R Patel, Bora Mankoč, MD Bin Sintang, Ans Lesaffer, and Koen Dewettinck. Fumed silica-based organogels and aqueous-organic bigels. *RSC Advances*, 5(13):9703–9708, 2015.
- [26] Ashok R Patel, Pinar Dumlu, Lien Vermeir, Benny Lewille, Ans Lesaffer, and Koen Dewettinck. Rheological characterization of gel-in-oil-in-gel type structured emulsions. *Food Hydrocolloids*, 46:84–92, 2015.

- [27] Thomas S Skelhon, Nadia Grossiord, Adam R Morgan, and Stefan AF Bon. Quiescent water-in-oil Pickering emulsions as a route toward healthier fruit juice infused chocolate confectionary. *Journal of Materials Chemistry*, 22(36):19289–19295, 2012.
- [28] Thomas S Skelhon, Patrik KA Olsson, Adam R Morgan, and Stefan AF Bon. High internal phase agar hydrogel dispersions in cocoa butter and chocolate as a route towards reducing fat content. *Food & Function*, 4(9):1314–1321, 2013.
- [29] Office of Food Additive Safety. Gras notification for synthetic amorphous silica. Technical report, 2014.
- [30] Evonik Industries AG. AEROSIL[®] 200F product safety information. Technical report, 2016.
- [31] Kevin W Smith, Krish Bhaggan, Geoff Talbot, and Kees F van Malssen. Crystallization of fats: influence of minor components and additives. *Journal of the American Oil Chemists' Society*, 88(8):1085–1101, 2011.
- [32] Andrew GF Stapley, Heather Tewkesbury, and Peter J Fryer. The effects of shear and temperature history on the crystallization of chocolate. *Journal of the American Oil Chemists' Society*, 76(6):677–685, 1999.
- [33] RC Basso, APB Ribeiro, MH Masuchi, LA Gioielli, LAG Gonçalves, AO dos Santos, LP Cardoso, and R Grimaldi. Tripalmitin and monoacylglycerols as modifiers in the crystallisation of palm oil. *Food Chemistry*, 122(4):1185–1192, 2010.
- [34] L Svanberg, L Ahrné, N Lorén, and E Windhab. Effect of sugar, cocoa particles and lecithin on cocoa butter crystallisation in seeded and non-seeded chocolate model systems. *Journal of Food Engineering*, 104(1):70–80, 2011.
- [35] L Svanberg, L Ahrné, N Lorén, and E Windhab. Effect of pre-crystallization process and solid particle addition on microstructure in chocolate model systems. *Food Research International*, 44(5):1339–1350, 2011.
- [36] Sonia Calligaris, Fabio Valoppi, Luisa Barba, Monica Anese, and Maria Cristina Nicoli. Mutual effect of fat and β -carotene on fat crystal network structure and carotenoid bleaching. *Food Research International*, 66:257–263, 2014.
- [37] Nuria C Acevedo and Alejandro G Marangoni. Nanostructured fat crystal systems. *Annual Review of Food Science and Technology*, 6:71–96, 2015.
- [38] Yuqing Zhou and Richard W Hartel. Phase behavior of model lipid systems: solubility of high-melting fats in low-melting fats. *Journal of the American Oil Chemists' Society*, 83(6):505–511, 2006.
- [39] M Kellens, W Meeussen, C Riekkel, and Harry Reynaers. Time resolved X-ray diffraction studies of the polymorphic behaviour of tripalmitin using synchrotron radiation. *Chemistry and Physics of Lipids*, 52(2):79–98, 1990.

-
- [40] M Kellens, W Meeussen, and Harry Reynaers. Crystallization and phase transition studies of tripalmitin. *Chemistry and Physics of Lipids*, 55(2):163–178, 1990.
- [41] Emmanuel Ohene Afoakwa, Alistair Paterson, and Mark Fowler. Factors influencing rheological and textural qualities in chocolate – a review. *Trends in Food Science & Technology*, 18(6):290–298, 2007.
- [42] USDA. National nutrient database for standard reference. Technical report, 2017.
- [43] L. H. Jensen and A. J. Mabis. Crystal structure of β -tricaprin. *Nature*, 197(4868):681–682, 1963.
- [44] LH Jensen and AJ Mabis. Refinement of the structure of β -tricaprin. *Acta Crystallographica*, 21(5):770–781, 1966.
- [45] Nuria C Acevedo and Alejandro G Marangoni. Characterization of the nanoscale in triacylglycerol crystal networks. *Crystal Growth & Design*, 10(8):3327–3333, 2010.
- [46] M Van den Tempel. Mechanical properties of plastic-disperse systems at very small deformations. *Journal of Colloid Science*, 16(3):284–296, 1961.
- [47] CJ Nederveen. Dynamic mechanical behavior of suspensions of fat particles in oil. *Journal of Colloid Science*, 18(3):276–291, 1963.
- [48] Alejandro G Marangoni, Nuria Acevedo, Fatemeh Maleky, Fernanda Peyronel, Gianfranco Mazzanti, Bonnie Quinn, David Pink, et al. Structure and functionality of edible fats. *Soft Matter*, 8(5):1275–1300, 2012.
- [49] David A Pink, Bonnie Quinn, Fernanda Peyronel, and Alejandro G Marangoni. Edible oil structures at low and intermediate concentrations. i. Modeling, computer simulation, and predictions for X-ray scattering. *Journal of Applied Physics*, 114(23):234901, 2013.
- [50] Fernanda Peyronel, Jan Ilavsky, Gianfranco Mazzanti, Alejandro G Marangoni, and David A Pink. Edible oil structures at low and intermediate concentrations. ii. Ultra-small angle X-ray scattering of in situ tristearin solids in triolein. *Journal of Applied Physics*, 114(23):234902, 2013.
- [51] Bonnie Quinn, Fernanda Peyronel, Tyler Gordon, Alejandro Marangoni, Charles B Hanna, and David A Pink. Aggregation in complex triacylglycerol oils: coarse-grained models, nanophase separation, and predicted X-ray intensities. *Journal of Physics: Condensed Matter*, 26(46):464108, 2014.
- [52] Fernanda Peyronel, Bonnie Quinn, Alejandro G Marangoni, and David A Pink. Ultra small angle X-ray scattering in complex mixtures of triacylglycerols. *Journal of Physics: Condensed Matter*, 26(46):464110, 2014.

- [53] David A Pink, Fernanda Peyronel, Bonnie Quinn, Pratham Singh, and Alejandro G Marangoni. Condensation versus diffusion. a spatial-scale-independent theory of aggregate structures in edible oils: applications to model systems and commercial shortenings studied via rheology and USAXS. *Journal of Physics D: Applied Physics*, 48(38):384003, 2015.
- [54] Alejandro G Marangoni and Leendert H Wesdorp. *Structure and properties of fat crystal networks*. CRC Press, 2012.
- [55] R Campos, SS Narine, and AG Marangoni. Effect of cooling rate on the structure and mechanical properties of milk fat and lard. *Food Research International*, 35(10):971–981, 2002.
- [56] D Fennell Evans and Hakan Wennerstrom. *Colloidal domain*. Wiley-Vch, 1999.
- [57] K Sangwal. Recent developments in understanding of the metastable zone width of different solute – solvent systems. *Journal of Crystal Growth*, 318(1):103–109, 2011.
- [58] C Himawan, VM Starov, and AGF Stapley. Thermodynamic and kinetic aspects of fat crystallization. *Advances in Colloid and Interface Science*, 122(1):3–33, 2006.
- [59] Kiyotaka Sato. Crystallization behaviour of fats and lipids - a review. *Chemical Engineering Science*, 56(7):2255–2265, 2001.
- [60] Kevin W Smith, Fred W Cain, and Geoff Talbot. Crystallisation of 1, 3-dipalmitoyl-2-oleoylglycerol and tripalmitoylglycerol and their mixtures from acetone. *European Journal of Lipid Science and Technology*, 107(9):583–593, 2005.
- [61] Laura Bayés-García, Ashok R Patel, Koen Dewettinck, Déricks Rousseau, Kiyotaka Sato, and Satoru Ueno. Lipid crystallization kinetics – roles of external factors influencing functionality of end products. *Current Opinion in Food Science*, 4:32–38, 2015.
- [62] John William Mullin. *Crystallization*. Butterworth-Heinemann, 2001.
- [63] Valerie J Anderson and Henk NW Lekkerkerker. Insights into phase transition kinetics from colloid science. *Nature*, 416(6883):811–815, 2002.
- [64] Alejandro G Marangoni, Dongming Tang, and Anand Pal Singh. Non-isothermal nucleation of triacylglycerol melts. *Chemical Physics Letters*, 419(1):259–264, 2006.
- [65] Laziz Bouzidi and Suresh S Narine. Evidence of critical cooling rates in the nonisothermal crystallization of triacylglycerols: a case for the existence and selection of growth modes of a lipid crystal network. *Langmuir*, 26(6):4311–4319, 2009.
- [66] Stefan B Irmscher, Monika Gibis, Kurt Herrmann, Reinhard Kohlus, and Jochen Weiss. Oil-fat mixtures with low solid fat concentration: influence of fat concentration and cooling conditions. *Journal of the American Oil Chemists’ Society*, 92(9):1277–1291, 2015.

-
- [67] Evonik Industries AG. Basic characteristics of AEROSIL[®] fumed silica: Technical bulletin fine particles 11. Technical report, 2006.
- [68] M Seipenbusch, S Rothenbacher, M Kirchhoff, H-J Schmid, G Kasper, and AP Weber. Interparticle forces in silica nanoparticle agglomerates. *Journal of Nanoparticle Research*, 12(6):2037–2044, 2010.
- [69] Srinivasa R Raghavan, Howard J Walls, and Saad A Khan. Rheology of silica dispersions in organic liquids: new evidence for solvation forces dictated by hydrogen bonding. *Langmuir*, 16(21):7920–7930, 2000.
- [70] Yasufumi Otsubo, Misao Horigome, and Kaoru Umeya. Effect of surface treatment of particles on the rheological properties of suspensions. *Journal of Colloid and Interface Science*, 83(1):240–245, 1981.
- [71] VM Gun’ko, VI Zarko, R Leboda, EF Voronin, E Chibowski, and EM Pakhlov. Influence of modification of fine silica by organosilicon compounds on particle-particle interaction in aqueous suspensions. *Colloids and Surfaces A: Physicochemical and Engineering Aspects*, 132(2-3):241–249, 1998.
- [72] Herbert Barthel. Surface interactions of dimethylsiloxo group-modified fumed silica. *Colloids and Surfaces A: Physicochemical and Engineering Aspects*, 101(2-3):217–226, 1995.
- [73] Jerzy Baldyga, Lukasz Makowski, Wojciech Orciuch, Caroline Sauter, and Heike P Schuchmann. Deagglomeration processes in high-shear devices. *Chemical Engineering Research and Design*, 86(12):1369–1381, 2008.
- [74] *Oxford English Dictionary Online*. Oxford University Press, 2017.
- [75] Ronald G Larson. *The structure and rheology of complex fluids*. Oxford University Press New York, 1999.
- [76] SS Velankar and D Giles. How do I know if my phase angles are correct? *Rheology Bulletin*, 76(2):8–20, 2007.
- [77] Jan Mewis and Norman J Wagner. *Colloidal suspension rheology*. Cambridge University Press, 2012.
- [78] Simon Gaisford, Vicky Kett, and Peter Haines. *Principles of thermal analysis and calorimetry*. Royal Society of Chemistry, 2016.
- [79] Robert L Danley. New heat flux DSC measurement technique. *Thermochimica Acta*, 395(1):201–208, 2002.
- [80] CW Hoerr. Morphology of fats, oils, and shortenings. *Journal of the American Oil Chemists’ Society*, 37(10):539–546, 1960.
- [81] Douglas B. Murphy and Michael W. Davidson. *Fundamentals of light microscopy and electronic imaging*. Wiley, 2012.

-
- [82] Colin JR Sheppard and David M Shotton. *Confocal laser scanning microscopy*. BIOS Scientific Publishers, 1997.
- [83] Helmut Günzler and Hans-Ulrich Gremlich. *IR spectroscopy – an introduction*. 2002.
- [84] George C Pimentel and Aubrey L McClellan. *The hydrogen bond*. Freeman, 1960.
- [85] Evonik Industries AG. Successful use of AEROSIL[®] fumed silica in liquid systems: Technical information 1279. Technical report, 2015.
- [86] JMP Papenhuijzen. The role of particle interactions in the rheology of dispersed systems. *Rheologica Acta*, 11(1):73–88, 1972.
- [87] JMP Papenhuijzen. Superimposed steady and oscillatory shear in dispersed systems. i. Experimental and some results. *Rheologica Acta*, 10(493):493–502, 1971.
- [88] JMP Papenhuijzen. Superimposed steady and oscillatory shear in dispersed systems. ii. Influence of the inhomogeneity of the large deformation. *Rheologica Acta*, 10(503):503–507, 1971.
- [89] Benoit B Mandelbrot and Roberto Pignoni. *The fractal geometry of nature*. WH freeman New York, 1983.
- [90] Paul Meakin. Fractal aggregates. *Advances in Colloid and Interface Science*, 28:249–331, 1987.
- [91] Wei-Heng Shih, Wan Y Shih, Seong-Il Kim, Jun Liu, and Ilhan A Aksay. Scaling behavior of the elastic properties of colloidal gels. *Physical Review A*, 42(8):4772, 1990.
- [92] R Vreeker, LL Hoekstra, DC Den Boer, and WGM Agterof. The fractal nature of fat crystal networks. *Colloids and Surfaces*, 65(2):185–189, 1992.
- [93] Suresh S Narine and Alejandro G Marangoni. Fractal nature of fat crystal networks. *Physical Review E*, 59(2):1908, 1999.
- [94] I Heertje. Microstructural studies in fat research. *Food Structure*, 12(1):10, 1993.
- [95] Suresh S Narine and Alejandro G Marangoni. Mechanical and structural model of fractal networks of fat crystals at low deformations. *Physical Review E*, 60(6):6991, 1999.
- [96] Pierre-Gilles de Gennes. *Scaling concepts in polymer physics*. Cornell University Press, 1979.
- [97] Giovanni Dietler, Claude Aubert, David S Cannell, and Pierre Wiltzius. Gelation of colloidal silica. *Physical Review Letters*, 57(24):3117, 1986.
- [98] Chrismono Himawan, William MacNaughtan, Imad A Farhat, and Andrew GF Stapley. Polymorphic occurrence and crystallization rates of tristearin/tripalmitin mixtures under non-isothermal conditions. *European Journal of Lipid Science and Technology*, 109(1):49–60, 2007.

-
- [99] DM Small. Handbook of lipid research. In *The Physical Chemistry of Lipids*, volume 4, page 512. Plenum Press New York, 1986.
- [100] Albert Einstein. Eine neue bestimmung der moleküldimensionen. *Annalen der Physik*, 324(2):289–306, 1906.
- [101] Brian M Haines and Anna L Mazzucato. A proof of einstein’s effective viscosity for a dilute suspension of spheres. *SIAM Journal on Mathematical Analysis*, 44(3):2120–2145, 2012.
- [102] Jeong-Yun Sun, Xuanhe Zhao, Widusha RK Illeperuma, Ovijit Chaudhuri, Kyu Hwan Oh, David J Mooney, Joost J Vlassak, and Zhigang Suo. Highly stretchable and tough hydrogels. *Nature*, 489(7414):133–136, 2012.
- [103] J. Hou. *Composite polymer electrolytes using functionalized fumed silica and low molecular weight PEO: Synthesis and characterization*. PhD thesis, Michigan State University, 1997.
- [104] Srinivasa R Raghavan, Jun Hou, Gregory L Baker, and Saad A Khan. Colloidal interactions between particles with tethered nonpolar chains dispersed in polar media: direct correlation between dynamic rheology and interaction parameters. *Langmuir*, 16(3):1066–1077, 2000.
- [105] Jacob N Israelachvili. *Intermolecular and surface forces: 2nd edition*. Academic press, 1991.
- [106] Orland W Kolling. Influence of hydrogen bonding solvents on the infrared absorption band of the carbonyl group in acetone. *Transactions of the Kansas Academy of Science*, pages 161–166, 1996.
- [107] Hesam A Ardakani, Evan Mitsoulis, and Savvas G Hatzikiriakos. Thixotropic flow of toothpaste through extrusion dies. *Journal of Non-Newtonian Fluid Mechanics*, 166(21):1262–1271, 2011.
- [108] Howard A Barnes. Thixotropy - a review. *Journal of Non-Newtonian fluid mechanics*, 70(1):1–33, 1997.
- [109] Howard A Barnes, John Fletcher Hutton, and Kenneth Walters. *An introduction to rheology*. Elsevier, 1989.
- [110] Katherine MN Oates, Wendy E Krause, Ronald L Jones, and Ralph H Colby. Rheopexy of synovial fluid and protein aggregation. *Journal of the Royal Society Interface*, 3(6):167–174, 2006.
- [111] Shukun Chen, Gisle Øye, and Johan Sjöblom. Rheological properties of silica particle suspensions in mineral oil. *Journal of Dispersion Science and Technology*, 26(6):791–798, 2005.

-
- [112] Toshimaro Sone. The rheological behavior and thixotropy of a fatty plastic body. *Journal of the Physical Society of Japan*, 16(5):961–971, 1961.
- [113] A Shukla and SSH Rizvi. Viscoelastic properties of butter. *Journal of Food Science*, 60(5):902–905, 1995.
- [114] Thomas G Mezger. *The rheology handbook: for users of rotational and oscillatory rheometers*. Vincentz Network GmbH & Co KG, 2006.
- [115] Omer Said Toker, Salih Karasu, Mustafa Tahsin Yilmaz, and Safa Karaman. Three interval thixotropy test (3itt) in food applications: A novel technique to determine structural regeneration of mayonnaise under different shear conditions. *Food Research International*, 70:125–133, 2015.
- [116] Yasuhiro Nakai, Yoshitaka Ryo, and Masami Kawaguchi. Transient and steady-state rheology of silica suspensions in hydroxypropyl (methyl) cellulose solutions. *Journal of the Chemical Society, Faraday Transactions*, 89(14):2467–2472, 1993.
- [117] H. Henning Winter. The critical gel - the universal material state between liquid and solid. NATO ASI Meeting, 1999.
- [118] Nobuyuki Otsu. A threshold selection method from gray-level histograms. *Automatica*, 11(285-296):23–27, 1975.
- [119] Suresh S Narine and Alejandro G Marangoni. Microscopic and rheological studies of fat crystal networks. *Journal of Crystal Growth*, 198:1315–1319, 1999.
- [120] Dongming Tang and Alejandro G Marangoni. 3D fractal dimension of fat crystal networks. *Chemical Physics Letters*, 433(1):248–252, 2006.
- [121] Meenesh R Singh, Jayanta Chakraborty, Nandkishor Nere, Hsien-Hsin Tung, Shailendra Bordawekar, and Doraiswami Ramkrishna. Image-analysis-based method for 3D crystal morphology measurement and polymorph identification using confocal microscopy. *Crystal Growth & Design*, 12(7):3735–3748, 2012.
- [122] M Kellens, W Meeussen, and Harry Reynaers. Study of the polymorphism and the crystallization kinetics of tripalmitin: a microscopic approach. *Journal of the American Oil Chemists’ Society*, 69(9):906–911, 1992.
- [123] Dorota Johansson and Björn Bergenståhl. Sintering of fat crystal networks in oil during post-crystallization processes. *Journal of the American Oil Chemists’ Society*, 72(8):911–920, 1995.
- [124] ML Herrera and RW Hartel. Effect of processing conditions on crystallization kinetics of a milk fat model system. *Journal of the American Oil Chemists’ Society*, 77(11):1177–1188, 2000.

-
- [125] Alejandro G Marangoni. The nature of fractality in fat crystal networks. *Trends in Food Science & Technology*, 13(2):37–47, 2002.
- [126] Eric R Weeks. *Soft jammed materials*. Tohoku University Press.
- [127] I Heertje, P Vlist, JCG Blonk, HACM Hendrickx, and GJ Brakenhoff. Confocal scanning laser microscopy in food research: some observations. *Food Structure*, 6(2):2, 1987.
- [128] JCG Blonk and H Van Aalst. Confocal scanning light microscopy in food research. *Food Research International*, 26(4):297–311, 1993.
- [129] ML Herrera and RW Hartel. Effect of processing conditions on physical properties of a milk fat model system: microstructure. *Journal of the American Oil Chemists’ Society*, 77(11):1197–1205, 2000.
- [130] R Hans Tromp, Fred van de Velde, Jan van Riel, and Marcel Paques. Confocal scanning light microscopy (CSLM) on mixtures of gelatine and polysaccharides. *Food Research International*, 34(10):931–938, 2001.
- [131] Markus B Dürrenberger, Stephan Handschin, Béatrice Conde-Petit, and Felix Escher. Visualization of food structure by confocal laser scanning microscopy (CLSM). *LWT-Food Science and Technology*, 34(1):11–17, 2001.
- [132] Nuria C Acevedo and Alejandro G Marangoni. Toward nanoscale engineering of triacylglycerol crystal networks. *Crystal Growth & Design*, 10(8):3334–3339, 2010.
- [133] Sopark Sonwai and MR Mackley. The effect of shear on the crystallization of cocoa butter. *Journal of the American Oil Chemists’ Society*, 83(7):583–596, 2006.
- [134] Veerle De Graef, Peter Van Puyvelde, Bart Goderis, and Koen Dewettinck. Influence of shear flow on polymorphic behavior and microstructural development during palm oil crystallization. *European Journal of Lipid Science and Technology*, 111(3):290–302, 2009.
- [135] AC Juriaanse and I Heertje. Microstructure of shortenings, margarine and butter - a review. *Food Structure*, 7(2):8, 1988.
- [136] Dérick Rousseau. Trends in structuring edible emulsions with Pickering fat crystals. *Current Opinion in Colloid & Interface Science*, 18(4):283–291, 2013.

List of Publications

To date the following publications based upon work in this thesis have been submitted or are in preparation:

Raamanand R. Chauhan, Roel P. Dullens, Krassimir P. Velikov and Dirk G.A.L. Aarts. *The effect of colloidal aggregates on fat crystal networks*. Food & Function, 8(1):352-359, 2017. (Chapters 3 & 6).

Raamanand R. Chauhan, Roel P. Dullens, Krassimir P. Velikov and Dirk G.A.L. Aarts. *Exploring concentration, surface area and surface chemistry effects of colloidal aggregates on fat crystal networks*. Submitted. (Chapter 4 & 6).

Raamanand R. Chauhan, Roel P. Dullens, Krassimir P. Velikov and Dirk G.A.L. Aarts. *The deformation and recovery of fat crystal networks with colloidal aggregates*. In preparation. (Chapter 5).

Acknowledgement of Funding

We gratefully acknowledge Unilever and the Engineering and Physical Sciences Research Council (Award Ref. 1379135) for co-funding this project.

Acknowledgements

First and foremost, I would like to thank Dirk. He has always been able to guide and help me with his brilliant ideas and even better sense of humour. He has made this process truly enjoyable and rewarding. I would like to thank Krassi for the opportunity to work on this project and for his continued help and insight. Some of the best ideas in this work came directly from our many Skype discussions.

I feel extremely fortunate to be part of a research group which has two supervisors like Dirk and Roel at the helm. I have also benefitted from useful conversations with Roel and I am always grateful for his direct approach. Moreover, they set a warm, friendly tone from the top down and have made my time in the group extremely fun and memorable.

In particular, I must thank Colin for helping me to develop the key ideas presented here, for teaching me to code and for making these years some of my favourites in Oxford. Josh, Michael and François have become great friends over the past few years and I feel lucky to have shared this time with them. I would also extend my gratitude to the entire group, including the many friends that have moved on since I started.

Hannah, my fiancée, never asked about rheology or fat crystal networks but she has endured years of my thrilling conversations. She has been patient and understanding and has helped me consistently throughout this process. I am truly proud and grateful to have her by my side.

Finally, my parents have been an inexhaustible source of support since I first came up to Oxford. They remain some of my best friends and I will always owe a great deal to them. Thank you.